TESIS DE LA UNIVERSIDAD DE ZARAGOZA
2025
68

Daniel Gallardo Artal

Development of metrological techniques for the evaluation of macro- and micro- geometries by additive manufacturing polymeric reference standards for X-Ray computed tomography

Director/es
Albajez García, José Antonio
Yagüe Fabra, José Antonio

ISSN 2254-7606

Prensas de la Universidad
Universidad Zaragoza

Universidad de Zaragoza
Servicio de Publicaciones

ISSN 2254-7606

Universidad Zaragoza
1542

Tesis Doctoral

DEVELOPMENT OF METROLOGICAL TECHNIQUES FOR THE EVALUATION OF MACRO- AND MICRO- GEOMETRIES BY ADDITIVE MANUFACTURING POLYMERIC REFERENCE STANDARDS FOR X-RAY COMPUTED TOMOGRAPHY

Autor

Daniel Gallardo Artal

Director/es

Albajez García, José Antonio
Yagüe Fabra, José Antonio

UNIVERSIDAD DE ZARAGOZA
Escuela de Doctorado

Programa de Doctorado en Ingeniería de Diseño y Fabricación

2024

Universidad Zaragoza
1542

Tesis Doctoral

Development of metrological techniques for the evaluation of macro- and micro- geometries by additive manufacturing polymeric reference standards for X-Ray computed tomography

Autor

Daniel Gallardo Artal

Director/es

José Antonio Albajez García
José Antonio Yagüe Fabra

Escuela de Ingeniería y Arquitectura

2024

Development of metrological techniques for the evaluation of macro- and micro- geometries by additive manufacturing polymeric reference standards for X-Ray computed tomography.

Daniel Gallardo Artal

Supervised by:

Dr. José Antonio Albajez García

Dr. José Antonio Yagüe Fabra

Universidad Zaragoza

Department of Design and Manufacturing Engineering.

A thesis presented for the degree of

Doctor by the University of Zaragoza.

August 2024.

Acknowledgements

First, I am extremely grateful to my supervisors, José Antonio Albajez and José Antonio Yagüe, for all the guidance during this four years, giving me the confidence and advice to develop this thesis. Their constant labour, professionally and personally, have allowed me to become a better researcher. Also, I am very grateful to Lucía, who has been my mentor in all my research and teaching activity in this period, and I could consider her, unofficially, my third supervisor.

I would like to thank to all the members of the Department of the Design and Manufacturing Engineering, as well as the SAI members of the manufacturing workshop, for their great welcome and their "helping hand" whenever I needed.

My sincere thanks to Professor Simone Carmignato and Professor Filippo Zanini for giving me the opportunity to work together during my research stay at the Department of Management and Engineering at the Università Degli Studi di Padova, as well as to Javi and Thiago, early-stage researchers of the department and my coworkers during this period. The experience there has been definitely enriching, and has helped me to improve my research skills, getting me out of my comfort zone.

Special thanks to my PhD colleagues at the University of Zaragoza, for their "intelligent" humour and the coffee breaks where I could find relaxing gaps during my most stressful periods. Their daily support have made my PhD experience way more comfortable.

Muchísimas gracias a mis amigos y a mi equipo de baloncesto (omitiré los nombres de los grupos para mantener la seriedad del documento), por acompañarme y motivarme en esta aventura, y por estar ahí siempre para alegrarme los días (y las noches…).

Por último, dar las gracias a mi familia y en especial a mis padres, Marie Carmen y Miguel Ángel, por su cariño y comprensión y porque siempre me han animado a perseguir mis metas por muy difíciles que fueran. Y por supuesto, a Andrea, por apoyarme incondicionalmente y darme su energía, tanto aquí como a 8000 km de distancia.

Abstract

In recent years, industrial metrology has experienced a drastic change as a result of the development of newly and innovative technologies based on the computational advances in the digitalisation of parts and assemblies. X-ray computed tomography (XCT) is among the most important; this technique, commonly used for medical purposes, has been adapted in metrology for the non-destructive evaluation of parts and assemblies. It is capable of measuring internal features, hidden cavities or even porosity, being able to evaluate macro and micro geometries. However, traceability of XCT measurements remains challenging due to the high number of factors to consider, and standards which regulates it is still in development.

XCT has supposed a significant advance; the quality control requirements of new designs have increased, due to the introduction of complex geometries. In this aspect, one of the main contributors is additive manufacturing (AM). This production technique allows the fabrication of these innovative complex features with a considerably save in material and time. The production improvement is not only limited to shapes, as a wide range of materials are available (mainly polymers and metals, but also ceramics and composites). In conclusion, these two technologies (XCT and AM) are strongly related due to their versatility in their field of application.

In this thesis, the main objective is the development of an evaluation methodology for the analysis of the XCT precision in the evaluation of polymeric additively manufactured parts, through experimental measurements performed in ad hoc designed test objects. After the identification of case studies with most promising research opportunities, separate experiments have been planned. A design-manufacturing-evaluation cycle is generated, adapted for each individual study. Nevertheless, the objective has been to maintain general guidelines in the procedure to be able to extrapolate methods and possible tendencies identified in the results.

Each experiment has provided deeper knowledge in its XCT field of actuation, producing advances in surface roughness characterization of different polymeric AM technologies (chapter 3), attenuation effect on metal-polymer assemblies (chapter 4), accuracy on the evaluation of polymeric lattice structures (chapter 5) and transversally, XCT uncertainty estimation for polymeric AM objects (chapter 6). As a result, further investigation is programmed in all the fields mentioned, with this thesis as a starting point.

Resumen

En los últimos años, la metrología industrial ha experimentado un cambio drástico como resultado del desarrollo de nuevas tecnologías de medición, basadas en los avances en computación y digitalización de piezas. La tomografía computarizada de rayos X (XCT) se encuentra entre los avances más importantes. Esta técnica, anteriormente usada en el ámbito médico, ha sido adaptada para la evaluación metrológica de piezas y ensamblajes de forma no destructiva, ya que es también capaz de evaluar elementos internos, cavidades e incluso porosidades, incluyendo macro y micro geometrías. Sin embargo, la trazabilidad de sus mediciones sigue siendo compleja, debido al alto número de factores para tener en cuenta; por ello, la normativa que la regula sigue en desarrollo.

La XCT ha supuesto un avance significativo; se han incrementado los requisitos de calidad de los productos, ya que es posible generar geometrías más complejas. En este aspecto, la fabricación aditiva (AM) es la principal responsable. Esta tecnología permite la fabricación de estas innovadoras geometrías complejas con un ahorro considerable en material y tiempo. La mejora no sólo se limita a las formas, puesto que se pueden emplear un gran número de materiales (principalmente polímero y metal, pero también cerámica y composites). En conclusión, XCT y AM están estrechamente relacionadas dada su versatilidad.

En esta tesis, el objetivo principal es desarrollar una metodología de medición para el análisis de la precisión de la XCT en piezas de AM polimérica, mediante mediciones experimentales en piezas de test específicamente diseñadas. Después de identificar las principales oportunidades de investigación, se han planeado estudios individuales en los que se ha generado un ciclo diseño-fabricación-evaluación adaptado a cada estudio. No obstante, el objetivo ha sido mantener unas directrices comunes para poder extrapolar los métodos y las tendencias identificadas en los resultados.

Cada experimento ha profundizado en el conocimiento sobre XCT para cada aspecto estudiado, produciendo avances significativos en caracterización de rugosidad superficial en diferentes tecnologías AM (capítulo 3), efecto de la atenuación en ensamblajes metal-polímero (capítulo 4), precisión en la medición de celosías poliméricas (capítulo 5) y de forma transversal, estimación de la incertidumbre en XCT para piezas de AM polimérica (capítulo 6). Como resultado, una serie de investigaciones futuras han sido planeadas, usando esta tesis como punto de partida.

Contents

List of Figures

List of Tables

List of Abbreviations

λc	Long wavelength filter
λs	Short wavelength filter
µm	Micrometres
2D	Two dimensional
3D	Three dimensional
AM	Additive manufacturing
b	Systematic error observed during the evaluation of the measurement uncertainty
BCC	Body-centred cubic
BCCZ	Body-centred cubic with vertical struts
CAD	Computer aided design
CMM	Coordinate measuring machine
DDM	Direct digital manufacturing
E_N	Normalized error
FCC	Face-centred cubic
FDM	Fused deposition modelling
FVM	Focal variation microscope
k	Coverage factor
LOM	Laminated object manufacturing
MJ	Material jetting
mm	Millimetres
PA6.6	Polyamide 6.6
PA12	Polyamide 12
PEEK	Polyether ether ketone
PETG	Polyethylene terephthalate glycol
PLA	Polylactic acid
PP	Polypropylene
POM	Polyoxymethylene
PTFE	Teflon
Ra	Average mean profile height
Ra’	Theoretical average mean profile height
Rku	Profile kurtosis
Rp	Profile mean peak height
Rq	Root mean square profile height
Rsk	Profile skewness
Rv	Profile mean pit depth
Rz	Profile maximum height
RP	Rapid prototyping

Sa	Average mean areal height
SD	Surface determination
SI	International System of Units
Sku	Areal kurtosis
SLA	Stereolithography
SLM	Selective laser melting
SLS	Selective laser sintering
Sp	Areal mean peak height
Sq	Root mean square areal height
Ssk	Areal skewness
Sv	Areal mean pit depth
Sz	Areal maximum height
U	Expanded uncertainty
u_b	Standard uncertainty of measurement of the correction of the systematic error b
u_{cal}	Standard uncertainty of measurement due to the uncertainty of calibration of the calibrated workpiece as stated in the calibration certificate
u_{drift}	Standard uncertainty of measurement due to the change (drift) in workpiece shape since the calibration referred to
u_p	Standard uncertainty of measurement due to the measurement process
u_w	Standard uncertainty of measurement due to variations in materials and production
Ti6Al4V	Titanium-aluminium-vanadium alloy
UV	Ultraviolet
XCT	X-ray computed tomography
Vx	Voxel size in XCT evaluation

1. Introduction

The application of X-ray computed tomography (XCT) in the field of industrial metrology has had a significant impact on the non-destructive evaluation of parts and assemblies. Its ability to characterize not only outer surfaces, but also the inner of the object, allows more complete inspections. XCT is typically based on the acquisition of 2D X-ray images along a complete rotation of the vertical axis of the workpiece, obtaining a 3D reconstruction of the object. It includes the measurement of features (freeform surfaces, lattices, hidden cavities) that are not accessible by traditional metrological devices and methods. Also, with a single XCT scan it is possible to measure macro geometries (diameters, distances between elements, form errors, etc) and micro geometries (surface roughness, porosity, etc).

However, this innovative technology has disadvantages. As XCT is dependent on the X-ray penetration of the part, a correct acquisition is determined by a correct selection of the settings of the X-ray source. Here, several aspects should be considered: object size, material density, thickness of the part, geometries measured, etc. As each part has differences in those characteristics, a generalisation in terms of settings definition becomes extremely difficult, mainly when the conditions are not the most optimal (for example, multi material parts with high differences in radiopacity). This results not only in a need of "case studies" for each specific evaluation, but also in a lack of standards to obtain uncertainty estimations for XCT measurements.

The aim of this thesis is to provide a deeper knowledge of XCT evaluations and uncertainty estimations through experimental results. Based on literature, relevant typologies of parts for industrial application have been studied and ad hoc test objects have been designed to perform the experiments. As a result, a cycle of design-manufacturing-evaluation has been applied to obtain sufficient data to provide guidelines for each specific situation. Studies have been focused on polymeric materials and additive manufacturing (AM); polymers have a different behaviour in XCT characterization in terms of X-ray attenuation (in comparison with metals, more widely studied) and are interesting for industrial purposes (commonly easier and more cost-effective to produce than other materials). On the other hand, AM allow to produce complex geometries that are not possible to manufacture with other technologies.

In this chapter, a summary of the background of the relevant research fields is presented, along with the aim and research objectives of this thesis.

1.1. Background

Since the beginning of mass production in industry, a quality control has been necessary to ensure an optimal accuracy of the products manufactured. This typically includes different tests and protocols performed by specific tools and devices to verify some key characteristics and to prove the correct functionality of the parts. The constant rise of the quality requirements has resulted in the development of a science which regulates the correct calibration and verification of the devices to ensure the accuracy of those measurements: industrial metrology [1,2].

One of the main aspects considered in quality control is the dimensional precision: in any mechanism or assembly, deviations in dimensions or forms in parts may result in bad adjustments, imbalances and other defects that lead to malfunctioning or failures. For simple measurements, this task is done by hand tools such as callipers, goniometers, gauges, etc., that allow a quick evaluation and no extra data processing. However, they are not suitable for more complex inspections or specific measurements which require a high accuracy. For this purpose, specialized devices and machines have been developed along history.

In dimensional metrology, there are two aspects which are highly important to consider when selecting the appropriate measuring device: range of evaluation (maximum distance, area or volume that the device is able to cover) and resolution (minimum feature size measurable). Both properties are inversely related; theoretically, trying to obtain high resolutions for a large area would result in a time-consuming task and a large amount of processing resources would be needed. Consequently, traditional devices are optimized for one purpose: whether the characterization of large areas with an acceptable resolution (macro geometries, geometrical elements with sizes bigger than 1 mm, such as planes, cylinders, spheres and their characteristics) or the evaluation of small areas (so-called micro geometries, including surface roughness and elements smaller than 1 mm) with high resolution.

For the evaluation of macro geometries, instruments as coordinate measuring machines (CMM) and laser trackers are widely used. Both systems use contact tools (probes in CMM, reflectors in laser trackers) to perform measurements on the objects, along with a coordinate system based on the location of single points in a three-dimensional space along 3 main axis: X, Y and Z.

CMMs rely on a structure which moves the probe along the 3 axis to contact the part directly, which is attached to a flat plate; this structure depends on the architecture of the CMM, but in all cases provides enough stability to the probe for high accuracy measurements. Points obtained by the probe are registered as XYZ coordinates in a cartesian system by optical rules and encoders.

Laser trackers use a laser beam which is directed to a reflector located in contact with the object and the position is registered by an interferometer or an absolute distance meter. In contrast to CMMs, laser trackers work in a spherical coordinate system, obtaining the distance and two orthogonal angles by angular encoders. They are capable of large distances evaluation [3] (CMMs are limited by their size and the effective measurement volume); however, due to the possible errors originated in the angular encoders [4], the level of accuracy is much lower than in a CMM.

For the characterisation of micro geometries, several devices have been developed, using contact or optical methods. Although in industry they are commonly used to characterize surface texture and roughness, their capabilities extend to the evaluation of geometric elements with sizes below 1 μm.

In general, those instruments are based on the acquisition of the height of a determined point for the obtention of a single point (confocal microscopes), a profile (laser and contact profilometers) or a surface (focal variation microscopes, FVM). Surface ones are considerably advanced methods for the reconstruction of micro geometries along a 2,5D surface. This technique acquires point data varying the height of a light beam in a defined range, achieving a vertical resolution of nanometres.

Together with the advance of digital technologies and computation, new metrological devices and techniques have appeared. They are able to acquire data from real parts and to reconstruct a 3D digital object, in which is possible to obtain dimensional and GD&T measurements. Laser scanners and photogrammetry are typically used for large scale characterization (buildings, geological excavations), while optical scanners (as a tool for portable measuring arms) are utilized to obtain a 3D point cloud of smaller industrial parts. Here, instruments are limited to the external surface, not being able to inspect inner parts [5].

As a newly developed technology in metrology, X-ray computed tomography (XCT) has become a solution for the non-destructive inspection of parts and assemblies due to its capability of measuring not only the external surface of the object, but also the inner features. This technique has been used for years [6] for medical imaging and internal

inspection of human bodies, and recently has been adapted for high precision measurements in the field of industrial engineering.

XCT is based on the acquisition of 2D X-ray images of the object measured, which is placed in a rotary plate. A detector registers the 360º projections and a reconstruction of the virtual object is done through a specialized algorithm. Here, post processing is required: specific software is used for the data filtering and surface determination, and in some cases for the extraction of metrological data.

As stated before, XCT has the advantage of characterizing both inner and outer elements of the object, being a solution for the inspection of internal defects as porosity. Also, its resolution and range of measurement gives this technology high versatility, allowing to evaluate macro geometries, micro geometries and complex elements as freeform surfaces and lattice structures.

However, several disadvantages are present. XCT relies on the penetration of the object by X-rays, producing a grayscale histogram which varies depending on the attenuation. This parameter is directly related to the density and the atomic number of the material and the thickness of the part. As a consequence, any variation on the geometry of the part could affect the result of the evaluation. Settings typically should be adjusted for each test object, so generalization in the measuring process have become challenging. This have difficulted the uncertainty estimation of XCT devices; currently, standards for the regulation of uncertainty calculations procedure are still in development, and approximations are done for each case.

The continuous improvement of metrological techniques such as XCT is motivated by the development of manufacturing processes, which are capable of producing innovative complex designs with higher quality requirements. Here, additive manufacturing (AM) rises as the most versatile technology in the field of industrial manufacturing. AM started as a new procedure which was able to replicate virtual objects into reality, based on a layer-by-layer process; however, its purpose was only formal prototypes due to poor mechanical and thermal characteristics. The improvement of this properties has led to the usage of AM for final products.

AM concept groups a variety of techniques: fused deposition modelling (FDM), laser powder bed fusion (LPBF), stereolithography (SLA), etc, in which different types of materials could be used depending on the process principle. Most common materials are polymers and metals. For example, in applications with high quality requirements, such as aeronautical, aerospace or precision tooling, AM of metal alloys usage is incrementing

due to their outstanding mechanical and thermal performance. However, the production of metallic AM parts is costly, as devices are expensive and have high technical and environmental requirements. On the other hand, polymeric AM has also high interest in industry as it is more cost-effective for certain applications. Additionally, improved materials as engineering plastics (polyether ether ketone (PEEK), polyethylene terephthalate glycol (PETG)) or fibre-filled reinforced polymers are utilized for end-use applications with quality requirements.

1.2. Research aim and objectives

The main aim of this thesis is the development of an experimental methodology for the analysis of the XCT precision in the evaluation of polymeric additively manufactured parts. For this purpose, several test objects are designed and manufactured, each one adapted specifically for the situation studied. Reference metrological devices are utilized for the calibration of the parts produced, and intercomparisons are done to identify systematic errors. The final goal is to provide deeper understanding of these XCT evaluations, being able to apply the developed process and guidelines to future measurements, improving their traceability and uncertainty estimation procedures.

This goal is subdivided into different research objectives that are developed along the thesis:

i. Review and identification of key aspects. A deep review of the state of the art to identify relevant aspects of both technologies studied: main characteristics of XCT, existing and prospective sources of error, opportunities in AM, material properties, etc.

ii. Analysis of current XCT procedures. Study of the common procedures for the evaluation of industrial parts by means of XCT, as well as uncertainty estimations.

iii. Analysis of the traditional evaluation methods on polymeric AM parts. Application of the common measuring processes in the evaluation of polymeric AM parts to identify systematic errors and trends, using test objects with conventional geometries.

iv. Design of test objects for each case study. With the knowledge obtained, test artifacts are designed, adapted and optimized for its measurement by the relevant reference device and XCT.

v. Development of an evaluation methodology. For each situation identified and planned, a design-manufacturing-evaluation cycle is created in which the test object is evaluated and re-designed or modified if necessary.

vi. Validation of the procedure. Through statistical calculations and uncertainty estimations based on existing standards, verification of the methodology developed is done and systematic trends are registered in guidelines for each specific situation.

1.3. Structure

The structure of the thesis, after this first introductory chapter, follows the next scheme:

- In the second chapter, a state of the art review is presented analysing the two main technologies in which the thesis is based on (X-ray computed tomography and polymeric additive manufacturing). Here, the main research opportunities are described, as well as the interconnection between studies and experiments proposed.
- Third, four, fifth and sixth chapters describe the main work developed in the thesis. In this chapters, it is included the methodology developed for the experiments: details of the design criteria followed for the test objects, the metrological instruments and devices used for the calibration of the artifacts (as well as the calibration procedures), the intercomparison done between results obtained by reference devices and X-ray computed tomography, and the validation of the procedure through uncertainty calculations if applicable.
    - In the third chapter, the work developed concerning the surface characterization and roughness evaluation of polymeric AM parts is presented. Study has been done in two phases: a first stage in which the test objects have been calibrated using a FVM to verify the real roughness values (comparing to the theoretical models), and a second stage in which the final test object has been measured both by XCT and FVM to compare results and evaluate the XCT performance.
    - In the fourth chapter, the investigation about attenuation in XCT evaluation of metal-polymer assemblies is described. The chapter is divided in two different studies, each one independent. In the first one, the effect of the presence of metal in the evaluation of polymeric features is

investigated, with the objective of evaluating the errors caused in dimensional measurements of different geometries and surface texture characterization. In the second one, the concept of relative intensity (I/I_0), which has been stated previously by other authors [7] is introduced and the effect on XCT accuracy of its variation in metal-polymer assemblies is investigated.

- In the fifth chapter, research described is focused on the evaluation of the accuracy of XCT measurements on polymeric lattice structures. The chapter is related to a single experiment, in which the precision of XCT when measuring a realistic lattice structure is presented. An intercomparison with a FVM is done, as this instrument is able to obtain high-quality 3D surfaces. As it has the limitation of the range of evaluation, an experiment is made using a test object adapted for the measurement by both FVM and XCT, simulating a 4 × 4 × 4 cubic lattice.
- In the sixth chapter, investigations concerning XCT uncertainty estimation for polymeric AM objects are described. The objective of the work presented in this chapter is to obtain a precise uncertainty estimation in the evaluation of parts made by polymeric AM. For this purpose, the aim is to define a procedure with a proper AM-based reference standard. This study has been done in parallel with investigations presented in chapters three, four and five, and some elements have been implemented as new knowledge and materials were acquired.

- Seventh chapter groups the closing remarks of the thesis, including the conclusions of the research, the key contributions to the field of study and the future work.
- Eight chapter is a translation to Spanish of the introduction, background, structure of the thesis and objectives planned in first chapter, and conclusions and future work described in seventh chapter.
- Finally, last chapter lists the main scientific production resulting from the thesis, including published papers in indexed and non-indexed journals, conference proceedings and a summary of the research stay at the University of Padova.

In Figure 1.1, a scheme of the organization of the research conducted in this thesis is presented, as explained in Section 2.3.

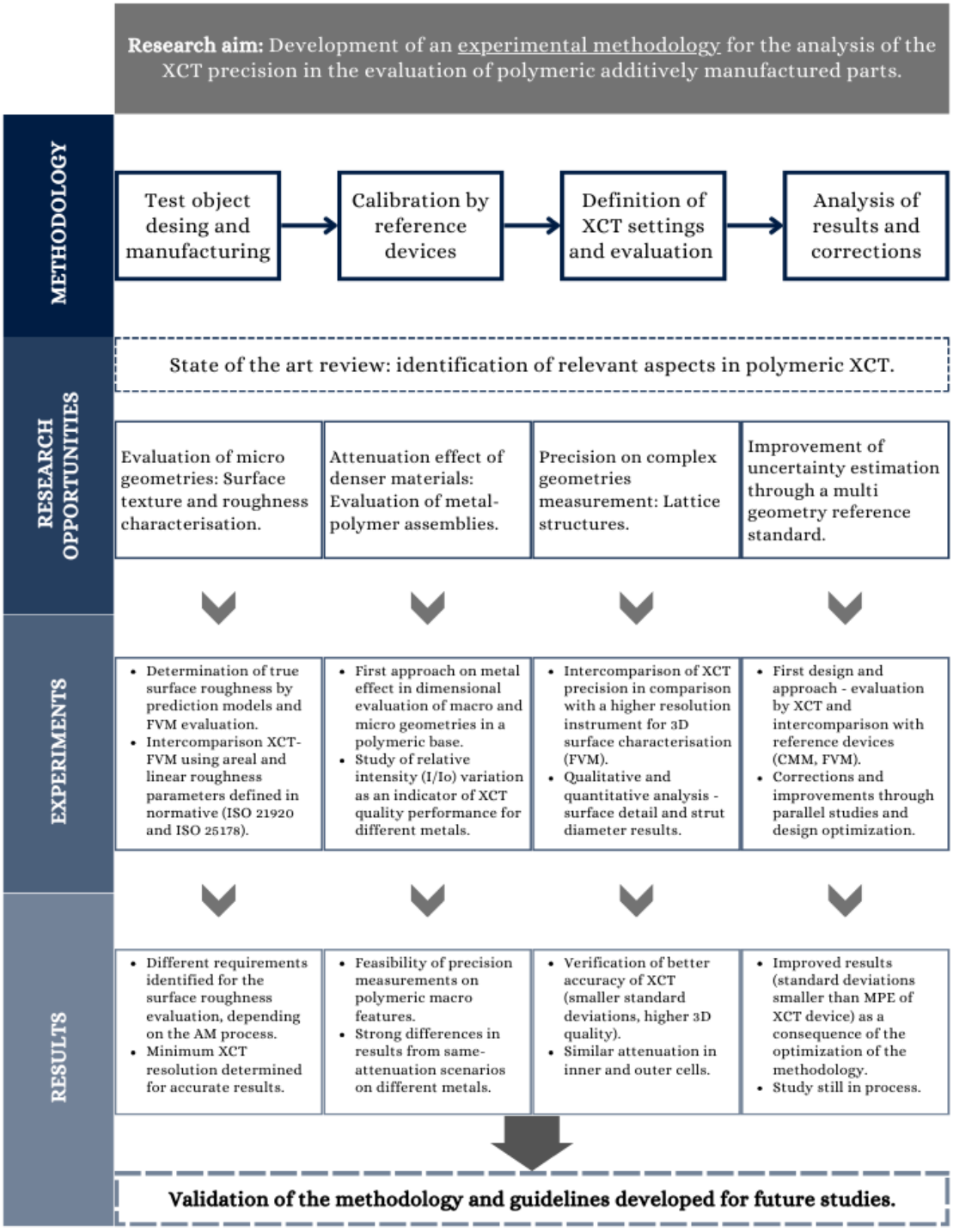

Figure 1.1. Graphic scheme of the research conducted in the thesis.

2. State of the art

A deep review of the literature existing about topics related to the thesis has been done. This section is divided into two subsections, according to the two main technologies utilized for this work: X-ray computed tomography (Section 2.1) and polymeric additive manufacturing (Section 2.2).

2.1. X-ray computed tomography

The discover of X-rays in 1895 by the physicist Wilhelm Conrad Röntgen (Nobel Prize in Physics in 1901) supposed a huge advance in the modern science; however, their implementation in practical 3D applications were not possible till the invention of the first XCT machine, in 1972, by Godfrey Newbold Hounsfield (also Nobel prize winner, in 1979 for Physiology and Medicine). First applications of XCT were purely medical, for the inspection of bones and tissues in human bodies, as it was able to create 2D sections of internal parts; for this reasons, medical community agreed on the importance of the invention of this machines for radiological diagnosis [8].

From here, XCT experimented a continuous development to improve its capacities, which led to an increasing interest from other fields of study [6,9,10]. In particular in industry, as this technology had a potential application for the non-destructive evaluation of parts and assemblies, allowing the inspection of internal defects, fractures or even porosity. This application was able thanks to the development of an algorithm to reconstruct 3D objects from a succession of 2D X-ray images of a rotating object: Feldkamp-Davis-Kress (FDK) algorithm, introduced by L.A. Feldkamp, L.C. Davis, and J.W. Kress in 1984. At this point, 3D volumes were useful for a qualitative analysis; the next step was the adaptation of this technique for its application in metrological quality control.

First measurements were taken in the earlies 1990's, and a focalization on metrology was done around 2005 as the manufacturers started to develop more precise XCT machines for dimensional evaluation purposes. Capacities of XCT devices are in constant improvement (higher resolutions, larger volumes of measurement, better algorithms for error correction), however, there are still challenges to overcome. An important aspect in metrology is the traceability of the measurements, and as a complex technology, the

number of factors and variables to consider is high, which difficult the standardization of uncertainty calculations and standards are still in development.

XCT functioning principle relies on the reconstruction of a 3D volume through the acquisition of a succession of 2D X-ray images of an object along a 360º horizontal rotation. X-ray beams penetrate the object, reaching a detector placed perpendicular to the beam source, generating a grayscale single image in which each pixel has a grey value depending on the beam energy at the detector. A determined number of single images are acquired varying the angle of rotation of the plate; with this projections, a 3D reconstruction is done by a reconstruction algorithm, which correlates each pixel from each image to obtain a single voxel resulting from all the projections. Most common reconstruction algorithm is FDK, as mentioned before.

With this information, a grayscale histogram is formed, in which each voxel has a grey value depending on the attenuation of the beam. Range of the histogram depends on the data codification: most common is 16-bits unsigned integer, resulting in 0-65535 (2^{16}) values (considering 0 – no attenuation and 65535 – maximum attenuation).

After the 3D volume reconstruction, a surface determination process is done to obtain the threshold between material and air, or between two materials with different densities. Here, calculations are done voxel by voxel; for this purpose, several algorithms have been developed, such as ISO50 and local gradient algorithms (Canny, Deriche [11–13]). Result of this process is a 3D object which contains the surface information of the part, and in which metrological evaluations could be performed. In Figure 2.1, a scheme of the complete process of an XCT evaluation is shown.

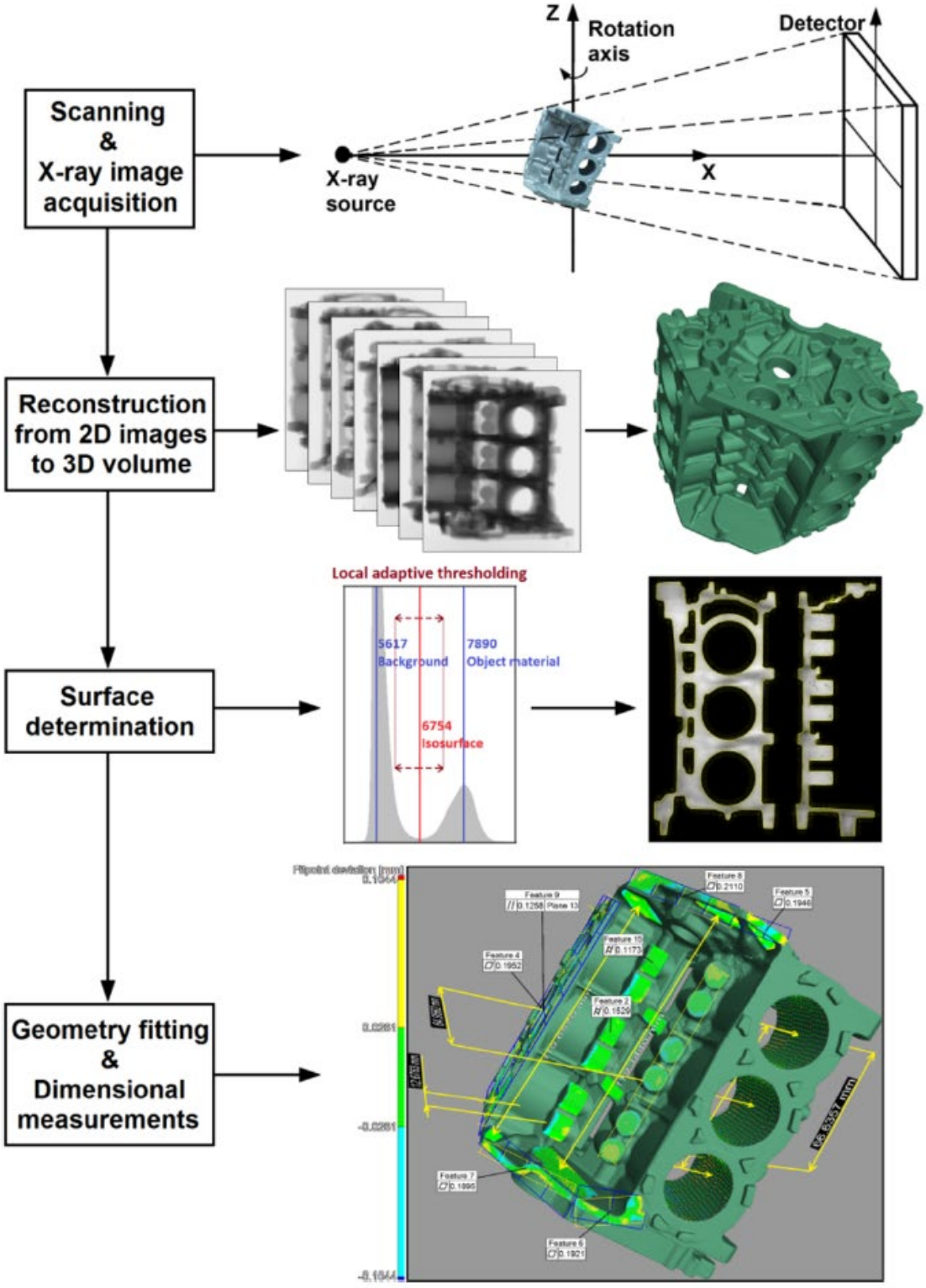

Figure 2.1. XCT process workflow from acquisition to dimensional measurement [6]

During all the process of an XCT evaluation, several factors could affect the measurement and should be considered to avoid or minimize errors. Here, a differentiation depending on the typology of the factors should be done:

- Hardware and environmental factors. XCT devices are machines which have a 3-axis coordinate system to move and locate the workpiece; therefore, geometrical errors in the alignment of the axis must be corrected: typically, this is done with multi-sphere reference parts. A proper calibration of the axis will avoid errors as ring artifacts, caused by the displacement of the vertical axis. Other critical hardware parts are the X-ray source, focal spot and detector, as they are the elements which acquire the volume data: poor filament alignment or non-ideal focal spot size and shape would result in blurred images, while a good magnification is needed for a proper resolution. An important aspect to consider also is the stability of the system, in which temperature plays an important role: controlled temperature of the hardware elements contributes to the repeatability and traceability of the measurements taken, to reduce uncertainties.
- Workpiece and device settings. Measurement of each part or assembly needs an adjustment of the X-ray settings to obtain a proper evaluation, selecting an appropriate voltage for controlling the X-ray penetration, current and integration time to control the brightness and including in some cases a physical pre-filter (typically, copper or aluminium sheets with variable thickness) to eliminate low-energy beams. This is particularly important for high-density materials as metals, in which distortions, artifacts and beam hardening (overemphasis on grey values on the edges of the workpiece) could occur. Number of projections should be enough to obtain an adequate resolution, but an elevated number will increase considerably the evaluation time. Placement and orientation of the workpiece in the coordinate system is also relevant, to obtain a proper magnification and avoid distortions derived from high thickness areas or symmetries.
- Data processing. Reconstruction of the 3D volume from 2D projections is done through FDK algorithm and, in some cases, a filter is applied right after to reduce noise and image blurring. Those filters sometimes could cause a loss of information or reconstruction artifacts, such as beam hardening or streaks caused by the edges of the part. Also, surface determination methods are strongly dependant on the noise of the XCT evaluation, and the real threshold air-material or between materials could

be diffuse and cause higher uncertainties in the measurements. For those data-related errors, correction methods are typically applied, as beam hardening correction and noise reduction filters.

An extended explanation of the factors affecting the XCT evaluation along with a detailed analysis of each one can be found in [14].

2.1.1. Surface roughness characterization

Dimensional measurements are typically divided into two separate categories according to the size of the feature evaluated: macro geometries (geometrical elements such as cylinders, spheres, planes and their dimensions, form error and distances, with dimensions greater than 1 mm) and micro geometries (elements with micrometrical dimensions). In this last category is included the characterization of surface roughness, which in manufacturing industry has a high relevance.

High precision parts require good surface finishing with low roughness in certain functional areas, which as a consequence is more costly. Therefore, an adequate surface quality control is needed to comply with the requirements. Contact and non-contact methods for roughness evaluation are widely used for this purpose [15,16], highlighting profilometers (which extract linear profiles through a contact probe) and focal variation microscopes (FVM, which obtains a 2,5D surface using variation of the contrast of each pixel in each vertical position). These instruments are specialized in the measurement of micro geometries with high resolution, up to nanometres; however, their range of evaluation is limited.

Here, XCT provides the opportunity for the evaluation of surface roughness of bigger areas with an acceptable resolution, along with the capacity of characterizing internal surfaces which are inaccessible for other devices. Nevertheless, this surface evaluation is directly linked to the geometrical magnification of the XCT measurement: higher resolutions could be obtained for bigger magnifications, reducing the scanned area. In other words, capacity of XCT will still be limited by the part size. Several experiments have been made to study factors affecting the surface measurements by XCT [17–19], as well as the influence of surface roughness in dimensional XCT measurements [20].

Numerically, surface roughness is evaluated by roughness parameters, which are defined in standard ISO 21920-2:2021 [21] for profile measurements and ISO 25178-2:2011 [22] for areal characterization. According to this standard, parameters could be classified into height, spatial, hybrid and material ratio parameters. Commonly used

parameters are employed to represent mean values (such as Ra, Rq, Sa, Sq), total values (such as Rz, Rp, Rv, Sz, Sp, Sv) and profile or surface form (such as Rsk, Rku, Ssk, Sku).

Prior to the calculation of roughness parameters, filtering is applied to the profile or surface to eliminate the form of the object and wave components present in primary profiles/surfaces which does not belong to the roughness itself [23]. As roughness is within a band of wavelengths, two filters are applied: a long wavelength filter (λ_c) for low frequency waves, and short wavelength filter (λ_s), for high frequency waves. Complete procedure for roughness measurement and filter selection is described in ISO 21920-3:2023 [24] for linear parameters and in ISO 25178-3:2012 [25] for areal parameters.

Roughness evaluation is an important part in metrological evaluation of AM parts [26–36], as their surface quality is typically poorer than conventional manufacturing methods due to its intrinsic properties. The layer-by-layer process of this technologies creates a stepped-stair effect (Figure 2.2) which has been studied, and it is possible to predict theoretical roughness parameters by mathematical models [37,38]. Also, as AM process produce exclusive elements (re-entrant features), new definition of parameters have been necessary to completely characterize AM surfaces [39].

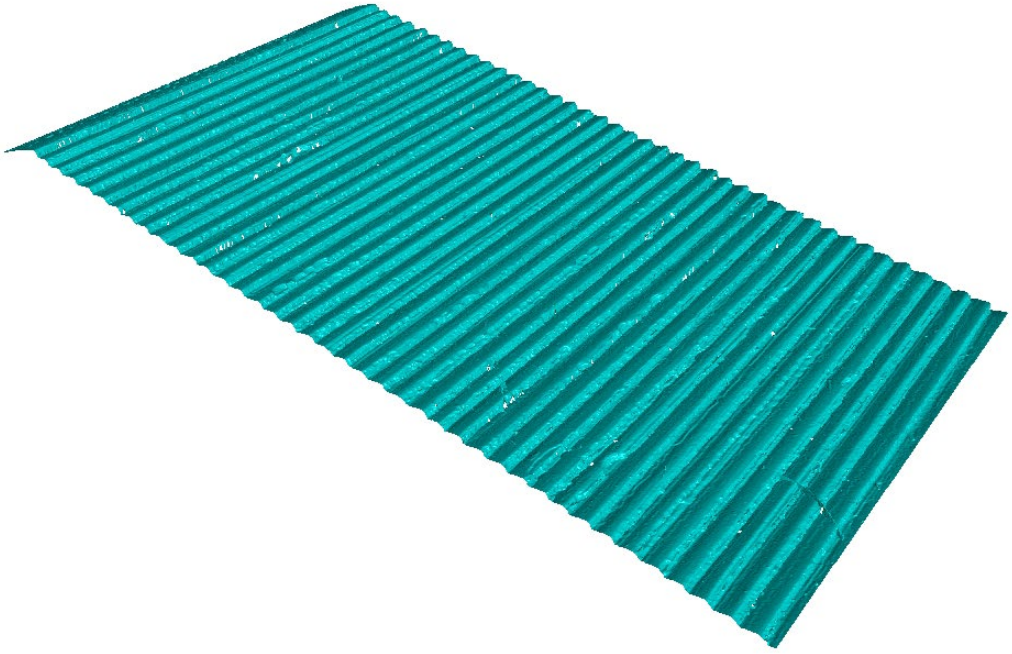

Figure 2.2. Stepped-stair effect observed in an XCT reconstruction of an inclined AM ramp.

XCT evaluation of AM surfaces has been widely investigated [40–42], due to its interest in the measurement of non-accessible surfaces and complex geometries. Studies have been done for the evaluation of the effect of geometrical magnification [43], to

provide guidelines to obtain traceability [44] or also to apply the procedures for non-planar surfaces in lattice structures [45,46].

2.1.2. Challenges in multi material assemblies

In industry, most of the parts and assemblies used in final products include more than one material. The objective is to improve product characteristics according to the design requirements, as each single material has different properties (mechanical, thermal, electrical, etc). In most industrial fields, combinations such as metal alloys (e.g. titanium-aluminium-vanadium alloy, Ti6Al4V), multi-metal assemblies (aluminium-steel, titanium-steel, etc), metal-polymer, polymer-polymer or ceramic-polymer are widely used.

In some cases, the inspection of assemblies to detect failures or defects require non-destructive methods. Here, XCT is capable of the characterization of internal parts, being able to perform quantitative analysis providing dimensional measurements of the elements. As stated before, XCT obtains a reconstruction of the object creating a grayscale histogram, in which each value depends on the attenuation of the X-ray through each voxel registered by the detector.

This attenuation relies on two main aspects: i) thickness penetrated by the beam and ii) attenuation coefficient, which is directly related to the density of the material [7]. XCT settings (voltage, current, physical filter, integration time, etc) are adjusted considering this attenuation and adapted to the material of the part [47,48]; however, for multi-material assemblies, this procedure could be challenging. This is more problematic in cases with considerable differences in density, as two situations are commonly observed:

- If settings are adjusted for a high-density material, beams will penetrate low-density parts without a significant loss of energy and therefore the sensibility of the XCT for the identification of less dense materials will be lower, even in worst cases not being possible to differentiate them from air.
- If settings are adjusted for a low-density material, beams will not have enough energy to penetrate denser parts, and the increase of artifacts will cause deformations in the reconstructed volume (Figure 2.3).

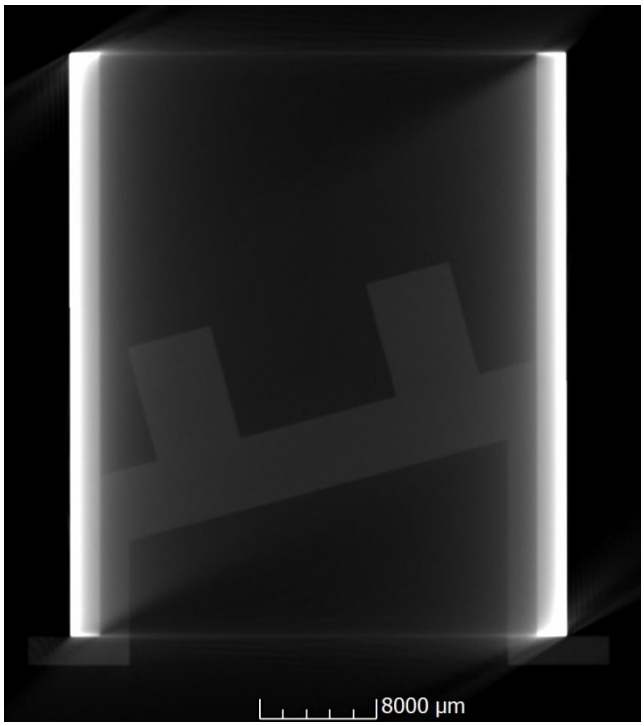

Figure 2.3. 2D slice of a simulated XCT evaluation of a metal-polymer assembly

Several studies have been conducted to try to optimize the measurement of multi material assemblies [49,50]. Two critical aspects that were identified are the surface determination [51] and the thickness of the outer material layer, especially when the denser material is on the outside [52,53]. Image artifacts generated by denser material combined with the contrast between materials could difficult the correct boundary location during surface determination in some cases, creating areas with high surface defects and deforming the resulting volume, therefore affecting the accuracy of XCT dimensional measurements [13,54]. Surface extraction methods for multi material assemblies have been studied for years [55,56], including common XCT surface algorithms such as Threshold, Canny and Deriche [57]. Correction of typical errors found in XCT measurements is also investigated and applied in multi material parts, such as beam hardening [58].

Although the difficulties in the XCT evaluation of multi material assemblies are clear, traceability of these measurements has been an objective for recent studies. Borges de Oliveira et al. [59] designed an experiment with low and high absorption materials using the length measurement error test (E-test) and probing error test (P-test) adapted for XCT in standards [60]. Apart from common material combinations (metal-metal, metal-polymer), XCT evaluation of composites [61,62] and fibre-reinforced polymers [63] have also been investigated.

2.1.3. Complex geometries: freeform surfaces, lattice structures

The development of new manufacturing methods (e.g. AM) has allowed industrial companies to improve the design of their products with the introduction of innovative complex geometries, such as freeform and organic elements, which optimize their characteristics and performance. Those improvements have a positive impact in the production, in which manufacturing time and cost are reducing significantly. However, as complexity of the parts increases, their evaluation becomes more difficult and for traditional measuring devices it is challenging to perform an accurate dimensional quality control.

A good example of complex geometries are lattice structures (Figure 2.4). The objective with the introduction of these features is to replace solid areas of an object maintaining similar or improved mechanical characteristics, with a significant material saving. Lattice structures are compound normally by a series of cells with a determined geometry [64], and although some traditional manufacturing processes may be able to produce them, AM is more optimal and more widely used for this purpose [65].

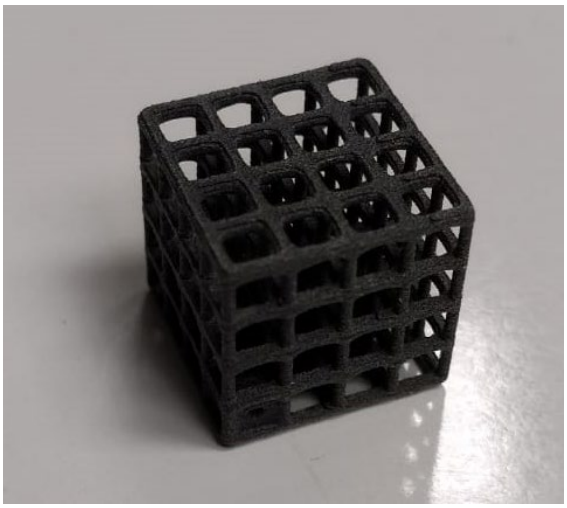

Figure 2.4. 4x4x4 cubic lattice structure.

In terms of dimensional evaluation, main challenge for traditional devices is the accessibility: normally, both tactile (such as CMMs) and optical methods (optical microscopes, laser scanners) are only able to measure the outer cells of the lattice. Here, XCT, as it is capable of the characterization of internal and external features, is the most optimal technique for the inspection of the whole structure.

With this metrological framework, obtaining traceability of the XCT measurements of lattice structures remain as a challenge. The use of an adapted reference standard to obtain task specific uncertainty calculations in a lattice structure is studied in [66], using the substitution method described in VDI/VDE 2630-2.1 [67]. Zanini et al. [68] investigated the application of two different uncertainty calculation methods: substitution method and multiple measurements approach [69,70], using a specific reference standard composed of vertical struts.

Other factors have been investigated, such as the concept of theoretical supplemental surface [71] for the verification of the external part of the lattice, or the effect of magnification in the XCT accuracy [72]. Defects in the lattice and porosity have also been widely studied [35,73–84]. Intercomparisons have been done between XCT and reference devices as CMM [85] for the measurement of outer cells or FVM [46] to replicate the surface texture of outer struts. Single strut measurements has been also considered for a general characterization of the complete part [86], in which orientation of the strut is evaluated as a parameter.

2.1.4. Uncertainty calculations

In metrology, obtaining traceability of the measurements performed is a key aspect to ensure the repeatability and reproducibility of the results. From the standard metre used by the International System of Units (SI), there should be an uninterrupted chain of calibrations (through calibrated reference standards and calibration procedures) to every measuring instrument to be able to estimate the uncertainty of the measurements taken.

Verification procedures are commonly performed following the recommendations registered in the standards. Most widely used sequences are length measuring error test (E-test) and probing error test (P-test) described in standard series ISO 10360 [87–89]; both procedures are based on the evaluation of predefined points on a test artifact to obtain repeatability in the measurements (unidirectional and bidirectional distances in E-test, sphere diameter in P-test). Verification procedures and performance tests have also been specifically adapted for XCT and described in standard ASME B89.4.23 [90].

In complex measuring systems, it is challenging to obtain a single measure which could provide the uncertainty for all possible measurements; therefore, uncertainty estimation is usually registered in “task-specific” guidelines. For example, standard ISO 15530-3:2011 [91] is adapted for CMMs, describing the procedure for the definition and estimation of factors affecting the uncertainty of these machines. This method is called

substitution method, and it requires a calibrated workpiece. Calculations used for the estimation of the expanded uncertainty U are shown in Eq. 1:

$$U = k * \sqrt{u_{cal}^2 + u_p^2 + u_w^2 + u_b^2} \quad (1)$$

where k is the coverage factor (k=2 for a level of confidence of approximately 95%), u_{cal} is the standard uncertainty of measurement due to the uncertainty of calibration of the calibrated workpiece as stated in the calibration certificate, u_p is the standard uncertainty of measurement due to the measurement process, (standard deviation of the repeated measurements), u_w is the standard uncertainty of measurement due to variations in materials and production (due to variations in, e.g., coefficient of expansion, form errors, roughness, elasticity and plasticity), and u_b is standard uncertainty of measurement of the correction of the systematic error b.

In XCT, variables and factors which affect measurements are more difficult to model, and therefore uncertainty calculations become more complex [14,44,66,92–97]. Consequently, a completely defined standard is still not available for XCT; here, an adaptation of the substitution method is done in directive VDI/VDE 2630-2.1 [67]. Following the same equation, VDI/VDE 2630-2.1 recommends an addition of parameter u_{drift}, which is the standard uncertainty of measurement due to the change (drift) in workpiece shape since the calibration referred to. The equation (Eq. 2), thus, will remain as following for XCT measurements:

$$U_{XCT} = k * \sqrt{u_{cal}^2 + u_p^2 + u_w^2 + u_b^2 + u_{drift}^2} \quad (2)$$

In addition, for the evaluation of the measurement compatibility between XCT and reference measurements, the E_N parameter is commonly calculated according to standard ISO/IEC 17043:2023 [98] following Eq. 3:

$$E_N = \frac{|y_{XCT} - y_{REF}|}{\sqrt{U_{XCT}^2 + U_{REF}^2}} \quad (3)$$

Where y_{XCT} = current measured value of the feature, y_{REF} = reference value of the feature, U_{XCT} = expanded uncertainty of the XCT measurement and U_{REF} = expanded uncertainty of reference value. Results are considered valid for $E_N \leq 1$ as stated in the standards.

In substitution method, it is necessary to use a calibrated workpiece which should have similar characteristics as the measured part, in terms of geometry, material and scale, to obtain the most realistic results possible. For this reason, studies that aim to improve the uncertainty estimation for XCT measurements are based on the development of specific reference standards with ad hoc designed geometries. In Table 2.1, a summary of test objects designed commonly used for this purpose is presented.

Table 2.1. Examples of reference standards used for XCT evaluation.

Reference Standard	**Geometries**	**Size**	**Material**	**Research group**
CT Tetrahedron	Spheres	Ø = 3; 4; 5 mm	Ruby	University of Padua, Italy [99]
	Cylindrical bars	Ø = 2 mm L = 25 mm	Carbon fibre	
	Framework	Not specified	Carbon fibre	
Dog bone	Bone shape	L = 11,8 mm W = 1,5; 3 mm T = 1 mm	POM	Denmark Technical University (DTU) [100]
Steps	Cylinders	$Ø_e$ = 40; 60; 80; 120; 160; 200; 220 mm $Ø_i$ = 20 mm	Aluminium	Swiss Federal Laboratories for Materials Science and Technology (EMPA) [101]
Silicon sheets cube	Sheets	4 × 4 × 1 mm^3	Silicon	University of North Carolina at Charlotte (UNCC) [102]
	Block	6 × 6 × 4 mm^3	Glass	
NIST Standard	Various geometries on a squared base of 40 × 40 mm^2		ABS	National Institute of Standards and Technology (NIST) [103]

* Ø = Diameter; $Ø_e$ = External diameter Ø; $Ø_i$ = Internal diameter Ø; L = Length; W = Width; T = Thickness; H = Height

Reference standards are typically designed for a concrete function, in which one type of geometry is included. Evaluation of macro geometries with basic shapes as cylinders, spheres or planes [99–101,103] ensure solid information of diameters, distances and form errors. In [102], the measurement of micro geometries is investigated, in a test object which includes coverings to convert the elements in hidden features. For the manufacturing of the parts, high quality materials provide low dilatation coefficient to avoid distortions caused by temperature and humidity; additionally, standards recommends the usage of reference standards as similar to the part evaluated as possible, including the material. It becomes more critical in XCT measurements.

2.2. Polymeric additive manufacturing

The design of industrial products has been always limited by the geometrical restrictions of the manufacturing process in which parts are produced. In this terms, the development of additive manufacturing (AM) has allowed the evolution of industrial products, including new designs with complex features which improve the characteristics of the object and reduces cost in the manufacturing process.

AM is a manufacturing technology based on the addition of material layer by layer, creating a 3D object from a virtual 3D file. AM is a concept which group several techniques, whose characteristics depend on the manufacturing principle and the material used. The application of AM technologies to the production of end-use products has transformed the manufacturing industry and the way of a product is conceptualized for both customers and providers.

2.2.1. From formal prototypes to end-use products

AM has originally been referred to as rapid prototyping (RP), and popularly as 3D printing [104]. These terms were usually employed to describe a process which aimed to create objects in a short period of time with the objective of representing a part before the commercial release of the final product [105]. Therefore, first design and conceptualization of AM technologies was focused on the quick production of formal representations, without considering functional aspects.

Basic principle of AM is the translation of a 3D CAD model, whether manually designed or extracted from a 3D measurement (scanning, XCT evaluation, etc), into a real object with the maximum simplification of the production process. In AM, there is not a need for planification of the manufacturing, as no additional tools are needed than the 3D printing device, the 3D CAD model and the printing instructions given directly to the machine. The process is done by the addition of material layers extracted from the CAD data; thickness of the layers depend on the physical limit of the AM technology used and the settings configured in the code. Here, no additional operator in-process actuation is needed but the configuration of the process settings prior to the production, and a post process of the part in case it is needed. The final objective of AM is to reduce process to the minimum expression.

The development of AM technologies is supported by various other technological evolutions which are directly related with this manufacturing technique. First, is the

continuous progress in computing capabilities: advances in processing power and graphics capability have led to a higher control of the manufacturing settings, allowing the monitoring of the process obtaining useful data for the improvement of future prints [106,107]. The creation of CAD models is another key aspect, as they are the base data for the prototyping. New CAD creation tools have allowed new complex features [65,108] and models which help designers to improve their products and simplify the printing process. Also, optimization of CAD formats (e.g. Standard Tessellation Language (STL) files) facilitates the interpretation of the geometries by the printing machine, decreasing the processing time. The improvement of material properties [109–112], being able to introduce fibre-reinforced and composites [113–118] and the development of specific configurations for 3D printing (filament, powder, liquid resin, material sheets) have also helped in the increase of the final products mechanical and thermal characteristics, being manufactured as end-use products and not only formal prototypes. Although this work is focused on polymeric AM, it is worth mentioning the huge evolution that has been the introduction of metal AM [119,120] for high-quality part production.

In conclusion, all developments in AM technologies aims the evolution of rapid prototyping (RP) into direct digital manufacturing (DDM).

2.2.2. Versatility and design freedom

In comparison to traditional manufacturing technologies (as machining, casting, etc), one of the most important improvements of AM is the new design possibilities offered for the parts produced. General information about AM technologies is found in standard ISO/ASTM 52900:2021 [121] Several AM processes have been developed based on different techniques for the addition of material, each one obtaining objects with diverse characteristics, finishes and material types:

- Liquid polymerization. Liquid resins are used in stereolithography (SLA) AM machines in a process called photopolymerization, in which the polymeric material is solidify by a laser beam forming the final part. Most of SLA parts need to be cured in an ultraviolet (UV) oven to improve mechanical and thermal properties; however, the characteristics of SLA printed objects are poor in terms of strength and durability comparing to other AM processes. Main advantages of this AM method is the part accuracy and surface finish; additionally, it is possible to produce flexible parts.

- Powder bed fusion. In this category, base material is used in form of micrometric particles with sizes around 50 μm which are fused using thermal sources. Most common technologies are selective laser sintering (SLS) for polymers and selective laser melting (SLM) for metals, in which power source used is a laser beam. Similarly, in electron beam melting (EBM), a high-energy electron beam is used to fuse the particles instead of a laser. Powder bed fusion (PBF) processes are able to process a wide variety of materials due to their nature, such as polymers, metals and even ceramics, and in contrast to other AM techniques, there is no need for support structures in polymer PBF as powder itself acts as a support (in metals, thermal residual stresses make support structures desirable for good printing results). Most of the powder remains not used in each print but is normally recycled for later batches with no performance loss. There is an improvement in mechanical and thermal characteristics in PBF produced parts; however, the dimensional precision and finishing is poorer than liquid-based AM and the manufacturing process is more time-consuming, as an additional post-processing is needed.
- Material extrusion. Material here is found in an initial solid state; it is fused by a thermal source and pushed through a nozzle by pressure, depositing layers of the melted material in a heated bed. Flow of material remains constant while a solid layer is being built, but this machines have the ability of stopping the process when a layer is finished. Material extrusion (MEX), similar to polymer extrusion, is also called fused deposition modelling (FDM) and is one of the first AM developments and also the first approach to low-cost and user-friendly 3D printing. Main advantages of MEX/FDM are the lower cost of the parts produced and the manufacturing time, as it requires no prior preparation and few post-processing (removing of support structures or improving surface finish). Material versatility is high, mainly in thermoplastic polymers; new developments in materials and nozzles allow to print with material-filled filaments, such as fibre-reinforced, metals or wood. However, their mechanical characteristics are poor, mainly in the vertical axis, as parts produced are not isotropic. Also, surface finishes are normally rough derived from the stepped-stair effect from the layer thickness.

- Material jetting. Similar to 2D traditional printers, material jetting (MJ) is based on the deposition of droplets of material by a printing head which are photopolymerized and cured into a solid object by an UV light. MJ printing devices are able to produce very thin layers (up to 16 μm), with high speed processing, no need of support structures and high versatility (possibility of multiple material and printing colours). MJ process is low-cost in comparison to other AM techniques such as PBF; however, the accuracy of the parts is worse, and the variety of materials is limited to photopolymerizable resins.
- Material adhesion. Laminated Object Manufacturing (LOM) is one of the first commercialized AM techniques, and it consists in layer-by-layer lamination and cutting of material sheets, which are glued together by a specialized adhesive. A variety of materials could be used in sheet lamination AM, including wood, metal, cork and plastic; butcher paper was the original material used in the original LOM process. Most recent and used adaptation of material adhesion AM is ultrasonic additive manufacturing (UAM), in which a combination of sheet lamination, ultrasonic metal seam welding and computer numerical control (CNC) milling. Parts here are built from bottom to top, trimming each layer of metal foils using CNC milling. This process has the disadvantage of randomly distributed voids, which give UAM parts highly anisotropic properties.

This variety of AM techniques have been studied for the identification of design opportunities and limitations [122–125]. Material itself is one of the main aspects to consider [126–128], and the monitoring of key parameters as density [129], environment humidity [130] and temperature [131] during the manufacturing process. Metrological approaches [132–134] have been done also, to estimate a better traceability on the measurement of complex AM geometries. To test the performance of AM devices, standard ISO/ASTM 52902 [135] has been developed, in which general principles for producing test artefacts are described.

2.3. Outcomes

The review of the state of the art regarding XCT and AM has served to obtain essential knowledge about both fields of study of this thesis, allowing to identify research opportunities and to define experiments in those areas.

Investigation planned for this thesis has been divided into four interconnected groups. The main objective is to develop a methodology for the optimal evaluation of polymeric AM parts by XCT, thus although experiments for each group of investigation are adapted for the characteristics evaluated, the intention is to modify the less possible the design, manufacturing and measurement process to provide solid guidelines which could be applied to generic inspections.

In the state of the art review, it has been detected that, in general, uncertainty estimation of XCT measurements is still in development, although there is currently some directives and methods [67,68,91] which describe procedures for this purpose. From an experimental point of view, the most important aspect is the suggestion of the usage of reference parts for the calibration as similar as the product, in terms of geometries, size and materials. Considering this requirement, it is reasonable to design a specific calibrated test object manufactured in polymers by AM if the purpose is to determine the uncertainties of measurements in polymeric AM parts.

An initial idea has been to create a series of experiments in which sufficiently solid dimensional measurements could be extracted from the evaluation by XCT of a test object, which should include as many representative geometries as possible. However, it has been detected that for certain cases there is few knowledge:

- Procedures for the characterisation of polymeric AM surface texture and roughness are not entirely defined, as each manufacturing method has its own surface finish and guidelines are typically generic, not considering particularities.
- Determination of the precision on the evaluation of complex geometries (such as lattice structures) is challenging, as there is not an optimal reference device for the calibration of the test parts.
- The effect of the inclusion of elements made by more dimensionally stable materials (as reference features, or for higher accurate measurements) in the tomographies is not evaluated. For this case, metals are commonly used.

Therefore, in parallel to the experiment regarding general estimation of XCT uncertainties in the measurement of polymeric AM parts, these 3 aspects are studied to solve the present problems, increase the knowledge on the topic and apply it on the multi geometry test object. As stated before, the objective is to develop a common methodology

for the design, manufacturing and evaluation of test parts, aiming to maintain similar guidelines for all the experiments.

Considering this, the four groups in which the investigation is divided, in the following order, are: surface texture and roughness characterisation, metal-polymer assemblies, lattice structures and, transversally, improvement of uncertainty estimation.

3. Surface characterization in polymer-based AM

Evaluation of micro geometries has been challenging for XCT due to the resolution limitations compared to other metrological devices which are specifically used for this purpose. This field has an interest in industry, mainly in the quality control of surface roughness of the parts and plays an important role in AM parts as their manufacturing technique create particularly rough surfaces due to the layer-by-layer process.

The aim here is to create a series of experiments for the evaluation of the surface roughness of parts made by different polymeric AM technologies – FDM, Polyjet and SLS have been selected, as they are commonly used in polymeric AM part production and their manufacturing principle and, therefore, their surface finish is different. For this purpose, theoretical models [37,38] are used to create a range of test objects with different theoretical surface roughness values. This investigation is focused on polymers: even though studies have been done for surface characterization of metallic AM parts [27,40,43], conclusions from experiments on one material cannot be extrapolated to other materials, as XCT settings must be adjusted.

Study has been done in two phases: a first stage in which the test objects have been calibrated to verify the real roughness values comparing to the theoretical models, using a focal variation microscope as the reference device for the measurements, and a second stage in which the final test object has been measured both by XCT and FVM to compare results and evaluate the XCT performance. Results of these studies are published in two articles: “Surface Characterisation and Comparison of Polymeric Additive Manufacturing Features for an XCT Test Object” [136], which details the first stage of the experiment, and “X-Ray Computed Tomography performance in metrological evaluation and characterisation of polymeric additive manufactured surfaces” [137], which describes the second stage. Therefore, this chapter is divided according to the organization of the two articles, and their content is included in the different subsections. As both articles describe a linear process in which results of the first stage are used for the final second stage, discussion and conclusions are focused on the outputs obtained in the second stage.

3.1. Methodology

In this section, methodology followed to conduct the experiment is described, including theoretical calculations for surface roughness prediction, details of the design and manufacturing process of the test objects, the procedure used for the measurement of

the parts, the areal and linear roughness parameters utilized and the data acquisition and filtering.

3.1.1. Theoretical calculations

First step of the experiment process has been to apply two different predictive models, which based on printing parameters are able to estimate the theoretical average roughness (Ra) of the surface of the part produced.

First predictive model used as a reference for the study has been Ahn model, described in [37]. Its aim is to estimate the theoretical average roughness (Ra') created by inclined ramps on AM parts. Principle of Ahn model is shown in Figure 3.1 and the calculations are based on Eq. 4:

$$Ra' = \frac{1000t}{2}\left|\frac{\cos((90-\theta)-\emptyset)}{\cos\emptyset}\right| \quad (4)$$

Where t is the layer thickness, θ is the angle of inclination of the ramp (from the vertical), and Ø is the angle deviation of the vertical walls. Considering Ø = 0 for a theoretical and, thus, ideal scenario, the two main parameters are layer thickness and angle of inclination, which is possible to control through the design of the test object and the adjustment of process parameters. With this theoretical knowledge, the aim of this experiment has been to create a range of surfaces with smoother (lower Ra') and rougher (higher Ra') features, with values measurable by XCT according to the voxel size obtained (which determines the resolution).

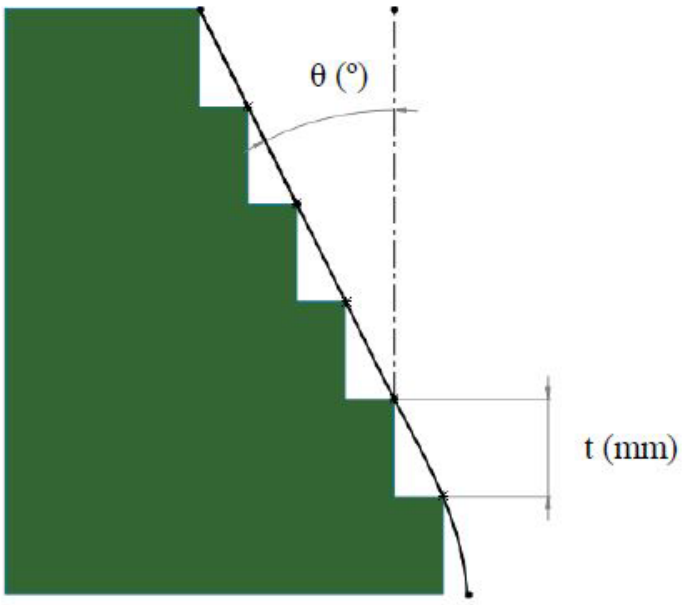

Figure 3.1. Representation of layer-by-layer process occurred in AM and parameters used in Ahn model.

Ahn model is able to estimate average roughness with an acceptable accuracy with an easy practical application, as configuring only two parameters it is possible to obtain a

prediction. As displayed in the image, steps are considered ideal and therefore with straight faces forming perfect 90º angles; however, even considering perfect geometries, AM technologies create rounded shapes in the manufacturing process: for example, in FDM parts, extrusion of the filament would rather produce cylindrical struts. In Figure 3.2, a representation of the ideal filament disposition against the geometries used in Ahn model predictions is shown.

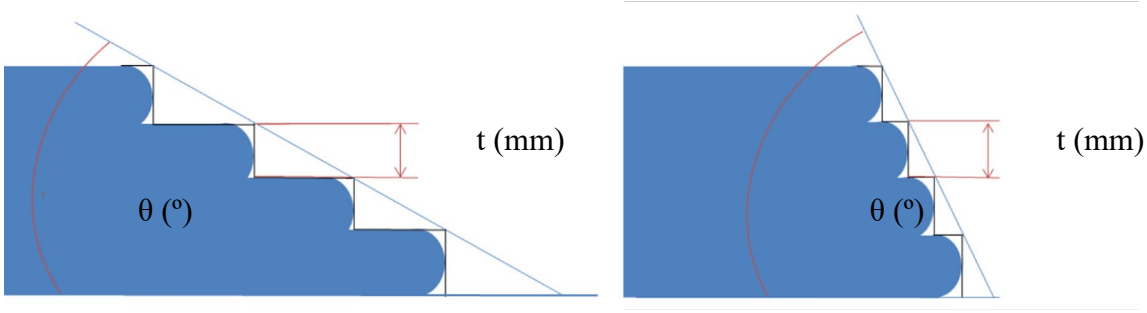

Figure 3.2. Ahn model straight stairs and rounded stairs representation.

Considering this geometrical difference, a second predictive model developed by Buj-Corral et al. [38] is used. Their objective was to obtain more accurate roughness estimations for FDM parts, creating a more realistic model in terms of geometry, taking into consideration the roundness of the deposited filaments. In this method, two consecutive filaments are considered for roughness evaluation. A cross section of the profile obtained is shown in Figure 3.3.

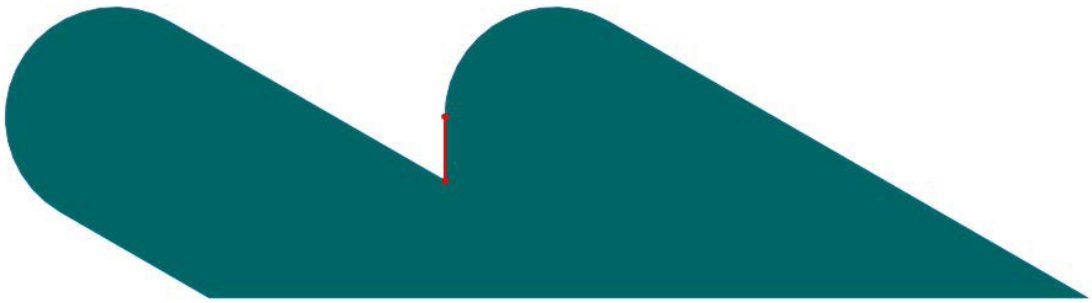

Figure 3.3. Cross-section of an FDM external profile, based on [38]

Here, a vertical red line is added in order to avoid negative values in the roughness theoretical calculations, as the procedure for the theoretical average roughness parameter (Ra') is based on the effective area divided by the profile length. Calculations are defined in Eq. 5:

$$Ra' = \frac{1}{L}\int_0^L |f(x)|\,dx \tag{5}$$

Where L is the horizontal length and f(x) is the function determined by the profile of the surface. In Figure 3.4, an approximation model in CAD is shown, used as a reference for the calculations:

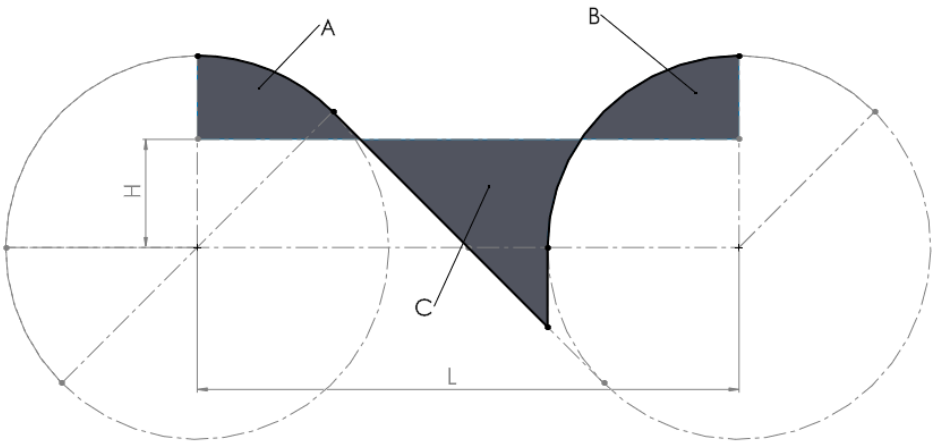

Figure 3.4. CAD representation of the model, used for calculations.

Here, inclined line corresponds to angle of inclination of the surface, radius of the circles is equal to layer thickness and height of the horizontal line is calculated in order to obtain an equal area above (marked as A and B) and below (marked as C) it in the grey areas. Effective profile used for the representation of the function (f(x)) is highlighted in black, while L is the horizontal length.

Both models are optimized for the roughness estimation of FDM parts; however, as the layer-by-layer principle is common to Polyjet and SLS process, the calculations have served also for the design of test objects made by these technologies.

3.1.2. Test object design and manufacturing

First stage of the experiment has consisted in the verification of real surface roughness values according to the predicted values calculated. For this purpose, several individual test parts have been designed.

As stated before, three AM technologies have been selected for the manufacturing of the test objects: FDM, Polyjet and SLS, as they present different surface finishes and are commonly used in industry for polymeric AM production. Materials chosen are polylactic acid (PLA) in FDM, a special polypropylene-like resin (Rigur RGD450) in Polyjet and polyamide 12 (PA12) in SLS. Parameters used for the design of the parts have been layer thickness (0.1 – 0.2 mm) and angle of inclination (30º – 45º – 60º – 75º). Polyjet 3D printer nominal layer thickness is between 16 – 48 µm, which creates surfaces with very low roughness (theoretical Ra around 1-2 µm according to calculations made by

theoretical models) which are out of the minimum measuring resolution of XCT measurements. Therefore, an approximation has been made with artificial steps of 0.098 mm and 0.196 mm in the object ramps, multiples of nominal layer thickness and similar values to the other AM technologies, with the objective of achieving comparable results with the rest of the parts. To create this artificial steps, CAD files were modified substituting plain ramps by stairs with the desired dimensions.

Two different morphologies have been created for the parts: two-faced, with complementary angles (30º – 60º and 45º – 75º, dimensions shown in Figure 3.5) and four-faced (30º – 45º – 60º – 75º, dimensions shown in Figure 3.6). Ramps dimensions are designed in order to obtain at least 15 mm profiles, to have a sufficient evaluation length for roughness evaluation. The opposite face of each ramp is printed with the same angle, in order to ease the evaluation and fixture in the measurement devices (allowing to place the geometries in a perpendicular position to the FVM beam). Only up-skin surfaces have been evaluated, as down-skin ramps could be affected by gravity and present high roughness differences from theoretical values, not following the same theoretical model.

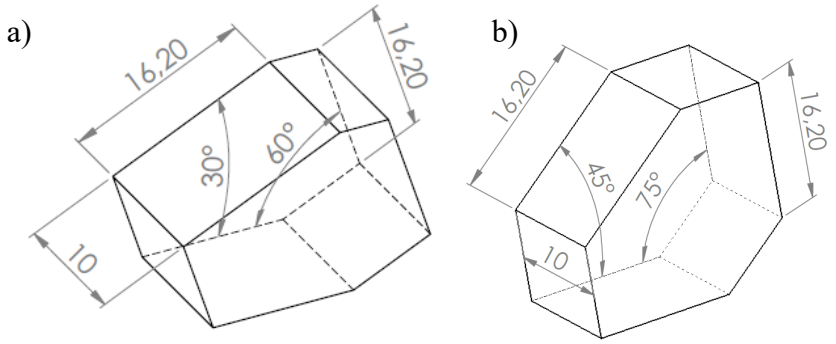

Figure 3.5. Dimensions of two-faced parts. a) 30º - 60º. b) 45º - 75º.

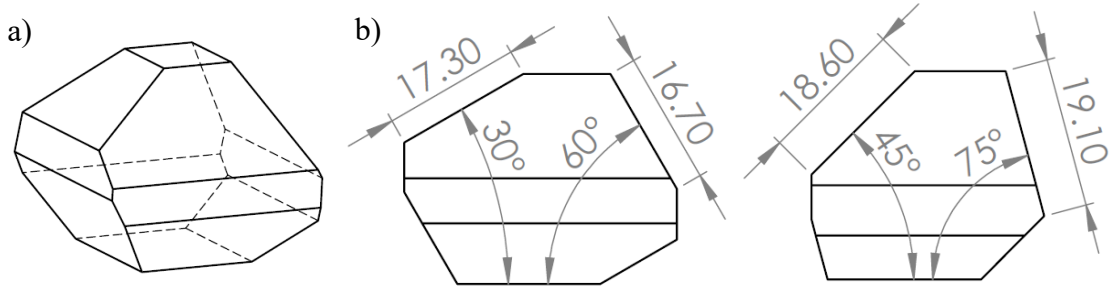

Figure 3.6. Four-faced parts. a) General view. b) Dimensions.

Various parts of each type (at least 3 replicas) have been printed and visually evaluated to detect possible manufacturing defects. Manufacturing parameters (layer thickness, ramp angle of inclination) were used to create a range of parts to be evaluated. Most suitable objects with none or few defects have been selected for each type of geometry.

Post processing has consisted in the cleaning of the parts by pressurized water (for Polyjet parts) and by compressed air (for SLS parts). No post processing was necessary for FDM parts.

For the second stage of the experiment, a single test object has been done in which certain parts from the first stage are included. These individual parts have been selected based on the measurements and verifications done in the first stage. As one of the objectives is to create an object of study as compact as possible, one part was selected for each AM technology. Second criteria used for the selection was the comparison between average roughness deviation (Ra) measured in FVM and theoretical average roughness (Ra') based on the predictive models [37,38] as explained before.

Other relevant aim of the ad hoc designed test object is to ease the orientation of the part for the reference measurements, as done for the first stage of the experiment. The objective is to fit every surface to be measured in a horizontal plane, thus, incorporating complementary-angled ramps in the opposite side of the part. Also, for the XCT measurements, the goal has been to make the design as much compact as possible, to improve the geometrical magnification. As the part is composed by components manufactured by different AM technologies, a polymeric FDM base to support those components is created. Additional ramps, similar to those present in individual parts, were added into the base to amplify the range of geometries evaluated. The result is an assembly with general dimensions 50 mm × 55 mm × 60 mm, shown in Figure 3.7. Sinusoidal profiles present in the assembly are intended for future experiments and, thus, their results were not included in the experiment.

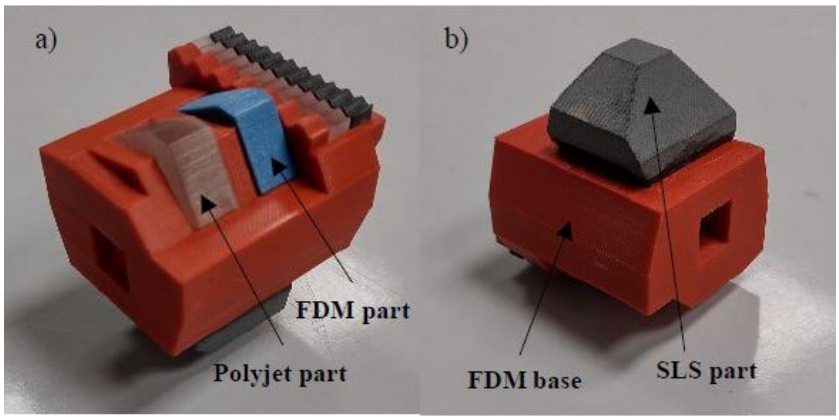

Figure 3.7. Second-stage test object design. a) Upper side. b) Lower side.

As a result of the test object design, a range of inclined ramps available for the evaluation are shown in Table 3.1.

Table 3.1. Summary of geometries evaluated and their expected average roughness.

Technology	Material	Angle of inclination	Layer thickness/mm	Expected Ra/µm
FDM	PLA	60º – 30º	0.2	25.00 – 43.30
FDM (base)	PLA	60º – 45º – 30º	0.1	12.50 – 17.67 – 24.14
Polyjet	Rigur RGD450	60º – 30º	0.1	12.50 – 21.65
SLS	PA12	60º – 45º – 30º	0.1	12.50 – 17.67 – 24.14

As shown in the table, additional ramps have been included in the base to amplify the range of the experiment. With this selection, expected roughness of the test objects oscillates between 12.50 µm and 43.30 µm, which is a common roughness value on polymeric AM parts.

3.1.3. Measurement procedure

First stage evaluation of the test objects has been done by a FVM InfiniteFocusSL of Alicona, which is used as a reference calibrated device for the verification of the trueness of roughness values; a 10x magnification lens was configured, with a lateral resolution of 8 µm and a vertical resolution of 130 nm. Contrast and brightness were adapted to the surface colour of each test object, with no additional effect on the resolution of the device.

In second stage, XCT evaluation has been performed to the single final test object with the integrated parts selected from the first evaluation. Three XCT measurements were taken for the whole assembly with a Zeiss Metrotom 1500/225 kV, with three different voxel sizes (28, 54 and 75 µm). The procedure for the obtention of the voxel sizes is the following:

- 28 µm is the smallest voxel size allowing the study area to be scanned in a single tomography.
- A voxel size of 54 µm is obtained under similar magnification conditions but applying a 2x binning. The binning process combines the information of several voxels (four voxels in 2x binning) to generate a single voxel, reducing the size of the generated files and accelerating the tomography analysis process.
- 75 µm has been obtained increasing the source-to-object distance and thus, reducing the magnification. 2x binning process is also utilised for this tomography.

In Table 3.2, settings selected for the evaluation of each scenario are displayed.

Table 3.2. XCT settings utilized for the evaluation of each scenario.

XCT settings	**Value**		
Voltage/kV	120	120	120
Current/µA	279	550	550
Physical filter	Al 2 mm	Al 2 mm	Al 2 mm
Nº of projections	3000	1500	1500
Exposure time/ms	1000	500	500
Image averaging	No	Yes (2)	Yes (2)
Voxel size/µm	28	54	75

A physical filter of aluminium with 2 mm of thickness was used for all the measurement to obtain the best contrast possible between polymer and background (air), and to ensure the correct penetration of all the geometries, since some areas could be too thick and create artifacts. Tomographies were processed in software VGStudio Max 3.4.2, with a preliminary general surface determination in Advanced mode, and local gradient surface determination for each geometry after ROI definition, with a 4-voxel search distance. For both general and local surface determinations, default ISO50 method was used in the software. A mesh for each element was exported in STL format, using the "manual" point reduction to set the tolerance in the minimum achievable (1/1000 voxel size), in Ray-based mode. 28 µm voxel size tomography has been made with no-binning process into the detector, while 54 µm and 75 µm tomographies have been made with a 2x2 binning. As a consequence, for 28 µm XCT a higher number of projections were required.

3.1.4. Roughness evaluation: linear and areal parameters

For the evaluation of surface roughness of the ramps, a series of linear and areal parameters were extracted according to the related standards:

- ISO 21920-3:2021 [138] for linear profile evaluation.
- UNE-EN ISO 25178-2:2011 [22] for areal evaluation.

Here, three surface characteristics of each feature are intended to be evaluated, both for linear profiles and areas:

- Average roughness parameters (Ra, Rq, Sa, Sq)
- Maximum and minimum values of peaks and valleys (Rz, Rp, Rv, Sz, Sp, Sv).

- Form and material distribution (Rsk, Rku, Ssk, Sku).

Average roughness parameters are divided into arithmetical average roughness (Ra, Sa), which are calculated by the mean value of the feature, and quadratic average roughness (Rq, Sq), which are calculated with the quadratic mean value.

Maximum roughness parameters consider the mean of several maximum values according to standards: 5 higher peaks (Rp, Sp), 5 lower valleys (Rv, Sv) and both (Rz, Sz). Therefore, Rz and Sz is a combination of Rv and Rp, and Sv and Sp, consecutively.

Skewness (Rsk, Ssk) and kurtosis (Rku, Sku) represent the form and material distribution of the feature. Skewness is related to the symmetry of the profile around the median lane; positive skewness indicates the presence of higher peaks, while negative skewness means deeper valleys. Kurtosis evaluates the sharpness of the profile; values of Rku, Sku > 3 are related to sharper peaks and valleys while values < 3 indicate flatter and rounder profiles.

3.1.5. Data acquisition and filtering

In first stage evaluation, integrated software IfMeasureSuite 5.3.6 (Alicona Imaging, Graz, Austria) in FVM has been used for the obtention of the roughness parameters of the ramps evaluated. Here, as the theoretical models are based on Ra, only this parameter has been necessary for the ramp selection, and consequently, only linear profile evaluation has been initially performed. Profiles extracted were located in the central part of the faces (see red lines in Figure 3.8). Three profiles along the central area of each ramp were extracted to obtain mean values for each geometry.

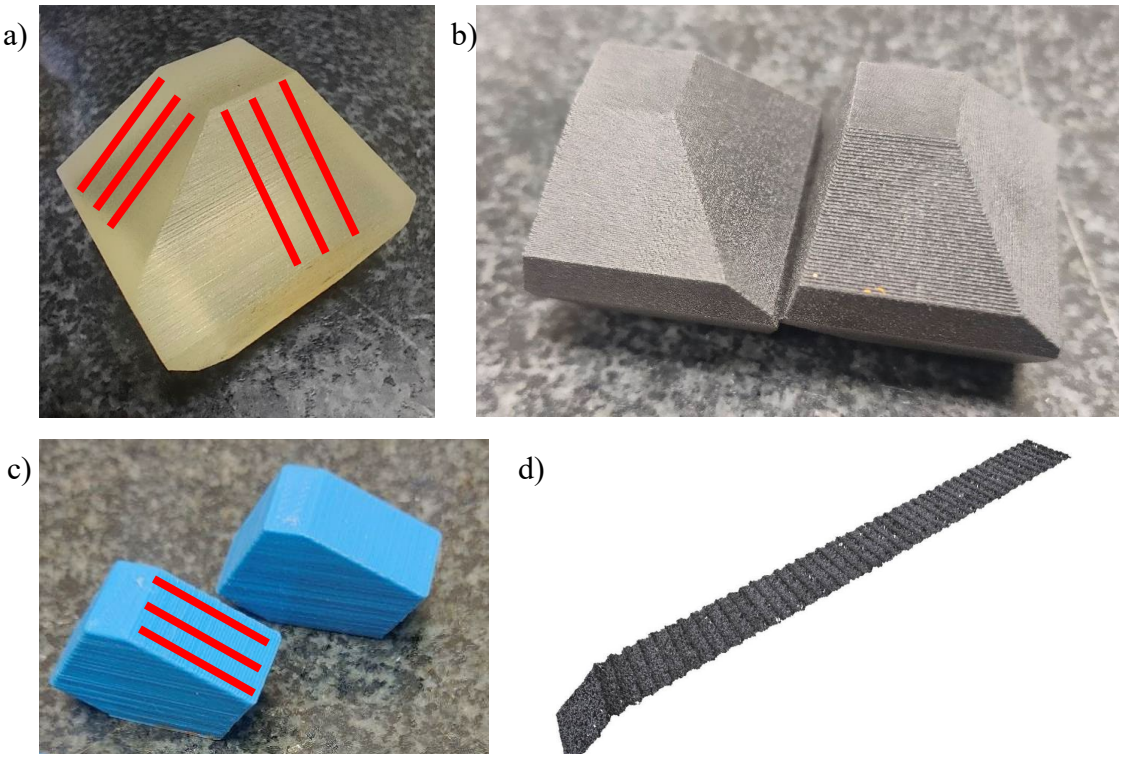

Figure 3.8. First stage part manufacturing and measurement. a) Printed four-faced Polyjet part. b) Printed four-faced SLS part. c) Printed two-faced FDM parts. d) Example of surface extracted by FVM.

In second stage, STL files were exported for each geometry and were processed by software Gwyddion 2.60, extracting both linear and areal parameters. Same software has been used for both FVM and XCT files in order to avoid software differences which could increase uncertainty. For each ramp, three profiles of 15 mm length and three areas of 4x4 mm, equally distributed along the surface.

Selection of the most suitable filtering cutoff for the surface evaluation in both stages have been made according to ISO 21920-3:2021 [138] for linear profile evaluation, and to UNE-EN ISO 25178-3:2012 [25] for areal evaluation.

Linear filtering, in roughness evaluation, is used to eliminate wave components present in primary profiles which does not belong to the roughness itself. As roughness is within a band of wavelengths, two filters are applied: a long wavelength filter (λc) for low frequency waves, and short wavelength filter (λs), for high frequency waves.

According to Ra predicted values, λc cutoff should be 8 mm. ISO 21920 recommends a profile length of 40 mm (five times larger than sample length). As indicated in Section 3.2, maximum profile length is 15 mm. For the best adaptation possible to the dimensions and the standards, two different λc filter cutoff values were selected for profile evaluation:

- 8 mm λ_c cutoff is selected according to the Ra predicted value (for Ra values larger than 10 µm).

- 2.5 mm λ_c cutoff is selected according to the evaluation length. (12.5 mm, more similar to profile length).

A λs filter of 80 µm is selected according to the maximum resolution achievable for the voxel size obtained, as investigated in [44]. In Figure 3.9 an example of profiles distribution with their nominal lengths (12.5 mm) are displayed.

Similar to linear roughness evaluation, a filtration is needed for the extraction of areal roughness parameters. For this purpose, 2D filters are applied: L-filter for low frequency waves and S-filter for high frequency waves.

Three 4 mm × 4 mm areas distributed across each ramp have been extracted, as displayed in the example in Figure 3.9. L-filter nesting index (hi-pass filter) of 0.8 mm and an S-filter nesting index (low-pass filter) of 2.5 µm were selected.

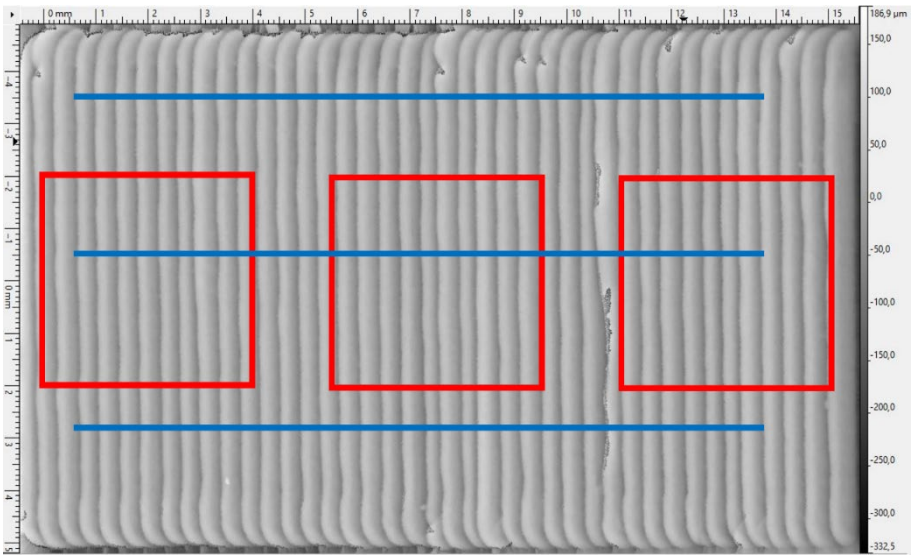

Figure 3.9. Representation of linear profiles (blue) and areal (red) distribution in a ramp.

3.2. Results

In this section, results obtained in first and second stage of the experiment are described.

3.2.1. Verification of predicted Ra

Results of first stage experiment measurements are compared with theoretical predictive models. Examples of roughness profiles of each technology (layer step ramps of 0.2 mm for FDM and SLS, 0.196 mm for Polyjet) extracted after filtration per ISO 21920-3:2021 [138] are shown in Figure 3.10.

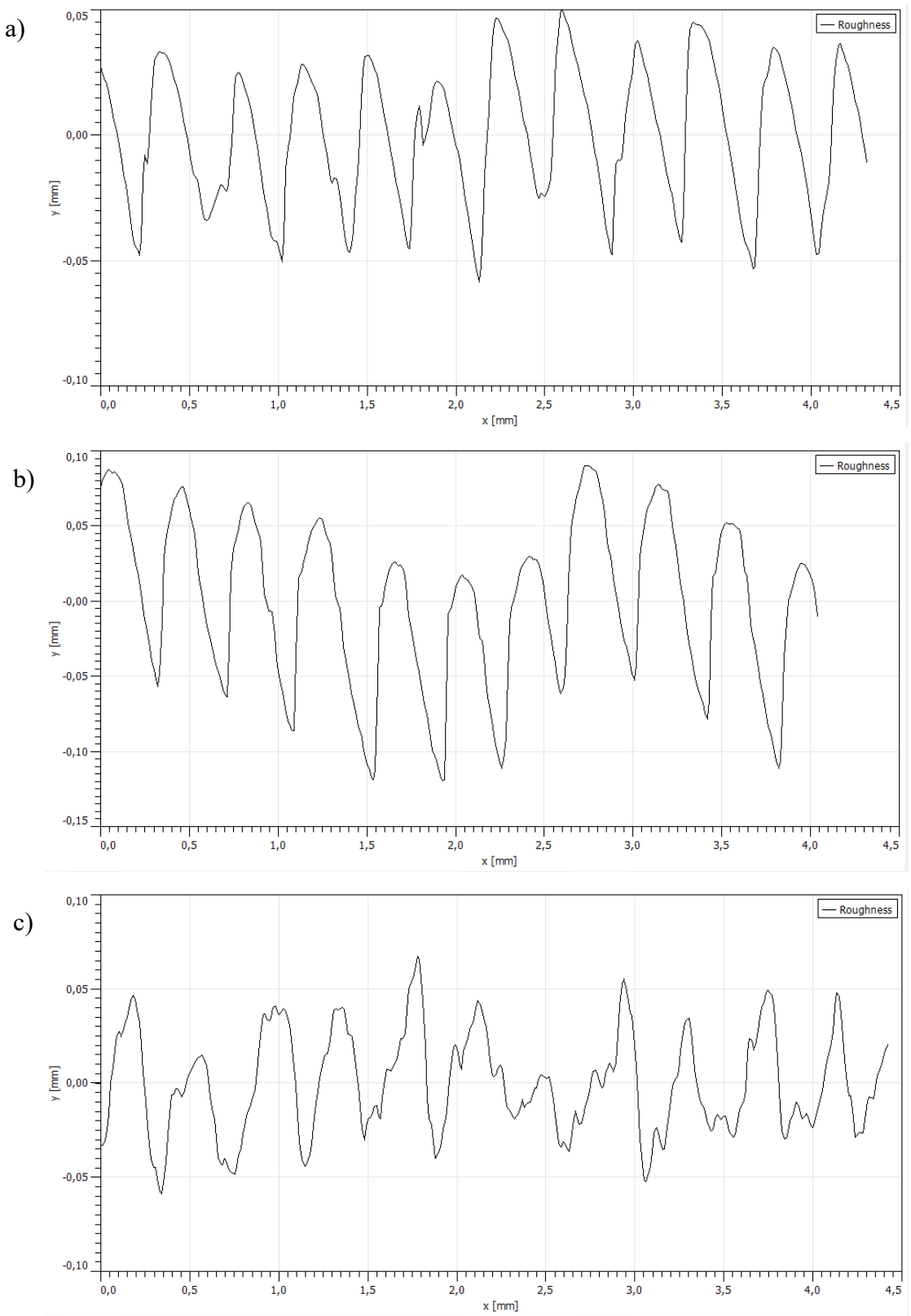

Figure 3.10. Examples of roughness profiles from 0.196-0.2 mm step ramps. a) Polyjet. b) FDM. c) SLS.

Visually, it is possible to observe that FDM profiles are more similar in terms of shape to the predictive models, mainly to the optimized model which consider rounded shapes

[38]. Higher irregularities are found in SLS profiles; one of the hypotheses is the partially fused powder present in the surface due to the air cleaning process required.

Values or theoretical and real Ra values have been extracted with IfMeasure integrated software in FVM. Graphics of measured Ra values compared to theoretical models are displayed in Figure 3.11. Several measurements of each geometry have been done, and mean values are considered. As stated, results are grouped and compared according to the layer thickness of the geometry evaluated.

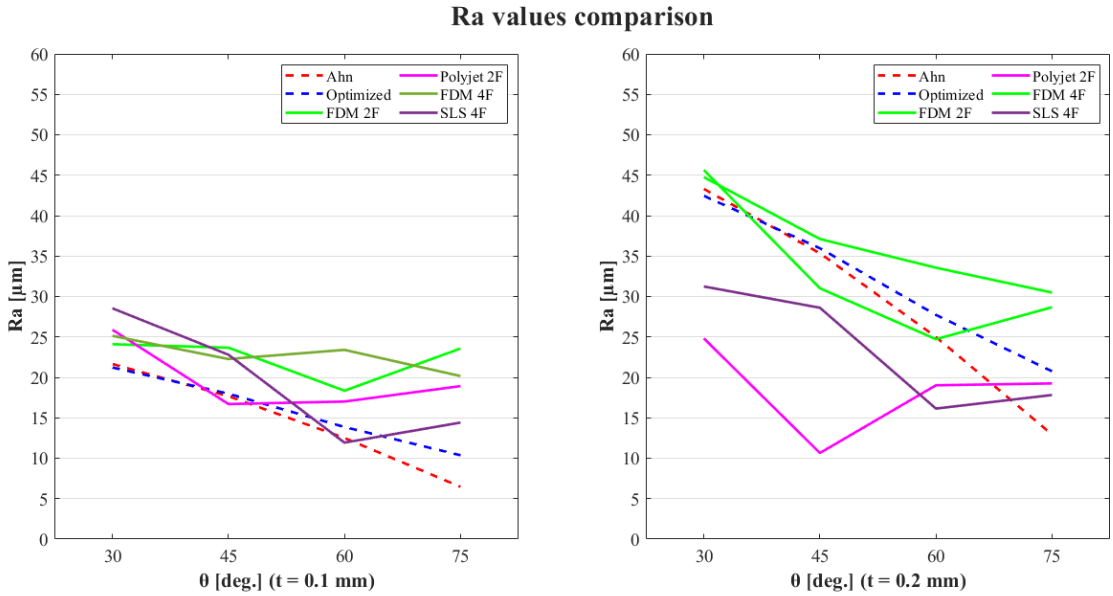

Figure 3.11. Comparison of theoretical and real values for each angle of inclination and layer thickness.

Several measurements of each geometry have been done, and mean values are considered. As stated, results are grouped and compared according to the layer thickness of the geometry evaluated.

As expected, a difference with theoretical calculations is found, in both predictive models. For FDM parts, the bigger accuracy of the optimized model [38] than the Ahn general model [37] is demonstrated, mainly for angles of inclination of $\theta \geq 60^{o}$ where bigger deviations occur, not following the theoretical values' tendency. For this build angles, approximations have been made by some authors, as Pandey model [37].

As a consequence, nominal value of Ra plays an important role, because as it decreases, higher precision of AM devices is required and therefore better resolution for measurements is necessary. Layer thickness is, indeed, a parameter to consider, but its influence is not as big as the angle of inclination in terms of manufacturing precision. No tendency in the differences between results of two-faced and four-faced parts has been identified.

3.2.2. XCT evaluation and intercomparison

Second stage of the experiment has consisted in the measurement of the second integrated test object, in which individual parts have been selected considering the design criteria and according to the results of the first stage (see Table 3.1 and Section 3.2.1).

3.2.2.1. Voxel size/Ra comparison

First comparison is made taking into consideration the two key parameters: voxel size of XCT measurement (Vx) and theoretical average roughness (Ra'), calculated following predictive models [37,38]. A coefficient Ra'/Vx is settled for the comparisons. Figure 3.12 summarizes the relationship between coefficient Ra'/Vx and the percentual deviation of XCT measurements from reference FVM evaluation, in terms of average roughness (Ra and Sa).

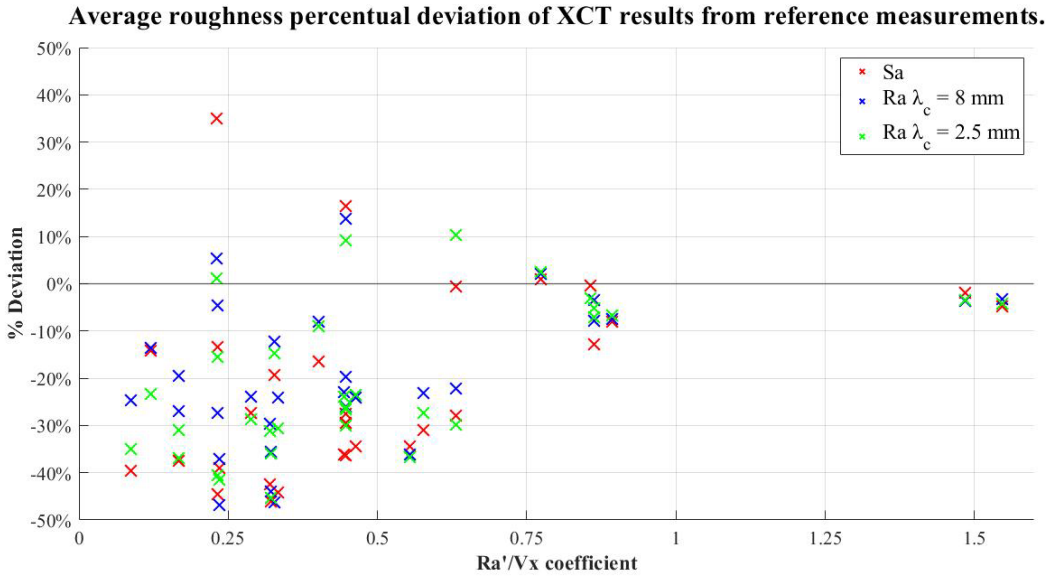

Figure 3.12. Average roughness % deviation comparison, considering Ra'/Vx coefficient.

Figure 3.12 shows that the tendency of deviation values is in general negative, indicating that roughness values registered by XCT are mostly lower than roughness values registered by FVM; this happens due to the lower resolution of XCT devices comparing to FVM. A trend is identified for values of Ra'/Vx ≥ 0.75, where deviations are found to be progressively smaller and under 10% of the reference measurement.

To validate the results, a measurement comparability evaluation using uncertainty calculations has been performed. E_N parameter is calculated, according to standard ISO/IEC 17043:2023 [98], following Eq. 3 described in Section 2.1.4:

Uncertainty calculations have been done following the procedures indicated in standards:

- ISO 15530-3:2011 [91] for reference FVM measurements. Uncertainty results registered are in a range of U_{FVM} = 2-3 µm.
- VDI/VDE 2630-2.1 [67] for XCT measurements, also following the recommendations suggested in [139]. There is still not a standard for the determination of the uncertainties of XCT measurements, but this directive defines with good detail the factors to take into consideration, and it is commonly used [66,93]. Uncertainty results registered are in a range of U_{XCT} = 4-6 µm.

Values selected for the uncertainty calculations are Ra and Sa parameters, as used in the calculations for the percent deviation displayed in Figure 3.12. In Figure 3.13, the relationship of E_N parameter values with the coefficient Ra'/Vx, for each voxel size, is shown.

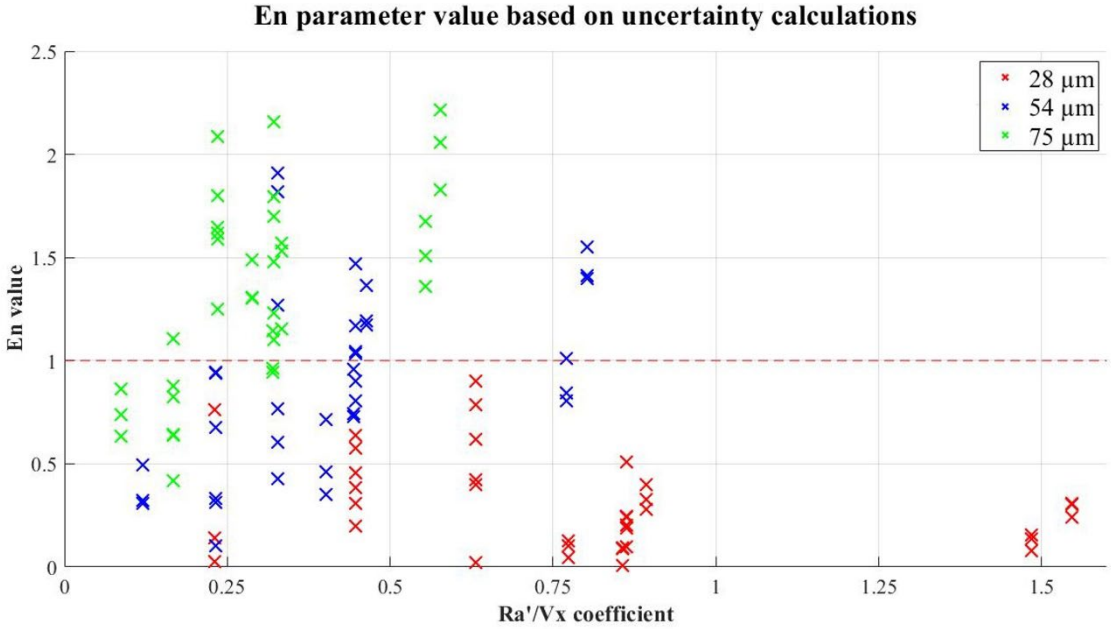

Figure 3.13. E_N parameter comparison for each voxel size and Ra'/Vx coefficient.

Distribution of values show that E_N < 1 complies for all measurements with Vx = 28 µm, which is not the case of measurements with Vx = 54 µm and Vx = 75 µm where most of values are over 1. It is shown also that the majority of the cases comply with the condition of E_N < 1 for a value of Ra'/Vx above 0,75; for the minimum voxel size achieved (28 µm), it will result in a theoretical limit value of Ra'= 21 µm.

No ramp Ra' value is over 0,75Vx for Vx = 75 µm, while the few cases for Vx = 54 µm do not fit into the E_N < 1 condition or are very close to 1. It is worth to mention that, even if it is true that E_N < 1, standard [51] recommends that if the value is very close to 1 (as it is the case of Vx = 54 µm results with Ra'/Vx above 0,75), validation should not be automatically done as desired value of E_N should be as close as possible to 0. Following

this advice, it can be seen that none of Vx = 28 µm results with Ra'/Vx above 0,75 are close to 1. Therefore, with this calculations, it is possible to conclude that for this roughness values, tomographies with Vx = 54 µm and Vx = 75 µm are not suitable for roughness evaluation, and the most trustworthy results are those which coefficient Ra'/Vx ≥ 0.75.

Additionally, a segmentation only by XCT voxel size is done according to Ra'=21 µm value calculated as mentioned in Eq. 5, considering all technologies. Results are displayed in Table 3.3, in terms of absolute and percentual deviation of the mean values.

Table 3.3. Absolute and % deviations of XCT results from reference measurements.

Ra/µm		***< 21***			***> 21***		
Voxel size/µm		***28***	***54***	***75***	***28***	***54***	***75***
Areal	**Sa/µm**	-1.3	-5.9	-7.3	-0.6	-5.4	-8.6
	%	-9.83%	-45.75%	-56.35%	-2.85%	-24.37%	-38.35%
	Sq/µm	-0.9	-6.6	-8.3	-0.3	-6.5	-10.1
	%	-5.86%	-42.36%	-53.69%	-1.30%	-24.61%	-38.33%
Linear λc = 8 mm	**Ra/µm**	-2.1	-4.8	-5.3	-0.3	-4.7	-7.5
	%	-13.24%	-30.61%	-33.98%	-1.29%	-18.66%	-29.71%
	Rq/µm	-2.4	-5.6	-6.3	-0.1	-5.4	-8.6
	%	-12.63%	-28.76%	-32.75%	-0.41%	-17.94%	-28.49%
Linear λc = 2.5 mm	**Ra/µm**	-2.8	-6.1	-6.5	-0.6	-5.1	-8.3
	%	-19.78%	-44.02%	-46.70%	-2.32%	-20.73%	-34.05%
	Rq/µm	-2.9	-6.8	-7.5	-0.5	-5.9	-9.7
	%	-16.72%	-39.57%	-43.86%	-1.63%	-20.47%	-33.61%

Table 3.3 shows that only for Vx = 28 µm results are into the acceptable gap, especially for Ra' values > 21 µm where absolute differences are below 1 µm. This also confirms the results obtained in Section 3.2.2.1. In general terms, it is shown that Sa and Sq values are more similar to Ra and Rq values with a λc = 2.5 mm cutoff than with a λc = 8 mm cutoff; however, for Ra' values < 21 µm and Vx = 28 µm higher differences are found. Thus, the influence of the AM technology has been investigated.

3.2.2.2. AM technology comparison

Focusing in Vx=28 µm XCT measurements, segmentation into AM technologies is presented in Figure 3.14.

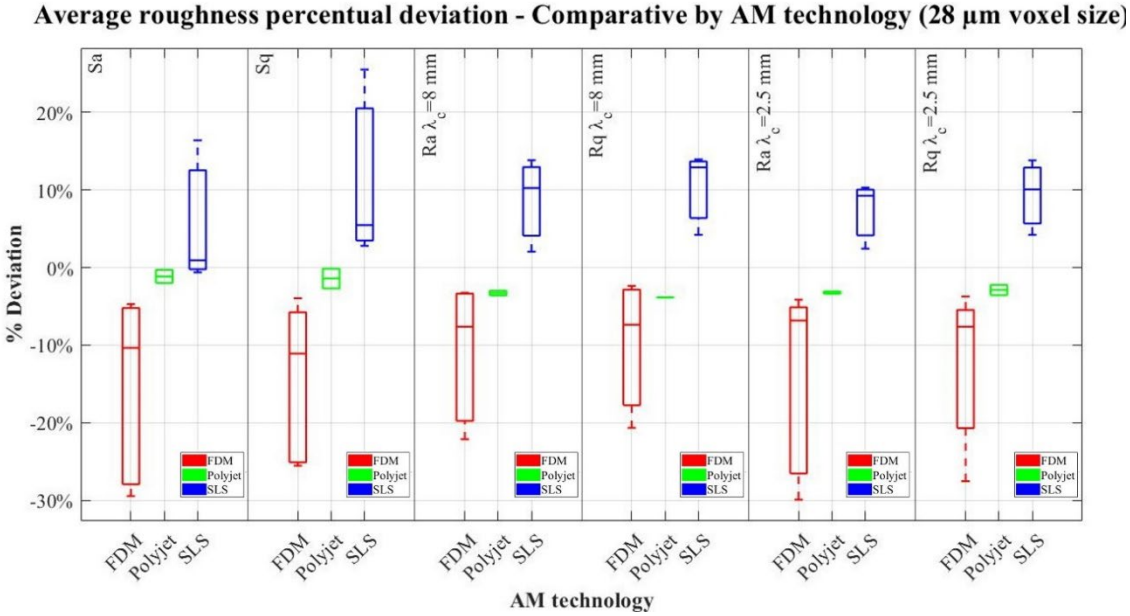

Figure 3.14. Average roughness % deviation comparison (segmented by AM technology).

Ra and Rq parameters are similar in both FDM and Polyjet features, with a higher negative % difference in FDM mean values due to higher volume of surfaces with Ra'< 21 µm in the sample. However, higher variances are displayed in Sa and Sq values for SLS geometries; also, differences are positive, indicating that average roughness values registered are higher than in reference measurements.

The reason for the variation in Sa-Ra and Sq-Rq results is the non-uniform surface. Unlike FDM and Polyjet processes, the presence of randomly distributed unfused dust in the surface creates unequal profiles in both X and Y directions. Although post process is done to remove the unfused dust, an amount of this remains in the surface because it is not possible to remove all the powder without damaging the surface. In FDM and Polyjet surfaces, roughness profiles are present predominantly in the perpendicular direction to the layer stairs. This dimension added to surface measurements increases the error in areal measurements.

A graphical view of an example of the reconstructed surfaces in each AM technology can be seen in Figure 3.15. The higher Ra values for SLS can be explained also due to the unfused surface powder (Figure 3.16). Its presence, added to the characteristics of AM technologies, could create re-entry features which cannot be evaluated by optical microscopes, because they are out of the field of view. However, XCT devices can

perform measurements of internal and non-accessible elements, being able to characterize re-entries and, thus, increasing the average roughness parameters' values.

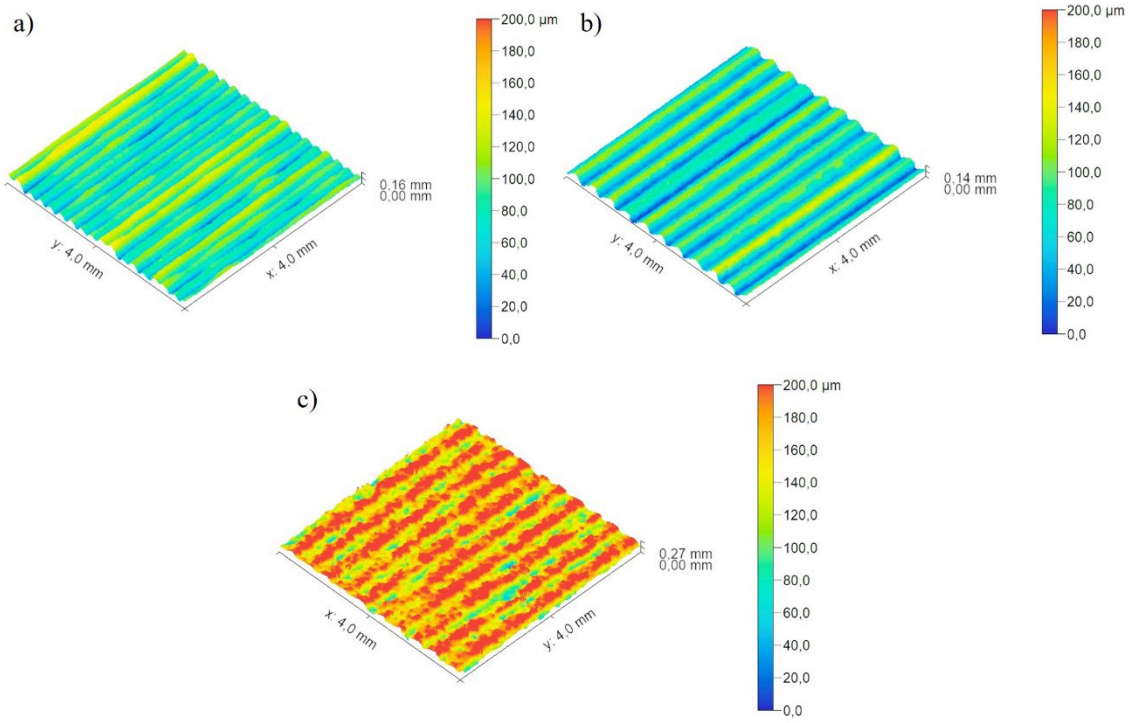

Figure 3.15. Surface height colour maps obtained from XCT reconstruction. a) FDM. b) Polyjet. c) SLS.

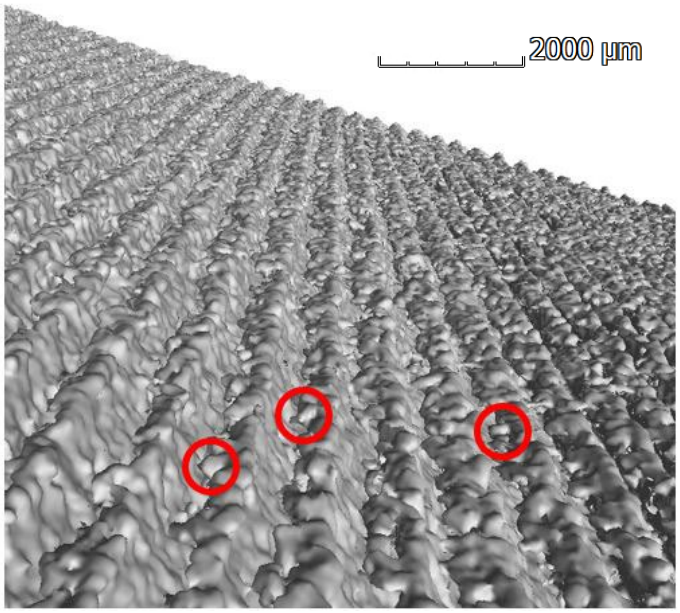

Figure 3.16. Close up of a SLS surface in XCT, showing the unfused powder representation (circled in red).

3.2.2.3. Skewness and kurtosis

Skewness and kurtosis determine the shape of the profile/area extracted. Higher values of skewness parameters (Ssk, Rsk) are indicatives of a predominancy of sharp peaks,

while lower values indicate a higher number of rifts. On the other hand, the lower are the kurtosis values (Sku, Rku), the smoother are the peaks and valleys.

Both skewness and kurtosis values have been evaluated. The mean value of the differences from the reference measurements are registered and shown in Figure 3.17 for skewness and kurtosis parameters. As in the previous section, results are focused on Vx=28 µm XCT measurements.

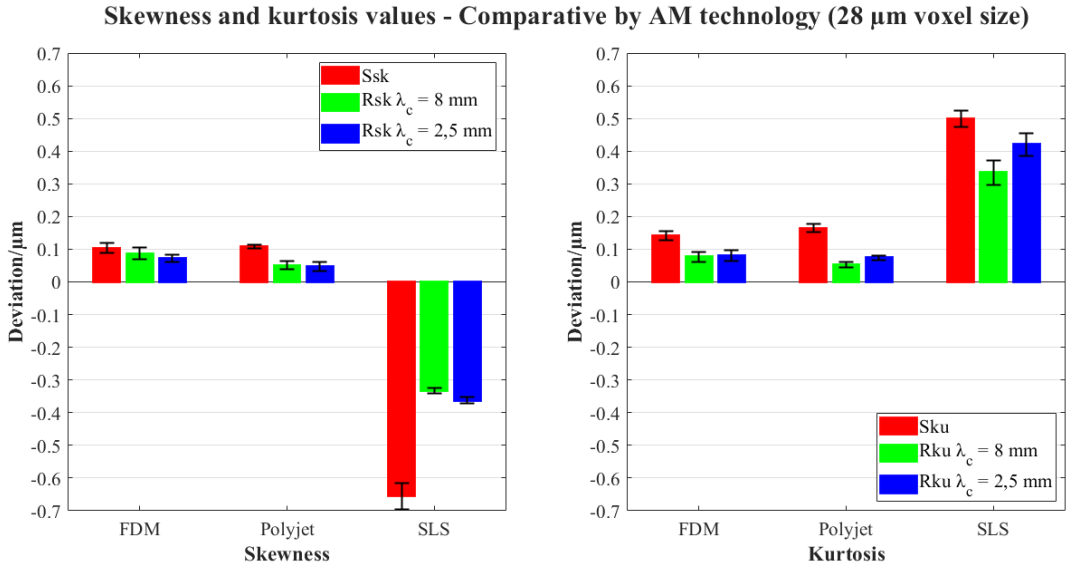

Figure 3.17. Skewness and kurtosis deviation values from reference measurements.

Results show that deviations from references are considerably low for FDM and Polyjet technologies, indicating a slightly higher skewness and kurtosis. For SLS technology, results show greater differences, presenting lower skewness and higher kurtosis.

XCT measurements, because their capacity of measuring elements out of direct sight, are able to produce sharper surfaces in spite of the lower resolution (Figure 3.18). It becomes clearer for SLS surfaces, where re-entries caused by unfused powder are more present, and thus differences are higher. It also produces a negative difference in skewness because some deep valleys are not accessible for optical measurements.

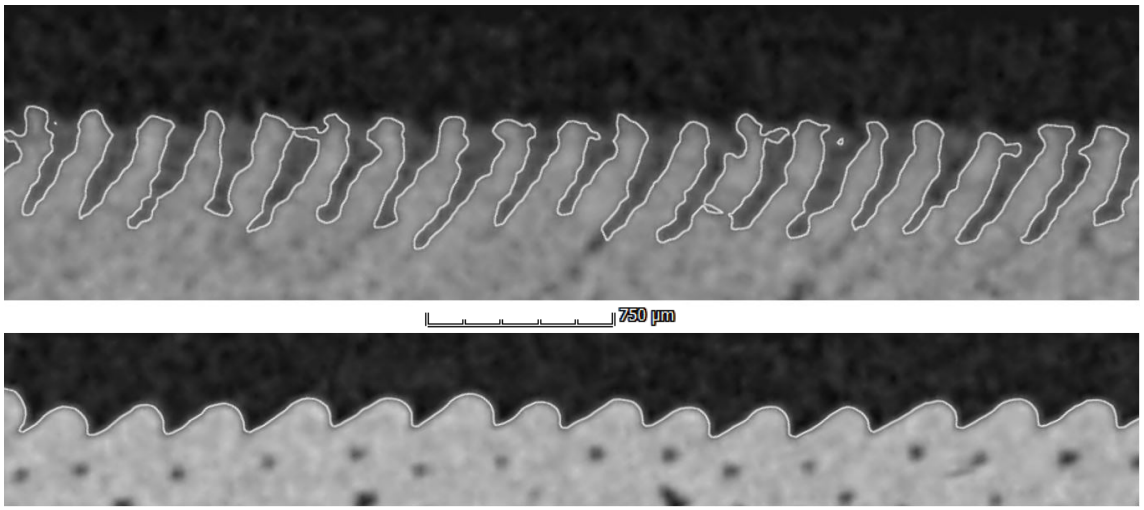

Figure 3.18. 2D view comparison of different profiles in XCT. SLS (upper) and FDM (lower).

3.2.2.4. Maximum roughness

The roughness values of highest peaks (Sp, Rp) and deeper valleys (Sv, Rv), apart from maximum roughness value (Sz, Rz) are studied. Percent deviations of areal (Figure 3.19) and linear (Figure 3.20) are presented. As mentioned before, results are focused on Vx=28 µm XCT measurements.

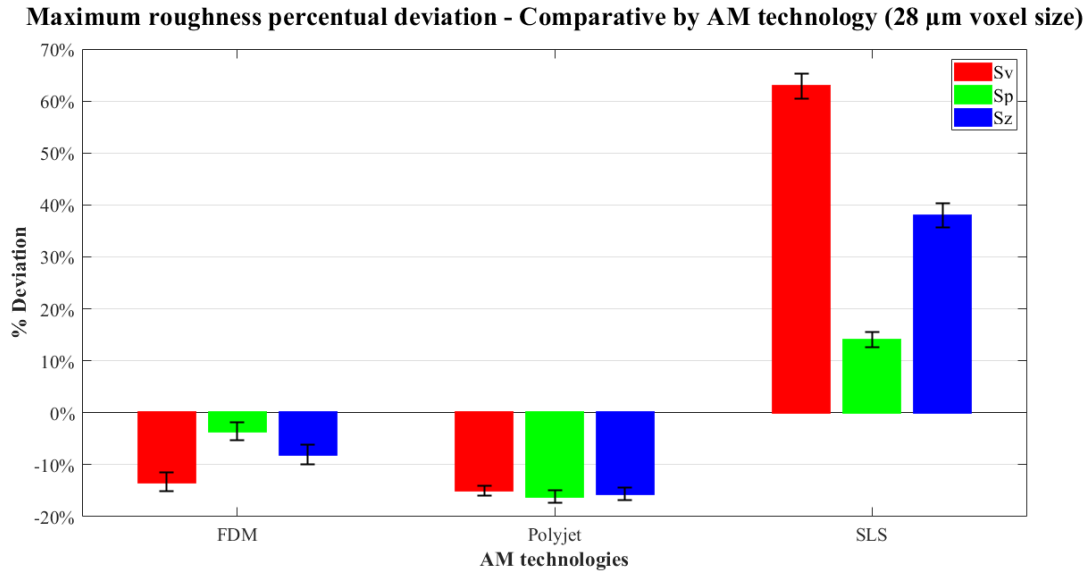

Figure 3.19. Average % deviation of areal maximum roughness parameters.

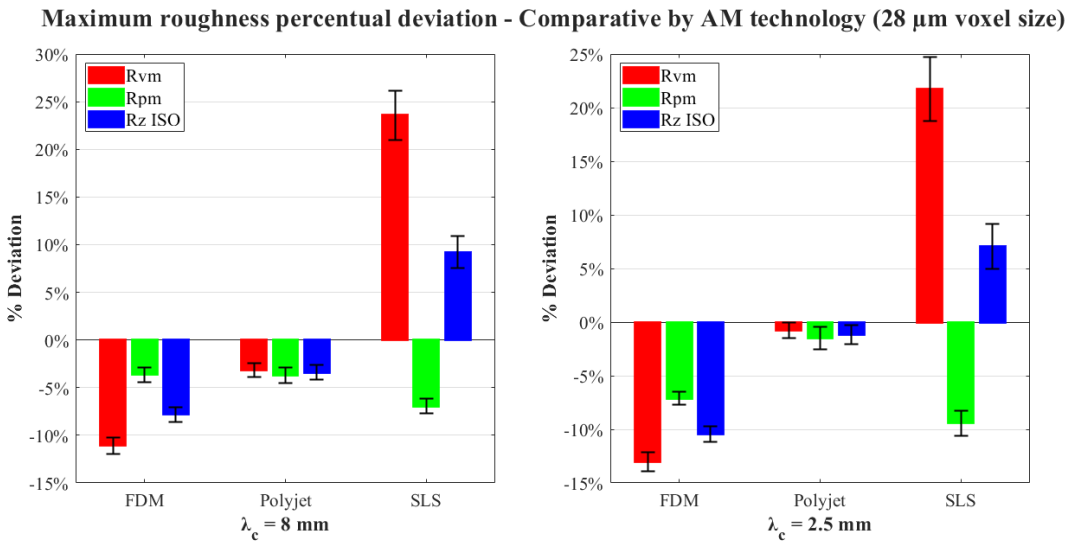

Figure 3.20. Average % deviation of linear maximum roughness parameters for Lc = 8mm (left) and Lc = 2,5mm (right).

Results show an equilibrium between peaks and valleys in Polyjet results, with a slight negative deviation. FDM surfaces presents higher deviations, with an emphasis on valleys; as resolution is lower than optical measurements, deep valleys tend to be smoothed and maximum values are lower. Opposite happens on SLS surfaces because, as mentioned before, re-entries and out-of-sight elements are not reached by optical FVM. Also, linear measurements show a different tendency than areal parameters due to the non-uniform stairs.

3.2.3. Discussion

First analysis from the results shows that, as expected, deviations of the XCT measurements and reference FVM measurements follow a tendency in which smaller XCT voxel size is correlated with better accuracy. A value of Ra'/Vx ≈ 0.75 is found to be a limit where, for higher values, it is possible to characterise surface texture for this type of polymeric AM parts with an acceptable accuracy. However, it is also found that small geometrical magnifications and, thus, high voxel sizes, remain non useful as deviations increase. In this experiment, Vx = 28 µm has been found suitable, which is an achievable geometrical magnification by a commercial XCT device for industrial parts with common dimensions. Analysis have been focused on this geometrical magnification from this segmentation, and validation by an uncertainty calculation [67,91] and measurement compatibility analysis [98] have been done.

Regarding the three polymeric AM technologies studied, post-processing has been seen as an important factor in the characterisation of the surfaces. No abrasive method

has been applied with the objective of reducing the possible damage originated; pressurized water is the recommended method for Polyjet by the manufacturer, and the pressure was controlled by the cleaning device. Support material sticked to the surface is weak enough to be removed by the water, not eroding the steps. Regarding SLS, compressed air was not filled with abrasive particles not to damage the surface; the main disadvantage is that the cleaning capacity of compressed air has been demonstrated not to be enough to remove all the powder. While theoretical values were achieved more precisely for FDM, which has no post process, therefore no surface modification (seen in the preliminary study), it has been found that it affects in a different way in terms of XCT accuracy comparing to optical devices (FVM in this case).

Polyjet surfaces, which are post processed by pressurized water, show same level of accuracy or even higher when characterised by XCT than FDM surfaces which has no post process. On the other hand, SLS parts, post processed by compressed air, have higher deviations and less predictable results. The reasons of this SLS surface behaviour are mainly partially unfused powder and re-entry geometries. Both aspects are linked because unfused powder create small voids out of the general stair-stepped shape of the surface. This unpredictable features can be reached by XCT but are out of sight of optical measuring devices, causing sharper surfaces with deeper valleys and higher roughness values.

In FDM and Polyjet features, unlike SLS, surfaces obtained by XCT are in general smoother than by FVM mainly because the lower resolution of the XCT devices, as expected. Increasing the voxel size and, thus, reducing the resolution, leads to less detailed surface data. This XCT smoothing effect is also present in SLS, but it is seen to be weaker than the effect of re-entrant features created by the unfused powder.

Additionally, roughness evaluation by linear and areal parameters shows no significant difference in FDM and Polyjet parts, while areal parameters have a better agreement between XCT and reference evaluation methods than linear ones for SLS parts. As seen in Figure 3.15, linear profiles can be extracted in the perpendicular direction to the AM layers with no big shape variation in FDM and Polyjet ramps, therefore those profiles are more similar along the feature. Consequently, results are more likely to be repeated along the surface, and thus more similar to the complete area evaluation. In SLS, again, unfused powder creates more heterogeneous profiles with different values. This is why an evaluation by areal parameters is demonstrated to be more suitable for the whole SLS surface.

Finally, regarding λ_s filter selected, value recommended by standards for the corresponding λ_c filter is 8 µm for the 2.5 mm λ_c cutoff, and 25 µm for the 8 mm λ_c cutoff. However, as investigated in [44], a λ_s filter of 80 µm (best resolution achievable for a voxel size around 20-30 µm) creates no difference in Ra measurements, because dominant surface texture components have a spatial wavelength larger than 80 µm. It becomes clearer for higher voxel size (54 µm and 75 µm), in which resolution is lower and, thus, wavelength of texture components is bigger.

3.3. Conclusions

In this paper, a metrological characterisation of polymeric additive manufactured surfaces by XCT for the evaluation of XCT resolution limit and performance is presented. Different additive manufacturing technologies and parameters as angle of inclination and layer thickness are used to create inclined ramps, with a range of theoretical average roughness (Ra) according to predictive models [37,38].

A preliminary study was made with the objective of a first feature characterisation, and as a result it has been a selection for this final experiment of only the most precise geometries according to the trueness of FVM measurements comparing to the theoretical predictions. This segmentation is made for creating a compact object of study, improving this way the geometrical magnification of the XCT measurement. Selected features are distributed along an ad hoc designed assembly, optimised for its evaluation both in an XCT machine, and in a reference device (FVM). Roughness areal and linear parameters are extracted, and a comparison has been made for a XCT performance evaluation.

Results show a tendency in the relationship between voxel size (Vx) and predicted average roughness (Ra'), in which a value of Ra'/Vx ≈ 0.75 is found to be a starting point for accurate XCT roughness measurements. Results have been validated by an uncertainty calculation following standards [52,53], with a measurement compatibility analysis [51] However, as previously studied, resolution remains as a handicap for XCT measurements regarding surface evaluation, but it is demonstrated that for a reasonably achievable geometrical magnification for a part with industrial dimensions (28 µm voxel size for a 50 mm × 55 mm × 60 mm part, in this case), it is possible to evaluate roughness with an acceptable precision.

Characterisation of 3 different polymeric AM technologies has been made, and therefore their topographical behaviour was possible to evaluate. Post process was found to be an important parameter to consider, working in a different way for Polyjet (where

post processing affects the trueness of the FVM results, but has little effect in XCT comparison) and for SLS (where unfused powder and re-entrant features creates different topography and roughness results between XCT and optical measurements). Although post process has been necessary for a correct cleaning of the parts, as expected, it has been found that is not entirely perfect, neither automated, as material remain unevenly in the surface in both technologies.

Linear and areal roughness parameters calculation have led to the conclusion that both FDM and Polyjet surfaces are suitable to be evaluated with linear profiles perpendicular to the steps created by the layer-by-layer technology. On the other hand, SLS surfaces need an areal characterisation for more robust results, again, because the unfused powder creates more heterogeneous profiles with high roughness differences between them.

To conclude, in this study a surface characterisation of a wide range of polymeric AM surfaces, made of different AM technologies with different AM principles (fused filament, Polyjet, powder sintering), considering dimensional parameters and optimising the object of study to be suitable for both XCT and optical reference devices has been made. However, as in a single study is difficult to evaluate every individual case, further research should be done to achieve a fully generalised characterisation of this type of parts. For this future work, including non-planar geometries could be interesting to check the effect of form in surface roughness, due to the effect caused by the printing process. Micro XCT could be used also for a more precise evaluation; however, geometrical magnification could still be a disadvantage depending on the size of the part.

3.4. Closing remarks and future work

In this chapter, an investigation of the capability of XCT for the characterisation of surface texture of polymeric AM parts is done, conducting an experiment which consists in two separated stages that are linearly dependent. First stage has allowed to test the accuracy of the theoretical models employed for the design of the individual parts, and to select the most optimal for the evaluation in XCT. Second stage has been focused on the comparison between these XCT measurements with the reference device (FVM), evaluating its performance and obtaining a proper characterization of the surfaces made by different AM processes [37,38]

To summarize, with the studies described in this chapter, better knowledge concerning surface evaluation of polymeric AM parts has been obtained. Roughness in AM products is an intrinsic characteristic of the manufacturing process; on the other hand, AM is

capable of producing complex geometries which are only possible to evaluate by XCT. Therefore, being able to properly characterise this feature by XCT is a critical aspect. For future work in this field, further investigation in the characterization of surface roughness in non-planar features will be studied, to be able to apply this obtained knowledge for more complex features which could be found in any industrial AM product.

The work presented till this section of the thesis only consider polymeric features; however, as stated before, material density is an important factor in XCT, as settings should be adjusted, and results will vary. In the next chapter, the study has been focused on the introduction of metallic elements and the effect caused by them on the polymeric parts.

4. Attenuation in XCT evaluation of metal-polymer assemblies

In XCT measurements, device settings such as voltage, current, physical filter, etc. normally should be adjusted for each object in order to optimise this characterization, reduce artifacts and improve the accuracy of metrological quality control. It depends on the attenuation of the X-rays, which is directly related to the penetration length and the attenuation coefficient of the material; here, material density plays an important role. Denser materials such as metals have higher attenuation ratios and require higher beam energies, which can produce distortions in the volume such as metal artifacts and beam hardening.

In multi material assemblies, optimal evaluation is challenging, as settings cannot be accurately adjusted for all the materials, and therefore the possibility of the appearance of artifacts is higher; this is more critical if there is a big difference in material density, such as metal-polymer assemblies. Here, optimising parameters for the denser material (metal) could result in a loss of information in the lighter material (polymer); however, if the adjustment is for the polymer, X-rays may not be powerful enough to penetrate metal and the number of artifacts will increase significantly.

In this chapter, the investigation conducted on the attenuation effect on the dimensional accuracy of XCT evaluation of metal-polymer assemblies is presented. The chapter is divided in two different studies, each one independent, both using steel and aluminium elements for the experiments, as this metals are widely used in industrial products and have a high interest in research. In the first one (Section 4.1), the effect of the presence of metal in the evaluation of polymeric features is investigated, with the objective of evaluating the errors caused in dimensional measurements of different geometries and surface texture characterization. Results of these experiments are published in the article “On the effect of material density in dimensional evaluations by X-ray computed tomography of metal-polymer multi-material parts.” [140]. In the second one (Section 4.2), the concept of relative intensity (I/I_0), which has been stated previously by other authors [7] is introduced and the effect on XCT accuracy of its variation in metal-polymer assemblies is investigated.

Although the correlation between these two experiments is evident, results obtained are independent; therefore, each experiment is detailed in a separate section.

4.1. Effect of material density

As stated in the introduction of this chapter, in this section it is presented the study of the effects caused by metals in the evaluation of polymeric macro and micro features in metal-polymer assemblies by means of XCT. The aim is to have a first approach on the evaluation of metal-polymer combinations in XCT, to observe trends and possible error sources caused by metals in these type of assemblies.

4.1.1. Materials and methodology

In this section, a description of the study is presented, including its details and the scenarios planned, materials selected for each feature, methodology followed for the evaluation and simulations performed to complete the XCT measurements.

4.1.1.1. Experiments

As the aim of the experiments is to evaluate the effect of metals (high-density materials) in XCT measurements on polymers (low-density materials), various scenarios with different metal proportions have been planned:

- Assembly with no metal (scenario named NM).
- Assembly with metal inserts where polymeric parts are not directly covered. In this case, inserts are screws and bolts (scenario named Scr).
- Assembly with metal coverings that hide polymeric parts:
    - Low-density metal coverings – aluminium (scenario named Al) + steel screws.
    - High-density metal coverings – steel (scenario named St) + steel screws.

A test object has been designed according to the scenarios planned (see Figure 4.1). Moreover, the design was conceived to enable both XCT measurements and reference measurements using conventional metrological devices (see section 4.1.1.2 for more details on the reference measurements).

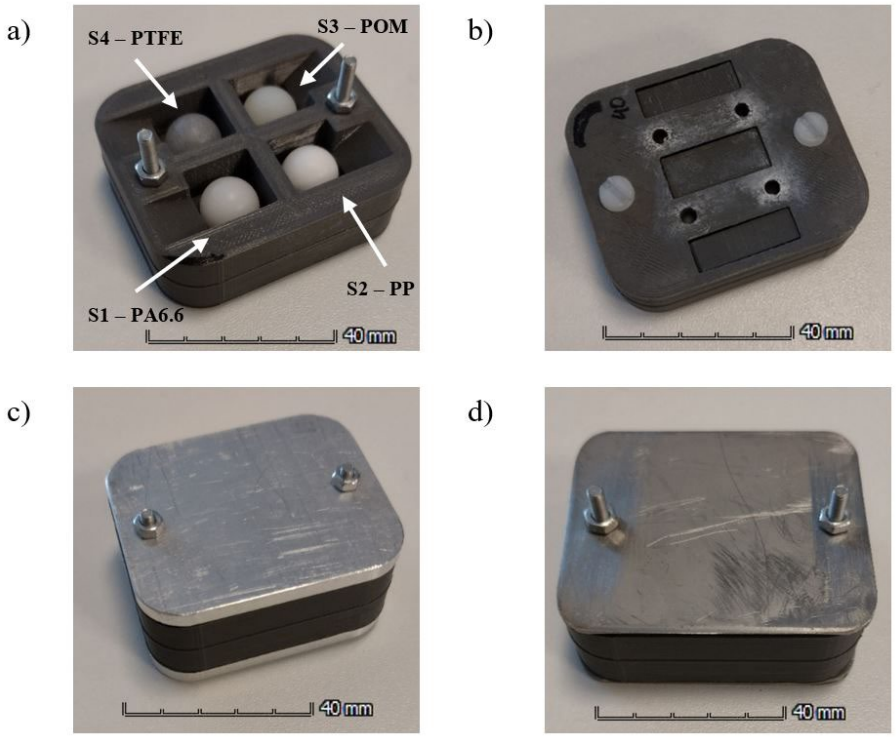

Figure 4.1. Metal-polymer assembly disposition. a) With metal inserts (upper view). b) No metal (lower view). c) Aluminium plates. d) Steel plates.

The main base is designed and manufactured in polyethylene terephthalate glycol (PETG) by FDM technology, with orthogonal shape and rounded corners, and general dimensions of 55 mm × 40 mm ×17 mm. The size of the assembly is intended to be as compact as possible but including large enough elements. The main base is divided into two halves to ease the reference measurements of the precision spheres; both parts of the base are mounted together for XCT evaluation.

Two sets of ramps are included in the base: four upper ramps, designed as a part of the upper base (Figure 4.1a), two with an angle of inclination of 20º and two with 40º, and three lower ramps, printed separately at an angle of inclination of 30º and stuck into the lower base (Figure 4.1b) in the holes designed for their placement. With this range of angles of inclination of the ramps (20º - 30º - 40º), and a constant layer thickness used for the manufacturing of the parts (0.15 mm), the expected surface texture (Ra, Sa) for the surfaces evaluated is in a range of 20 – 30 µm according to predictive models [37,38].

Four commercial precision spheres (with tolerances of Ø25 µm in diameter and 12 µm in form error) of 12 mm in diameter are located in the base as seen in Figure 4.1a, placed as vertices of a square with a distance of 18 mm between each sphere. Each sphere is made of a different polymeric material: polypropylene (PP), Nylon (PA6.6), polyoxymethylene (POM) and Teflon (PTFE).

Two types of metal coverings are designed: aluminium plates (low-density metal, thickness of 3.85 mm) and steel plates (high-density metal, thickness of 2 mm) with the same shape as the main base. For each scenario, two metallic parts of the same material are used (one placed over the upper base and one placed under the lower base).

Screws and bolts are used for fixing the assembly. The material used for the fixture objects included in the no-metal assembly is PA6.6, while in the rest of the scenarios the chosen material is steel. In the assembly with metal inserts, screws and bolts also play the role of metal inserts. In Figure 4.2, the distribution of the elements in the CAD model is shown.

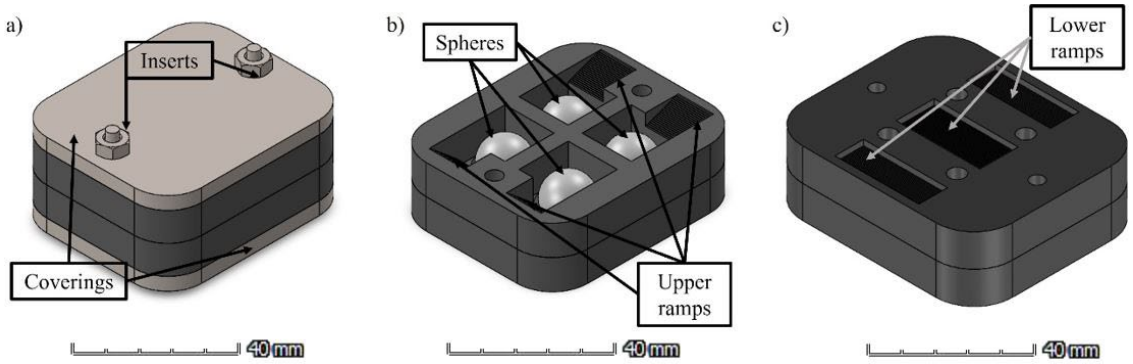

Figure 4.2. CAD model and element distribution. a) Complete assembly. b) Top face. c) Bottom face.

In Table 4.1, a summary of the materials used for each part and its density is presented.

Table 4.1. List of materials used and corresponding density.

Material	**Parts**	**Density (g/cm^3)**
Polyethylene terephthalate glycol (PETG)	Main base, polymeric screws/bolts.	1.27
Polypropylene (PP)	1 precision sphere (S2)	0.87
Nylon (PA6.6)	1 precision sphere (S1)	1.11
Polyoxymethylene (POM)	1 precision sphere (S3)	1.37
Teflon (PTFE)	1 precision sphere (S4)	2.16
Aluminium (Al)	Metal plates	2.70
Steel	Metal plates, metal screws and bolts.	7.85

4.1.1.2. Evaluation

In Figure 4.3, a summary of the workflow followed for the measurements is shown.

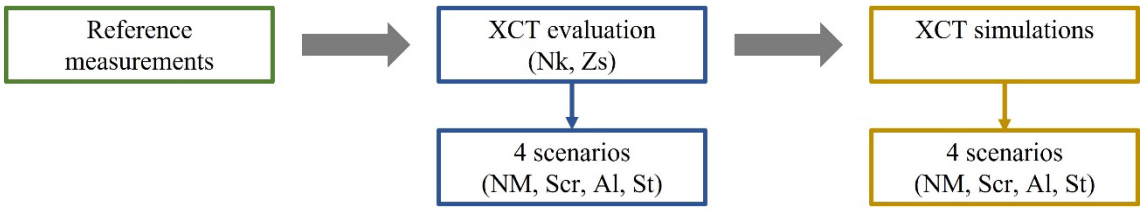

Figure 4.3. Methodology workflow followed in the experiment.

Reference measurements have been taken prior to XCT evaluation:

- Spheres were measured by a coordinate measuring machine (CMM) ZEISS PMC-876 CNC, with a 3 mm in diameter spherical ruby probe. Expanded uncertainty results registered are in a range of U_{CMM} = 2.4-2.6 µm for diameters and distances and U_{CMM} = 2.1-2.2 µm for spheres form error.
- Ramps have been characterized by a focus variation microscope InfiniteFocusSL of Alicona. A 10× magnification lens was used, with a lateral resolution of 8 µm and a vertical resolution of 130 nm. STL files were exported for each ramp. Expanded uncertainty results registered are in a range of U_{FVM} = 2-3 µm for *Sa* parameter.

Two different devices have been used for the XCT measurements: a Zeiss Metrotom 1500 (Zs in the results) and a NikonMetrology MCT225 (Nk in the results). Performance verification of the devices has been done according to the guideline VDI/VDE 2630 Part 1.3 [60]; this protocol, along with the geometrical and thermal stability systems present in both devices, ensures that scaling errors are minimized, preventing unnecessary re-scaling of the voxel size [141]. Settings were optimized and three iterations have been performed for each device and for each scenario; values are presented in Table 4.2.

Table 4.2. Parameters used for each XCT measurement.

Parameter	**Nk NM**	**Nk Scr**	**Nk Al**	**Nk St**	**Zs NM**	**Zs Scr**	**Zs Al**	**Zs St**
Voltage/kV	130	215	215	220	140	140	195	175
Current/µA	108	75	75	73	410	410	294	328
Physical filter	-	Cu 0.5 mm	Cu 0.5 mm	Cu 0.85 mm	Al 2.0 mm	Al 2.0 mm	Cu 0.75 mm	Cu 0.75 mm
Projections	1500	1500	1500	1500	1500	1500	1500	1500
Exposure time/ms	1000	1420	1420	2000	500	500	500	500
Voxel size/µm	36.02	36.02	36.02	36.02	47.56	47.56	47.56	47.56

Post processing has been performed with the software VG Studio Max 3.4.2 (Volume Graphics GmbH, Germany). First general surface determination (SD) has been made in Advanced – multi material mode, with a differentiation between polymers in no metal scenarios and differentiation between polymers and metals in the rest of the cases; a search distance equal to 4 times the voxel size has been selected. Regions of interest (ROIs) have been created for each element (4 spheres, upper ramps lower ramps) and a second local SD for each ROI has been done using the same parameters. Multi material differentiation has been made in local SD when applicable. Uncertainty estimations have been done according to guidelines (see Section 4.1.2.3 and VDI/VDE 2630 Part 2.1).

In addition to the XCT measurements, XCT simulations have been performed by the software aRTist 2.12 (BAM, Germany). One simulation has been made for each scenario (see Section 2.1). Settings of the simulations have been used also to adjust the parameters utilized for scanning with the Nikon Metrology MCT225 system, as it was possible to access directly to the device; on the other hand, as Zeiss tomographies have been made in an external laboratory, not all necessary data to simulate the process were available.

The selected elements of the simulation results are the diameters, distances and form errors of the spheres, which have been evaluated and compared to the real XCT results.

4.1.2. Results and discussion

In this section, details of the results obtained in the evaluation are presented, including general remarks about the tomographies and the contrast between materials, results related to the spheres measurements and surface texture characterisation. Finally, discussion of the results is added in Section 4.1.2.8.

4.1.2.1. Image contrast

In Figure 4.4, 2D slices of each XCT scenario are displayed. Slices are longitudinal to the ramps and focused on the central ramp and fixtures (screws and bolts).

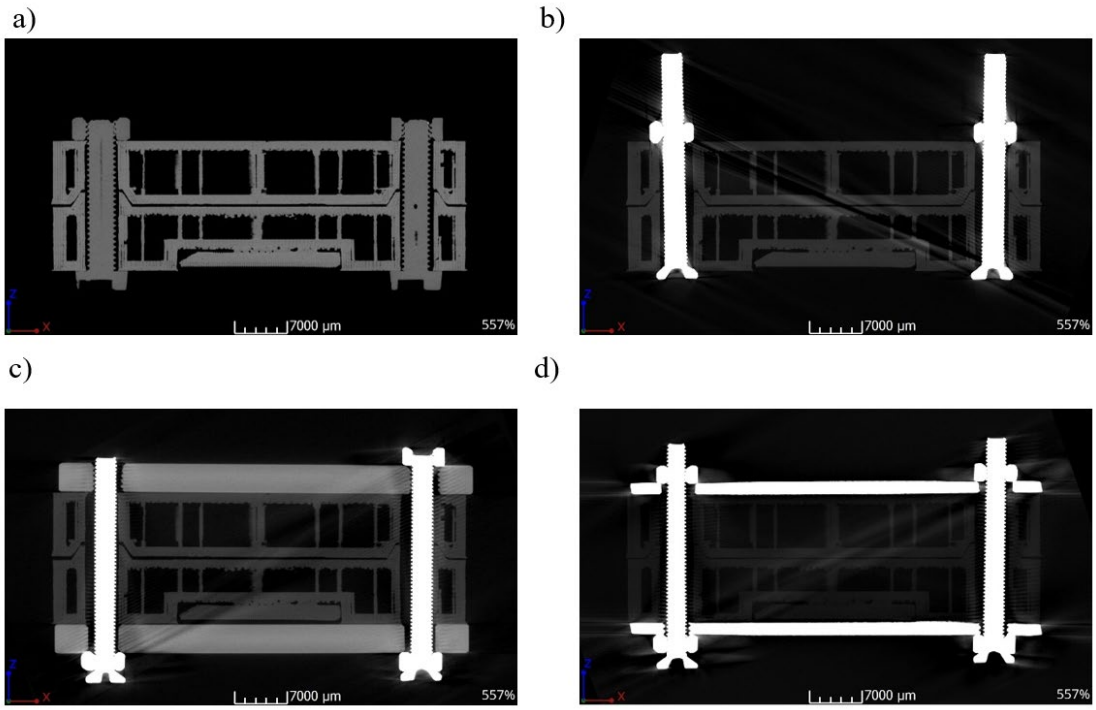

Figure 4.4. X-ray slices of XCT reconstruction. a) No metal. b) Steel inserts added. c) Aluminium coverings. d) Steel coverings.

The contrast between denser elements (brighter) and lighter parts (darker) is shown in Figure 4.4. Contrast between background and polymer is clear in no metal (NM) scenario (Figure 4.4a). High metal artifacts and noise levels were found in the assembly with steel coverings (St) (Figure 4.4d), creating difficulties to differentiate between background and polymer. In the remaining tomographies (Scr, Al), the presence of metal has less impact in the contrast background – polymer, therefore allowing to observe and characterise the threshold with an acceptable clearance.

To numerically validate the trend suggested by the X-ray slices, contrast-to-noise ratio (CNR) has been calculated from the grey value data obtained in software VG Studio Max 3.4.2 (Volume Graphics GmbH, Germany), following the procedure described in [142], using Eq. 6:

$$CNR = \frac{|A_{Material} - A_{Background}|}{\sqrt{\sigma^2_{Material} + \sigma^2_{Background}}} \quad (6)$$

where $A_{Material}$ and $\sigma_{Material}$ represent the mean and standard deviation of the material ROIs, respectively; $A_{Background}$ and $\sigma_{Background}$ represent the mean and standard deviation of the background ROIs, respectively.

In Table 4.3, CNR values and peak difference (material-background) obtained for the grey value analysis of the polymeric base (ROI of the material separated from the metal)

Table 4.3. CNR results for polymeric ROIs in each scenario.

Scenario	**Peak difference (A_M-A_B)**	**CNR**
NM	2793.33	2.18
Scr	1021.37	2.13
Al	1638.92	2.01
St	1162.31	0.92

Results confirm that contrast between polymer elements and background (air) is significantly lower in scenario with steel coverings (St). Values found in the rest of scenarios are similar, observing slight less contrast in Scr and Al scenarios; this suggests that presence of a higher amount of steel affects considerably the quality of the tomographic reconstruction, but it is not the case of aluminium.

4.1.2.2. Spheres – numerical comparison

Diameter, form error and distances between spheres have been obtained and compared, registering mean values of the measurements for each feature. A search distance has been established for all macro geometries in 200 μm. A quality threshold of 2σ (95%) of the points registered has been used, to reduce overestimation of form errors caused by aberrations. For graphics of diameters and form errors, density has been considered for comparison in the x axis; a vertical red line has been included in diameters and form errors graphics representing the density of the material of the base (PETG).

A summary of the absolute form error of the four spheres for each scenario and each evaluation is shown in Figure 4.5, including the results obtained by using the CMM and results obtained by simulations. Deviations of XCT diameter values from CMM measurements are shown in Figure 4.6, and deviations of XCT distances between spheres values from CMM measurements are shown in Figure 4.7.

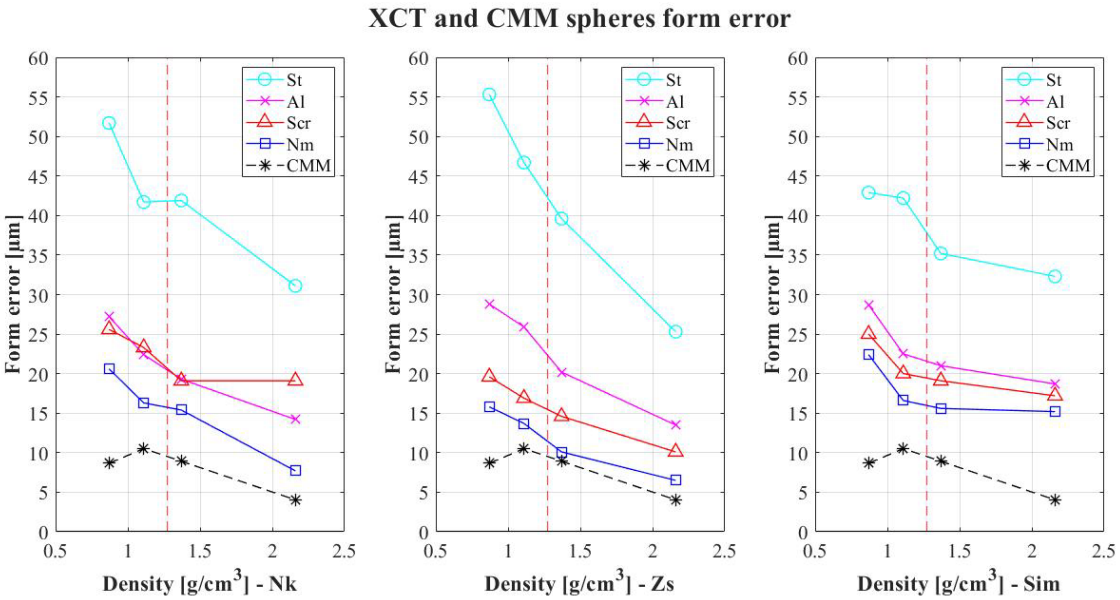

Figure 4.5. Form error of polymeric spheres for each scenario in XCT measurements, simulations and CMM.

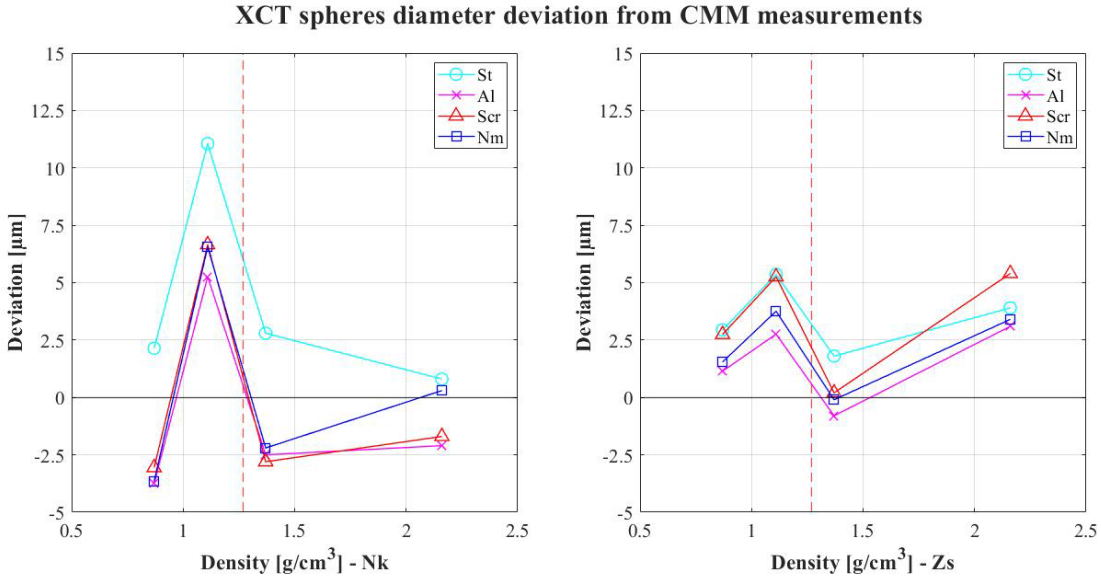

Figure 4.6. Mean deviations of diameters and distances from NM scenario.

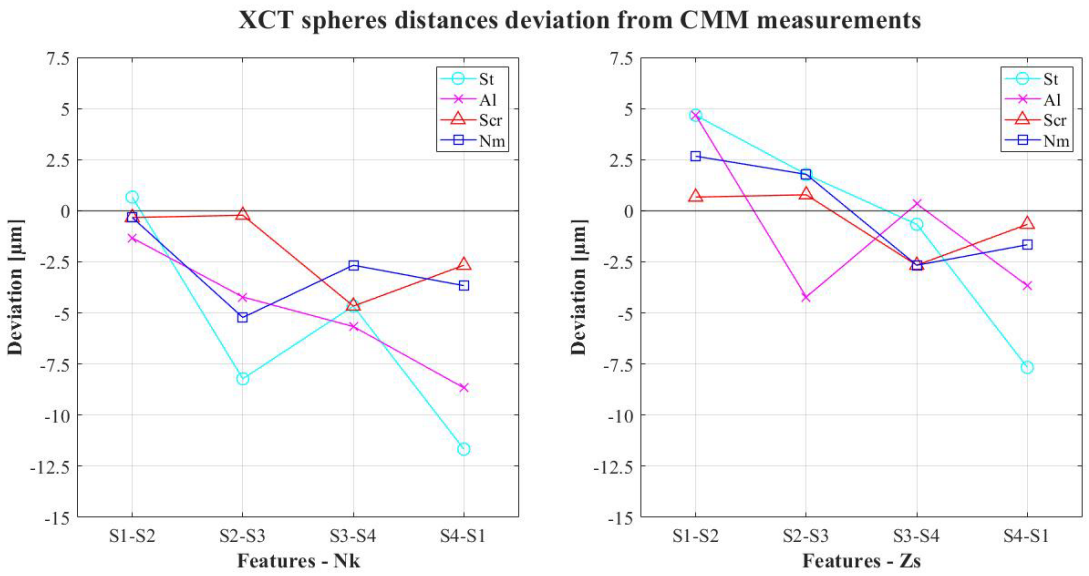

Figure 4.7. Deviation of XCT measurements of distances between spheres from CMM measurements.

Higher form errors were found in scenarios with higher amount of metal, mainly in St scenario (steel fixtures and plates). A trend is also observed regarding the density of the sphere's material: as the density increases, form error decreases. It suggests that even for the NM scenario where noise is significantly lower, differences in density between materials causes that an optimisation of XCT settings favours the denser material, at least for highly surface determination dependant features as form error. This tendency is not observed in diameters and distances; similar results are obtained in each sphere for diameters, while the deviations distribution for distances seems more random. The reason is that both diameters and distances are not as dependant on surface determination and external noise as form error. Simulations also confirm such observations; but results in simulated and real tomographies are slightly different. Distances and diameters obtained in simulations are not used for comparisons, as in simulation the object measured is the CAD model and, therefore, manufacturing deviations of the real part are not considered.

Regarding reference measurements, higher form error in XCT is found compared to CMM. Different measuring principles are used for each technology; XCT surface determination allows to obtain a more detailed characterisation of the features in terms of points acquired while accuracy of the measurements is better for CMM since uncertainties are in general lower. Profile filtration is also different: CMM resolution is limited by the diameter of the probe [143], causing a mechanical filtering when reaching deep valleys of the surface, while in XCT it is limited to the achieved magnification (voxel size).

4.1.2.3. Spheres – measurement compatibility and uncertainty calculations

For the evaluation of the measurement compatibility between XCT and CMM measurements, the E_N parameter is calculated, according to standard ISO/IEC 17043:2023 [98], following Eq. 7:

$$E_N = \frac{|y_{XCT} - y_{CMM}|}{\sqrt{U_{XCT}^2 + U_{CMM}^2}} \quad (7)$$

Where y_{XCT} = current measured value of the feature, y_{CMM} = reference value of the feature, U_{XCT} = expanded uncertainty of the XCT measurement and U_{CMM} = expanded uncertainty of reference value. Results are considered valid for $E_N \leq 1$ as stated in the standards.

Uncertainty calculations have been done following the procedures indicated in standards:

- ISO 15530-3:2011 [91] for reference CMM measurements. Expanded uncertainty results registered are in a range of U_{CMM} = 2.4-2.6 µm for diameters and distances and U_{CMM} = 2.1-2.2 µm for spheres form error.
- VDI/VDE 2630-2.1 [67] for XCT measurements, also following the recommendations suggested in [139]. This standard is commonly used for this type of measurements [66,93]. Expanded uncertainty results registered are in a range of U_{XCT} = 12-13 µm for diameters and distances and U_{XCT} = 6-7 µm for form error.

For both devices, coverage factor for the expanded uncertainty calculations is k = 2 for a 95% confidence interval.

In Table 4.4, E_N results obtained for each feature and in each scenario are shown. Features evaluated are diameters (*Sx*), form errors (*EFx*) and distances (*Sx-Sx*).

Table 4.4. E_N parameter for each feature and scenario.

	Zs				**Nk**			
Feature	**NM**	**Scr**	**Al**	**St**	**NM**	**Scr**	**Al**	**St**
S1	0,31	0,43	0,22	0,42	0,55	0,55	0,42	0,89*
S2	0,13	0,22	0,10	0,36	0,34	0,25	0,29	0,17
S3	0,01	0,02	0,05	0,16	0,17	0,24	0,21	0,22
S4	0,28	0,44	0,26	0,32	0,01	0,14	0,18	0,06
EF1	0,47	0,93*	**2,27**	**5,45**	0,78*	**1,38**	**1,27**	**4,58**
EF2	**1,05**	**1,60**	**2,95**	**6,83**	**1,63**	**1,93**	**2,14**	**6,33**
EF3	0,17	0,83*	**1,64**	**4,48**	0,92*	**1,13**	**1,12**	**4,84**
EF4	0,36	0,89*	**1,40**	**3,15**	0,53	**1,77**	**1,16**	**3,99**
S1-S2	0,20	0,07	0,32	0,32	0,03	0,03	0,10	0,10
S2-S3	0,13	0,06	0,31	0,16	0,34	0,04	0,34	0,66
S3-S4	0,15	0,17	0,01	0,03	0,17	0,34	0,39	0,37
S4-S1	0,15	0,05	0,30	0,61	0,27	0,20	0,64	0,84*

Values of $E_N > 1$ are highlighted in bold, as they are not considered acceptable; also, values of $0.75 < E_N < 1$ are marked with an asterisk because although values are valid, they approach 1.0 and therefore have to be taken with caution. Results show that all values for diameters and distances are valid and almost all are not close to 1, while in form errors only NM scenarios have valid results. However, *EF2* show higher E_N value mainly because, as shown in Figure 4.5, it has higher form error due to its lower density. Also, E_N value increases for scenarios with higher amount of metal, which is related with higher form errors as stated in Section 4.1.2.2.

4.1.2.4. Spheres – material differentiation

In Figure 4.8, grayscale histograms of the ROI of the four spheres in each scenario are displayed. Each peak is labelled in Figure 4.8a with its corresponding sphere.

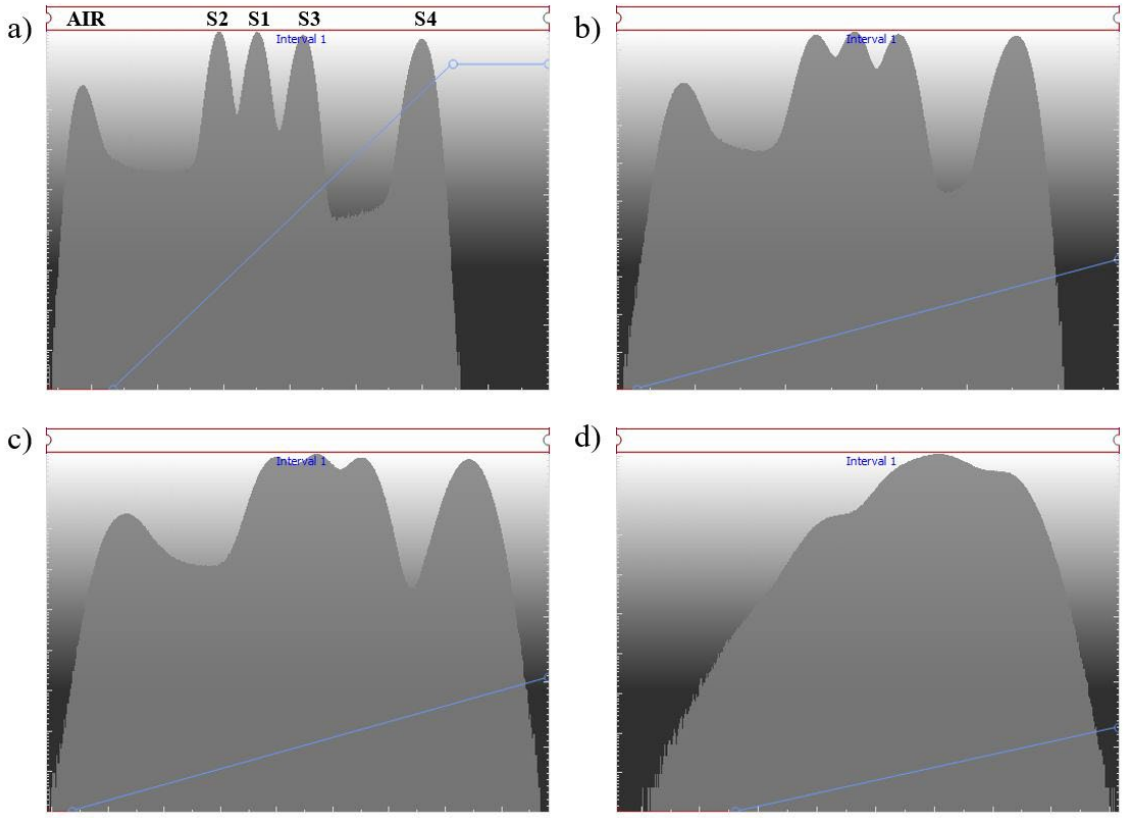

Figure 4.8. Grayscale histograms of spheres' ROI. a) NM. b) Scr. c) Al. d) St.

Histograms of ROI extracted of the four spheres show a variation on the distribution of the grey values: the more metal is present in the tomography, the more diffused is the boundary between the peaks of the materials; the most extreme case is St (Figure 4.8d) where even the background peak is not distinguishable. This clearly indicates that the denser material decreases the contrast between the lighter materials. However, a good polymer differentiation is possible with the presence of a certain amount of metal in XCT evaluation. As the density of aluminium is significantly lower than the density of steel, it affects less to the characterisation of the geometries, as seen in Figure 4.4.

4.1.2.5. Ramps – surface comparison and irregularities

For each XCT measurement, STL files are extracted from each surface and false colour height maps of an 8x8 mm area are created. Examples of this features are displayed in Figure 4.9a for NM scenario, Figure 4.9b for Scr scenario and Figure 4.9c for Al scenario. Noise created by steel inserts and coverings in XCT evaluation made not possible to obtain proper surfaces of the ramps in St scenario.

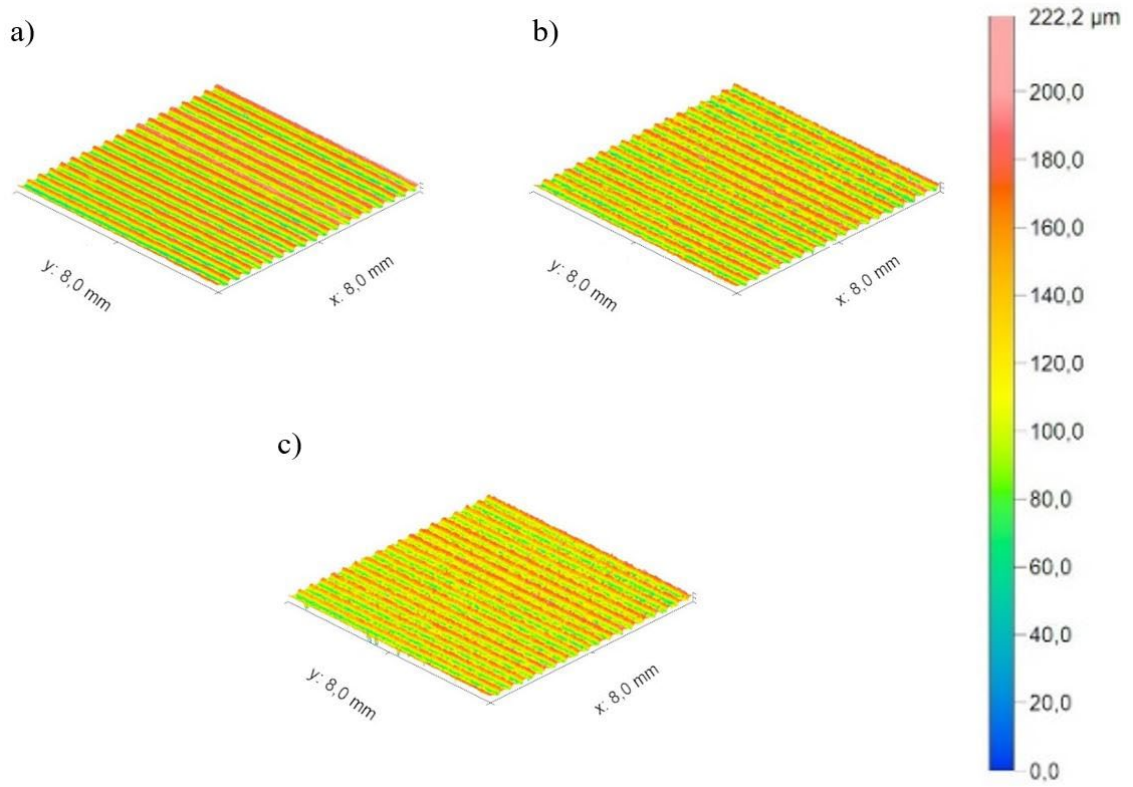

Figure 4.9. False height colour maps of STL extracted. a) NM. b) Scr. c) Al.

Ramps displayed have an angle of inclination of 30º. Irregularities in the surface extracted become more evident when the metal quantity is increased in the assembly. For a more detailed analysis, individual profiles of each STL shown previously are extracted and displayed in Figure 4.10.

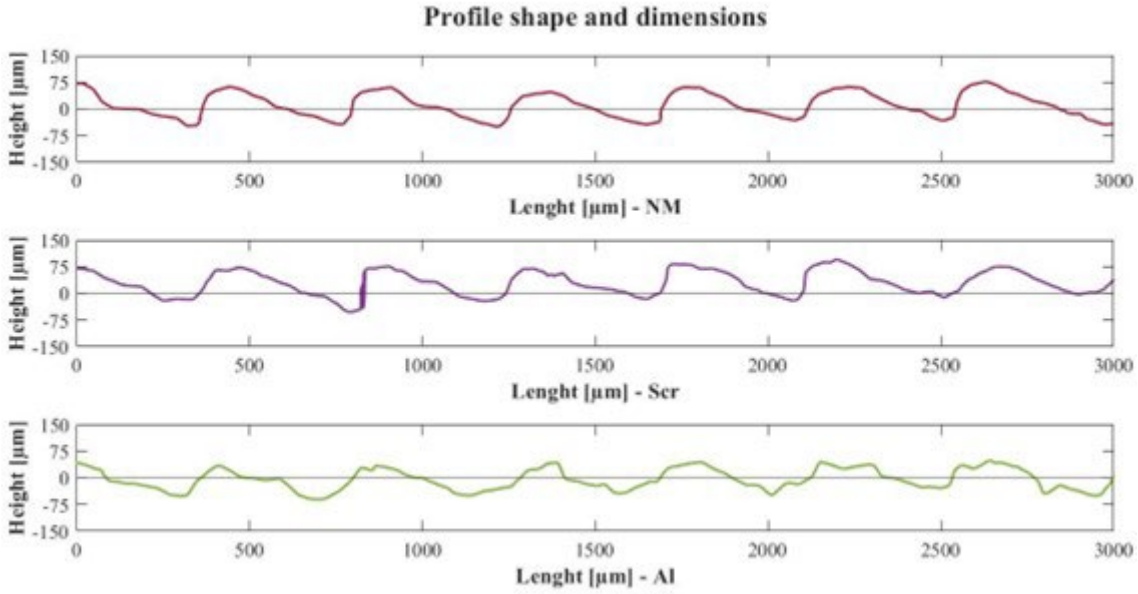

Figure 4.10. Individual profiles extracted from the ramps' STL.

When observing profiles, it is clearer that the shape is more irregular for metal scenarios (Scr and Al). However, peaks and valleys remain visible, suggesting that

although the presence of noise in the tomographies, profiles for surface texture evaluation are feasible to obtain. To verify it, surface texture parameters *Sa*, *Sq* and *Sz* have been computed.

4.1.2.6. Ramps – reference measurements

A first evaluation of the parts has been done with the FVM reference device (see Section 4.1.1.2). XCT scenario selected for the comparison has been NM (no metal), as no distortion caused by metals is present. Areal parameters used for the numerical comparison of ramps have been *Sa*, *Sq* and *Sz*.

Three areas of 4x4 mm along each ramp have been measured. L-filter nesting index (hi-pass filter) of 2.5 mm and a S-filter nesting index (low-pass filter) of 8 μm were selected according to standard UNE-EN ISO 25178-3:2012 [25].

As the nominal parameters' values of each ramp are different, percentual deviations have been calculated to equalize the results. Reference measurements are shown in Figure 4.11.

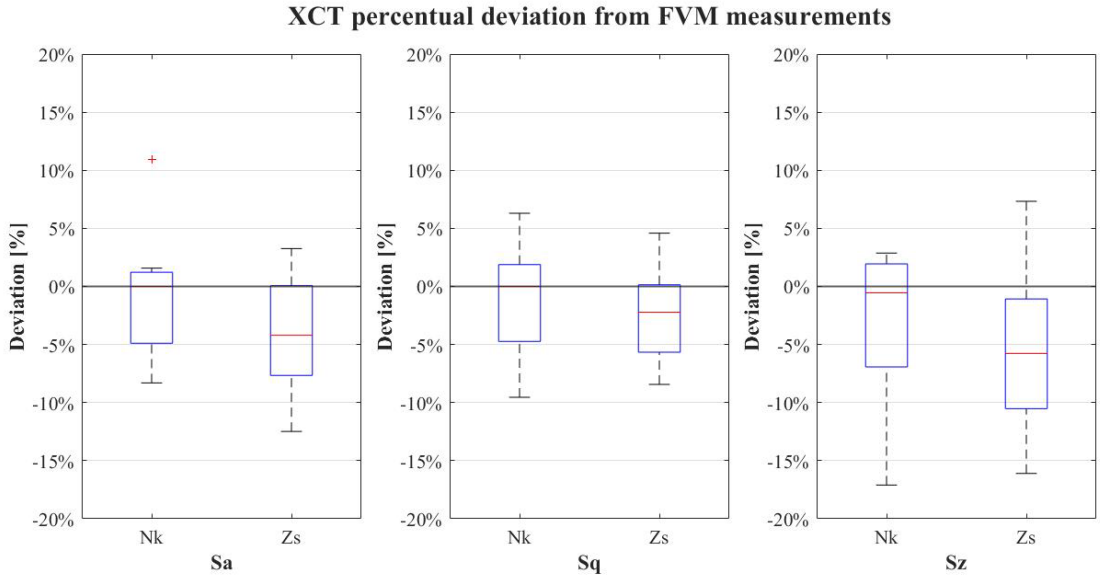

Figure 4.11. Mean values of inclined ramps deviations from reference measurements.

Sa and *Sq* values follow the same trend in both devices, having found a negative difference in Zeiss machine. The main reason is the slightly worse geometrical magnification obtained which is a consequence of the geometrical conditions of the device, causing a less precise resolution and, therefore, smoother surfaces; however, negative deviations are not too high (in the range of 10-15% maximum). Deviations found in *Sz* values are higher, more randomly distributed and almost all negative; this indicates that some peaks/valleys have not been characterised properly as expected by XCT due to

its lower resolution than FVM (in both XCT devices). However, as the main objective is to compare different XCT scenarios mutually, this comparison XCT-FVM has been done just to be aware of possible errors that occur in the main scenario (no metal, NM).

4.1.2.7. Ramps – surface texture comparison

As stated in Section 4.1.2.6, to equalize the results of all ramps, percentual deviation from reference scenario (NM) has been calculated. Nikon device results are shown in Figure 4.12 and Zeiss device results are shown in Figure 4.13.

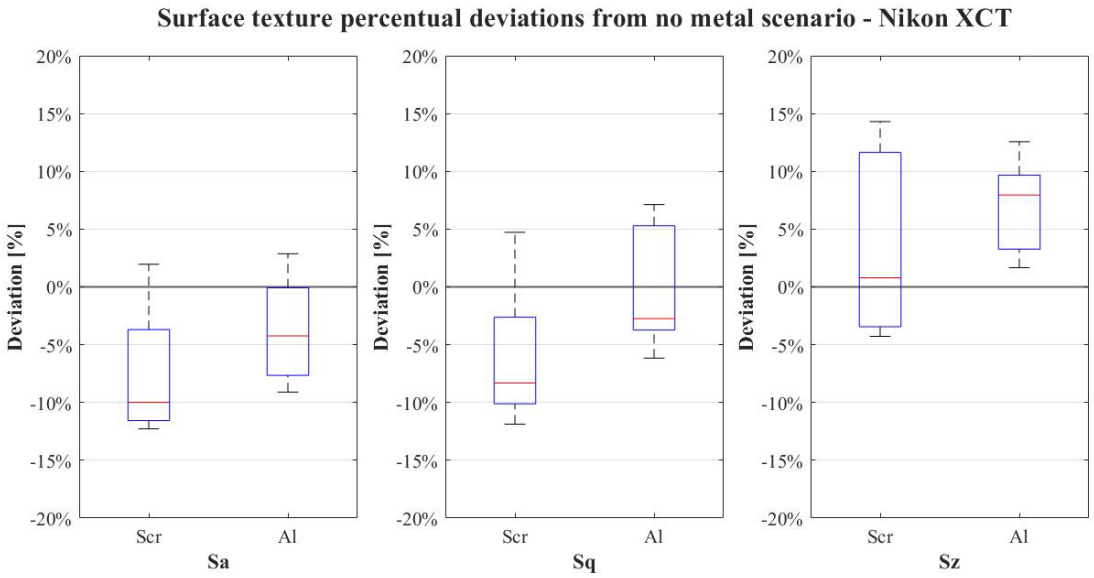

Figure 4.12. Nikon device XCT surface texture results.

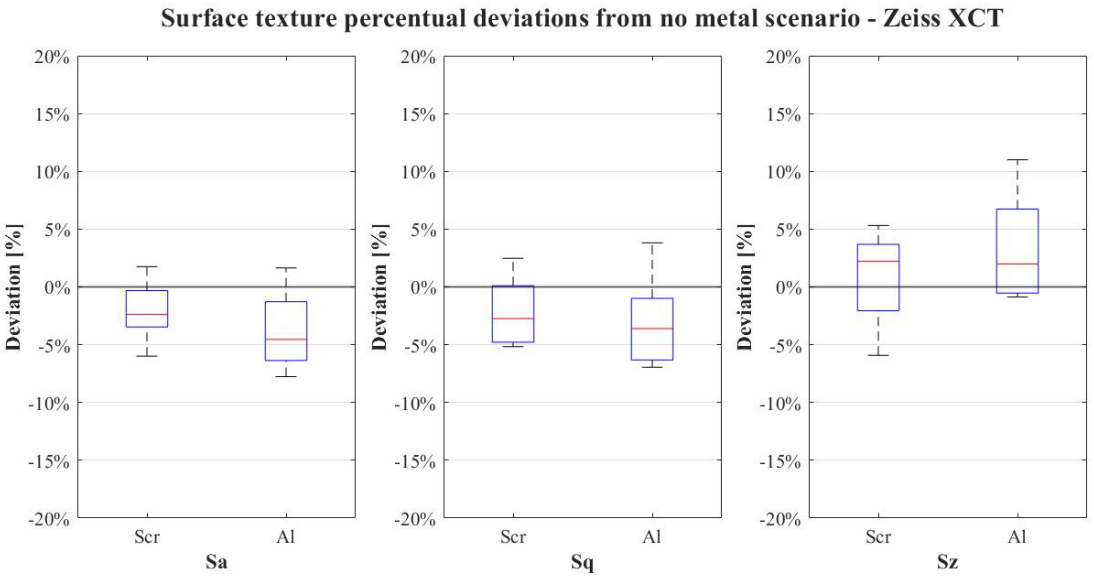

Figure 4.13. Zeiss device XCT surface texture results.

Results show that maximum deviations in *Sa* and *Sq* are in the +/- 15% range for both scenarios, and are slightly higher for Al. It indicates that amplitude of the surface texture

profile is not highly affected by the noise created by metal added, and therefore with the same resolution of the XCT evaluations (geometrical magnification), acceptable values of average surface texture may be obtained. Regarding *Sz*, as irregularities are present in the ramps in scenarios with metal, errors such as empty regions or spikes could appear and create more random variations in the results since this parameter is much more sensible to abrupt changes in the surface.

4.1.2.8. Discussion

In general, results show a correlation between less accurate surface obtained on the polymeric features by XCT and quantity of metal present in the XCT characterisation. Numerical results show higher deviations in features where surface determination has a high influence (as form error and maximum surface texture *Sz*); however, for diameters, distances and average values of surface texture (*Sa*, *Sz*), whose value is more independent to the obtained surface, variations found are in an acceptable range according to the measurement comparability parameter calculation (E_N) based on uncertainty calculations.

Focusing on highly influenced parameters, it is clear that noise created by the presence of metal artifacts in the XCT characterisation affects the variations in both form error and maximum surface texture *Sz* proportionally. Scenario with steel plates has been the most conflictive to obtain a proper surface determination: spheres evaluation has been possible with important distortions, while boundaries between ramps and background were not sufficiently clear to adequately extract the features. Logical reason is the high density of the metal and the high contrast with the polymers, and low contrast between polymer and air. Nevertheless, it has been demonstrated that when the amount of steel is not high (as in Scr and Al scenarios, where steel is only present as inserts), the level of noise and artifacts does not prevent from obtaining accurate dimensional results. Other important aspect is that, for this moderate quantity of metal, it has been possible to differentiate between polymers with similar density with an acceptable accuracy (Figure 4.8).

On the other hand, influence of aluminium has been much lower. Al plates create distortions, but the influence of the steel inserts was higher; differences between Al and Scr scenarios were much lower than between Scr and NM. This suggests that the lower density of this material comparing to steel and its closer value to the polymers' density are the main reasons for these results.

Additionally, it has been found that density of the polymer also creates different deviations in the spheres, as the optimisation of the XCT parameters for the correct

measurement of polymers also favour the denser ones. All tomographies follow the same trend; the lighter is the polymeric material, the higher is the form error in the sphere.

4.1.3. Conclusions

In this paper, an evaluation of the influence of denser materials such as metallic parts on dimensional measurements by XCT of polymeric features in metal-polymer assemblies is presented. Polymeric macro and micro geometries are included as test elements in an ad hoc designed test object, previously measured with reference devices, and four different scenarios have been planned with variations in the amount and type of metal present (considering aluminium and steel for the study). The objective of the workpiece design has been to i) simplify the design and to ii) equalize the number of projections affected by metal elements. As the aim is to evaluate exclusively the differences in the results of dimensional evaluation of polymeric features produced by the introduction of metallic elements, XCT parameters and post processing of the reconstructed volume has been optimized for each scenario as it is usually done in common XCT measurements.

Results quantified the correlation between the amount of metal present in the assembly and the deviations of the XCT evaluation with respect to the no metal scenario. These deviations are more relevant for objects that are sensible to changes in surface determination: spheres' form error and maximum surface texture *Sz*. Diameters, distances and average surface texture (*Sa* and *Sq*), as less surface-dependent features, are less affected by the variations caused by metals. Visually, it is possible to observe the irregularities created in the surface extracted from the inclined ramps; this confirms together with the dimensional macro and micro evaluation the higher deviations caused by metals.

Due to its high density difference, and therefore high attenuation coefficient, increasing the amount of steel significantly hinders the surface determination of the polymeric features, creating a high amount of noise and image artifacts that amplify form error evaluated on the spheres and it makes impossible to characterise properly the ramps. On the other hand, good results have been achieved in Scr and Al tomographies (steel inserts and steel inserts with Al coverings, successively), even being able to differentiate between polymers with similar densities. It indicates that aluminium effect on the polymeric parts is lower, mainly because its attenuation is also lower than steel. Also,

lighter polymers in multi-polymeric assemblies are affected by the noise created by denser polymers, even though the effect is smaller.

With this investigation, better knowledge regarding metal influence on the evaluation of polymeric macro and micro geometries is provided. Although this study is focused on a particular designed test object, some tendencies are identified but results may vary for different configurations, geometries, amount of metal and materials used.

4.2. Influence of relative intensity variation

As stated in the introduction at the beginning of this chapter, in this section is presented the effect of the variation of relative intensity (I/I_0) in the dimensional evaluation by XCT of metal-polymer assemblies. The concept of relative intensity is directly related to the energy of the beam source [144], the penetration length [52,145] and the attenuation coefficient of the material. Theoretically, the lower the relative intensity that reaches the detector is, the poorer the quality of the tomography is and, hence, more defects will appear. The final aim of this experiment is to verify the level of correlation between relative intensity and XCT quality, which could help to simplify the setting adjustment in future metal-polymer multi material XCT measurements.

4.2.1. Materials and methods

In this section, the description of the procedure for the I/I_0 calculations, the design of the test objects based on the attenuation curve and the methodology followed to perform the experiments are presented.

4.2.1.1. Attenuation curve

Main objective of this study is to find a correlation between I/I_0 and dimensional accuracy in XCT; therefore, first step is to design an appropriate experiment in which this parameter could be monitored.

For this purpose, attenuation curve is necessary to be described for the selected materials (St and Al). Described by Beer-Lambert law [7], each material has its own attenuation curve, which is calculated by the following Eq. 8:

$$I = I_0 \cdot e^{-\mu x} \tag{8}$$

Where I = intensity received by the detector, I_0 = intensity emitted μ = linear attenuation coefficient of the material and x = penetration length.

XCOM database from NIST [146] has been utilized for the obtention of mass attenuation coefficients (μ_m), which is used for the calculation of linear attenuation coefficients (Eq. 9):

$$\mu = \mu_m/\rho \tag{9}$$

Where ρ = density of absorbing material. Mass attenuation coefficient curves for the materials employed in this experiment are displayed in Figure 4.14.

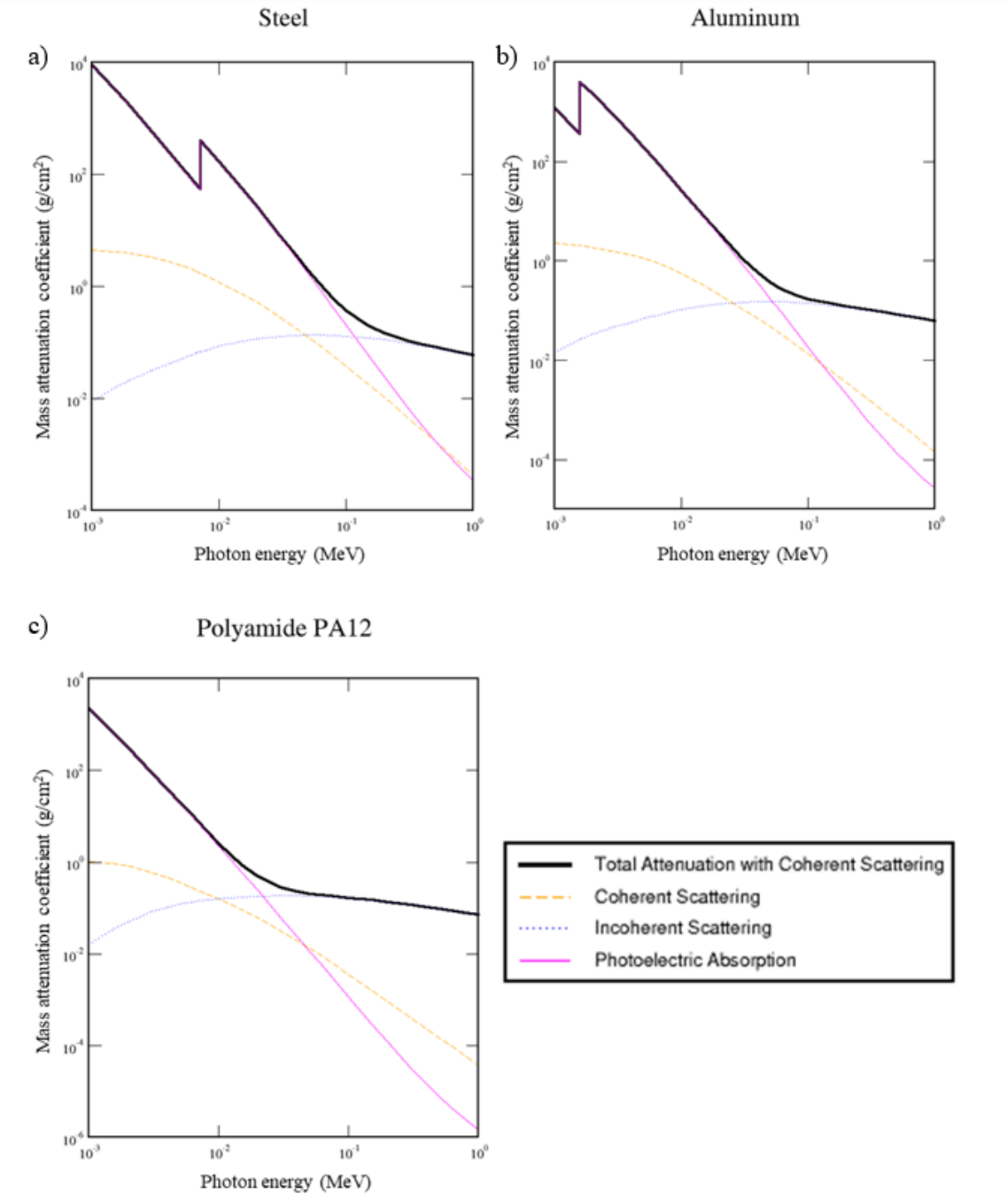

Figure 4.14. Mass attenuation coefficient curves for the materials used. a) Steel. b) Aluminium. c) Polyamide PA12. Curves are based on the data obtained from NIST database XCOM [146].

In this graphics, mass attenuation coefficients (which are obtained from the total attenuation with coherent scattering curve) vary depending on the average energy (E_{av}), parameter obtained from the characteristic energy spectrum of the tube, which consequently modifies the linear attenuation coefficient differently for each material and also the attenuation curve. Characteristic energy spectrums have been obtained using software SPEKTR 3.0 [147], introducing the voltage and physical filter selected for each scenario (see Section 4.2.1.2) and calculating the corresponding E_{av}. An example of the attenuation curves calculated for St and Al in two different values for E_{av} are displayed in Figure 4.15.

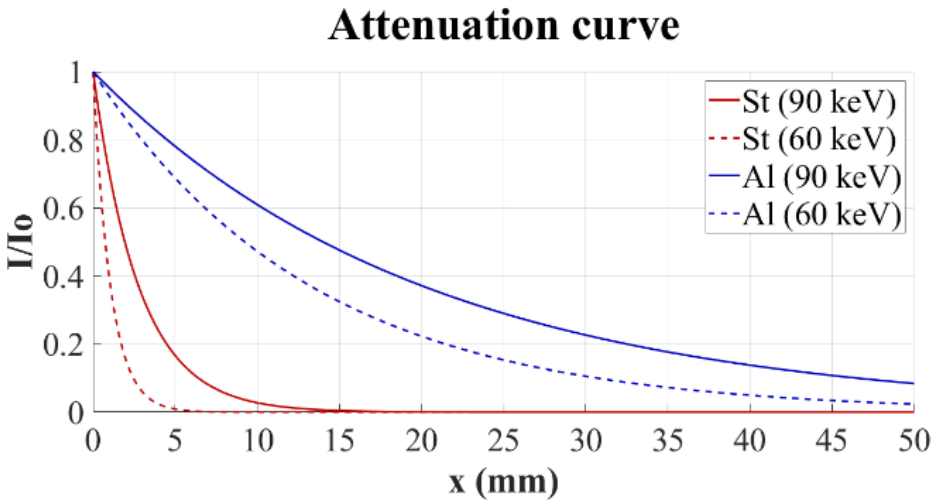

Figure 4.15. Attenuation curve for St and Al for 2 examples of E_{av} values.

It is shown that attenuation strongly varies for each material, while slight modifications occur depending on the average energy obtained. Four theoretical values of I/I_0 have been selected for the experiment. Based on the study of Villarraga et. al. [7], $I/I_0 = 0.08$ and $I/I_0 = 0.16$ have been chosen, amplifying the experiment to $I/I_0 = 0.24$ and $I/I_0 = 0.48$ to obtain results at different points of the curve.

4.2.1.2. Test object design

An ad hoc test artefact has been designed to perform the experiment, consisting in a polymeric base made in polyamide PA12 by selective laser sintering (SLS), with four Ø12 mm cylinders placed in a square disposition (distanced 12 mm one to another) and various metallic hollow cylinders which are switched from case to case. External diameter of metallic cylinders varies according to the I/I_0 calculations; thickness of the cylinder will vary according to the attenuation curve and the I/I_0 aimed. In Figure 4.16, rest of relevant dimensions of the assembly are presented.

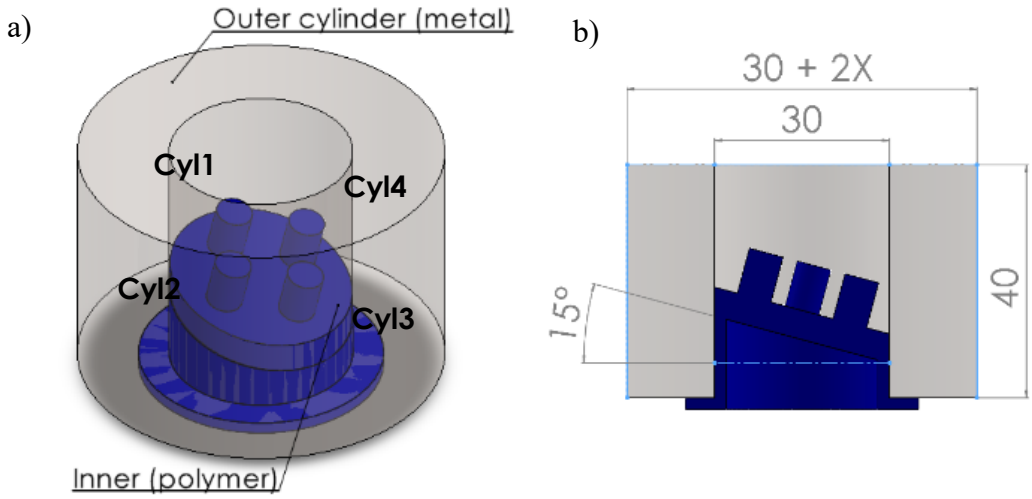

Figure 4.16. Test object design. a) Assembly disposition. b) Relevant dimensions (in mm).

Here, x is the penetration length derived from the previously calculated attenuation curves. An adjustment of E_{av} and x is done for the obtention of each I/I_0, through the modification of hollow cylinder thickness and XCT related settings (voltage, current and physical filter). In Table 4.5, a summary of penetration length and average energy selected for the obtention of each I/I_0 situation is displayed, along with the XCT settings used for the obtention of the selected E_{av}.

Table 4.5. XCT settings and attenuation parameters for each scenario.

I/I₀	**Al**					**St**				
	x (mm)	*E_{av} (keV)*	*Voltage (kV)*	*Filter (mm)*	*Vx (µm)*	*x (mm)*	*E_{av} (keV)*	*Voltage (kV)*	*Filter*	*Vx (µm)*
0.08	40	73	190	Al 2.0	47.47	8	96	195	Cu 1.0	47.47
0.16	**30**	**73**	**190**	**Al 2.0**	**47.47**	**6**	**96**	**195**	**Cu 1.0**	**47.47**
0.24	**20**	**63**	**160**	**Al 2.0**	**47.47**	**4**	**92**	**195**	**Cu 0.75**	**47.47**
0.48	10	60	160	Al 1.0	47.47	2	88	190	Cu 0.75	47.47

Penetration length and, consequently, thickness of hollow cylinders has been rounded to an integer number to optimize the manufacturing of the test parts; from this starting point, XCT settings were adjusted for their correspondent E_{av} (modifying voltage and physical filter) aiming to approximate as much as possible the real I/I_0 to the proposed theoretical values. The two central scenarios are highlighted in the table for each material: after first simulations with all cases, $I/I_0 \approx 0.16$ and $I/I_0 \approx 0.24$ situations are selected for the experimental evaluation and verification. In Figure 4.17, manufactured hollow

cylinders and polymeric base, an example of the assembly (Al 20 mm) and test object positioned in the XCT for the measurement is displayed.

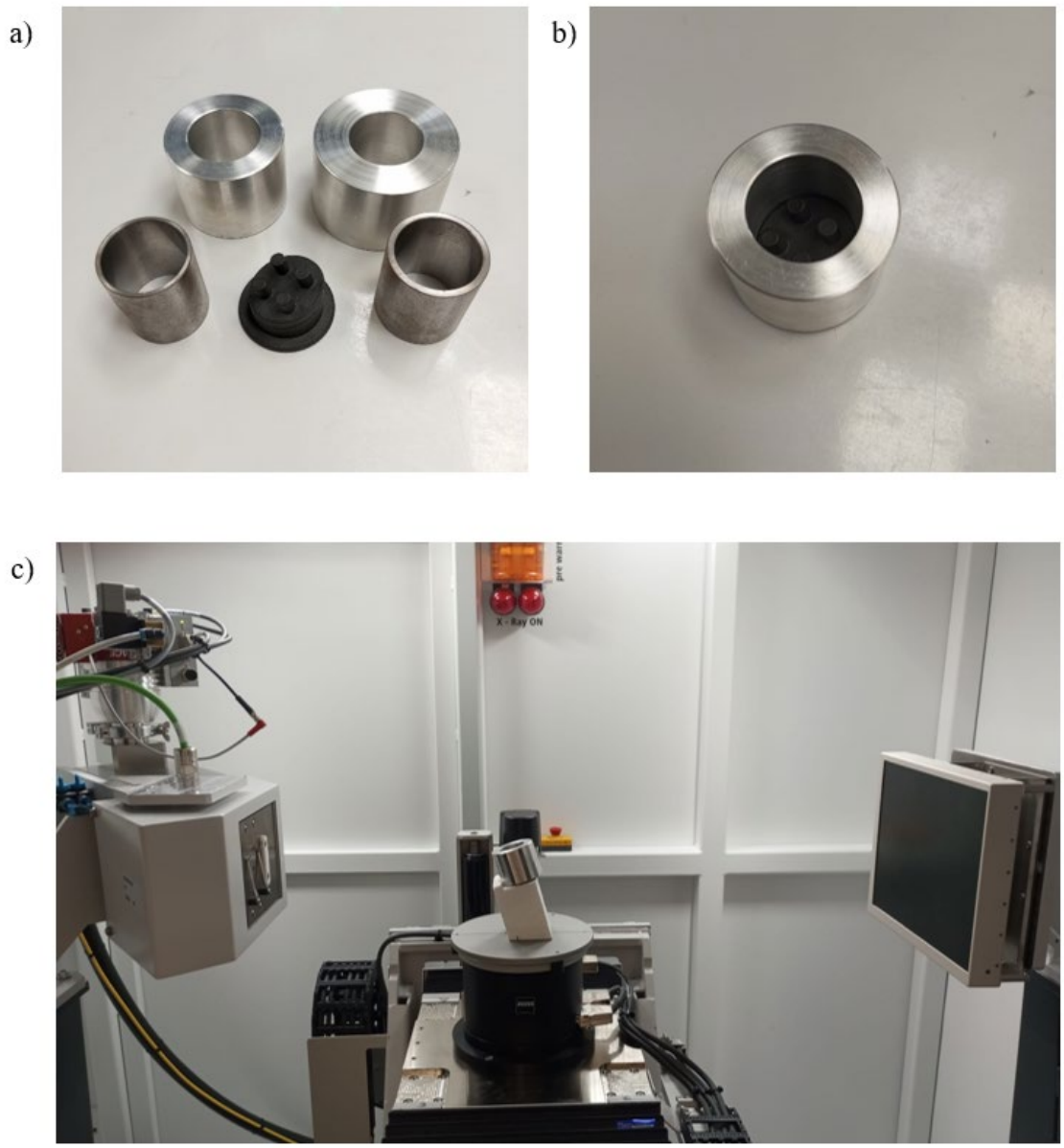

Figure 4.17. Details of the manufactured test object. a) Individual parts (hollow cylinders and base). b) Assembly (Al 20 mm). c) Test object positioned on the XCT device.

As seen in Figure 4.17c, test object is slightly tilted (≈ 15º) in order to avoid artifacts derived from an inappropriate part position [148]; this, added to the 15º that cylinders are inclined in the polymeric base (Figure 4.16b), ensures the correct geometrical conditions for the evaluation of the parts. To obtain this base position, test object is placed as shown in Figure 4.18. Even though this inclination in the hollow metallic cylinders affects the real penetration length x, the effect on the experiment is negligible as i) 15º only enlarge the penetration length in $x/\cos 15^{o} = x/0.966$ and ii) in al the scenarios the variation is proportional.

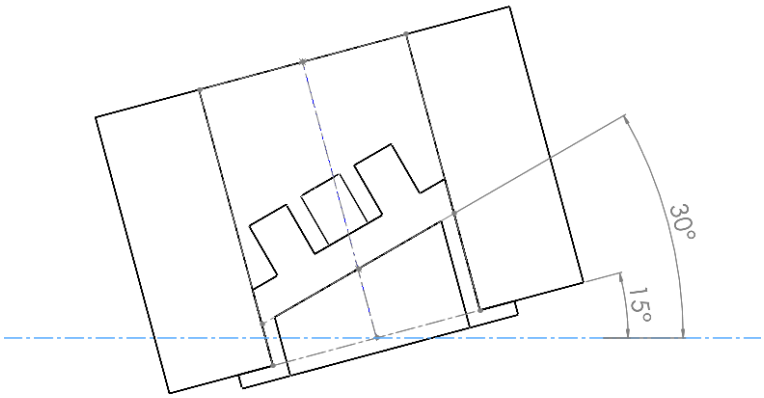

Figure 4.18. Schematic representation of the test object tilting in the positioning in the XCT.

In addition to Al and St scenarios, evaluation of the polymeric base alone (no metal, NM) is done to obtain reference measurements for the intercomparison with the rest of the cases. For this reference situation, same magnification as the rest of the cases are used ($Vx = 47.47\ \mu m$), voltage of 120 kV and physical filter of Al 1.0 mm, resulting in $E_{av} = 54\ keV$ and $I/I_0 = 0.78$ considering the thicker element (Ø12 mm cylinders) as the penetration length.

4.2.1.3. Evaluation methodology

First XCT simulations have been conducted using software aRTist 2.12 (BAM, Germany) to obtain a first reference for each case, including a scenario with no metal which has been used for dimensional intercomparison and calibration. After these simulations and as stated before, central cases for St and Al have been manufactured and XCT evaluations have been done by XCT device Zeiss Metrotom 800 G3/225 kV, using integrated software Metrotom OS for settings adjustment. Calibration of the device has been done according to standard VDI/VDE 2617 Part 13 / VDI/VDE 2630 Part 1.3 [60], using automated procedures; therefore, no voxel size re-scaling has been necessary for the experiment.

Post processing of the simulations and tomographies has been done in software VG Studio Max 3.4.2, using a local gradient threshold surface determination in Advanced – multi material mode, with a search distance of 4 voxels. No filter or correction has been added to any volume. Regions of interest (ROI) of each material have been created after surface determination process.

Dimensional values have been extracted from the evaluation of the four polymeric cylinders (diameters, form errors and distances between cylinders), as well as the internal

and external features of the metallic hollow cylinders (diameters and form error). Additionally, contrast-to-noise ratio (CNR) has been calculated following the procedure described in [142], using Eq. 6 as stated in Section 4.1.2.1:

$$CNR = \frac{|A_{Material} - A_{Background}|}{\sqrt{\sigma^2_{Material} + \sigma^2_{Background}}} \quad (6)$$

where $A_{Material}$ and $\sigma_{Material}$ represent the mean and standard deviation of the material ROIs, respectively; $A_{Background}$ and $\sigma_{Background}$ represent the mean and standard deviation of the background ROIs, respectively.

4.2.2. Results

In this section, the details of the evaluation of the test objects are presented, including a comparison of the CNR values and the dimensional measurements obtained.

4.2.2.1. CNR

CNR values have been calculated for both polymer and metal ROIs in each scenario, in simulated and experimental tomographies. In Figure 4.19, a comparison of results considering I/I_0 of each case is displayed.

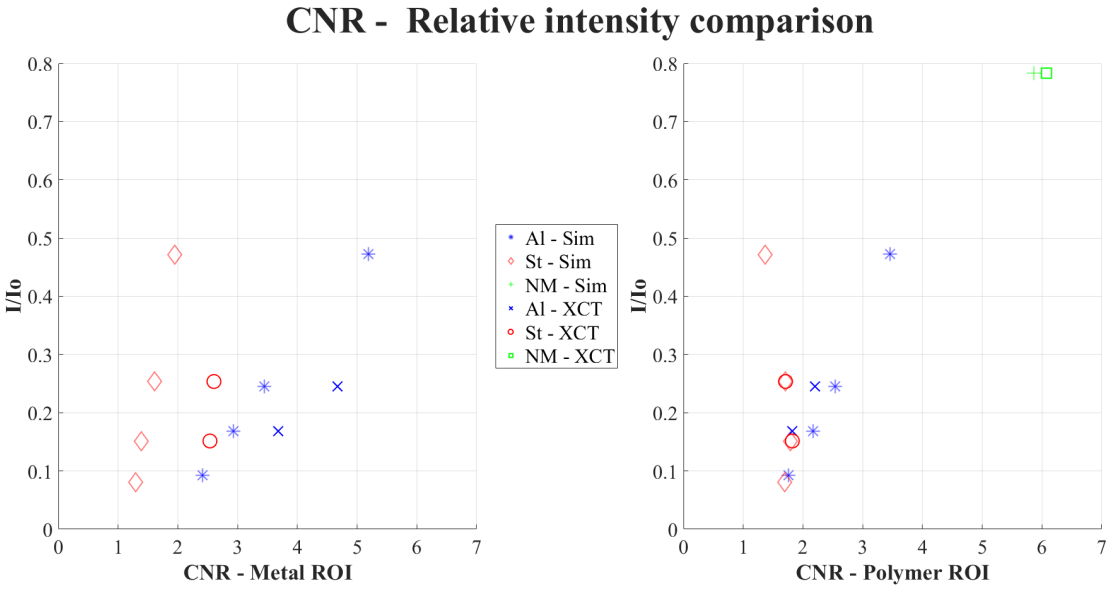

Figure 4.19. CNR values obtained for each scenario and in each material.

Results show, in general, a correlation between higher I/I_0 values and better CNR results, however, tendencies are different in Al and St scenarios, as better results are obtained in Al cases and trend is more evident and consistent, even correlated with the results obtained for the polymeric base alone (NM). Same correlation is found in experimental and simulated results, with slight differences due to the possible errors

associated with the simulation software and the uncertainty created by environmental conditions in real XCT; however, this similarities in results indicates that simulated tomographies can be used as a valid starting point. As expected, denser material ROIs obtain better contrast results, while polymer definition is affected by artifacts and noise; in this aspect, it is observed that for low I/I_0 values, CNR differences in polymer ROI are less significant, suggesting that a minimum difference with air will be present no matter the attenuation of the denser material.

In Figure 4.20 and Figure 4.21, a 2D slice from simulated and experimental tomographies of both cases with the same I/I_0 value and their correspondent grey values histogram is shown.

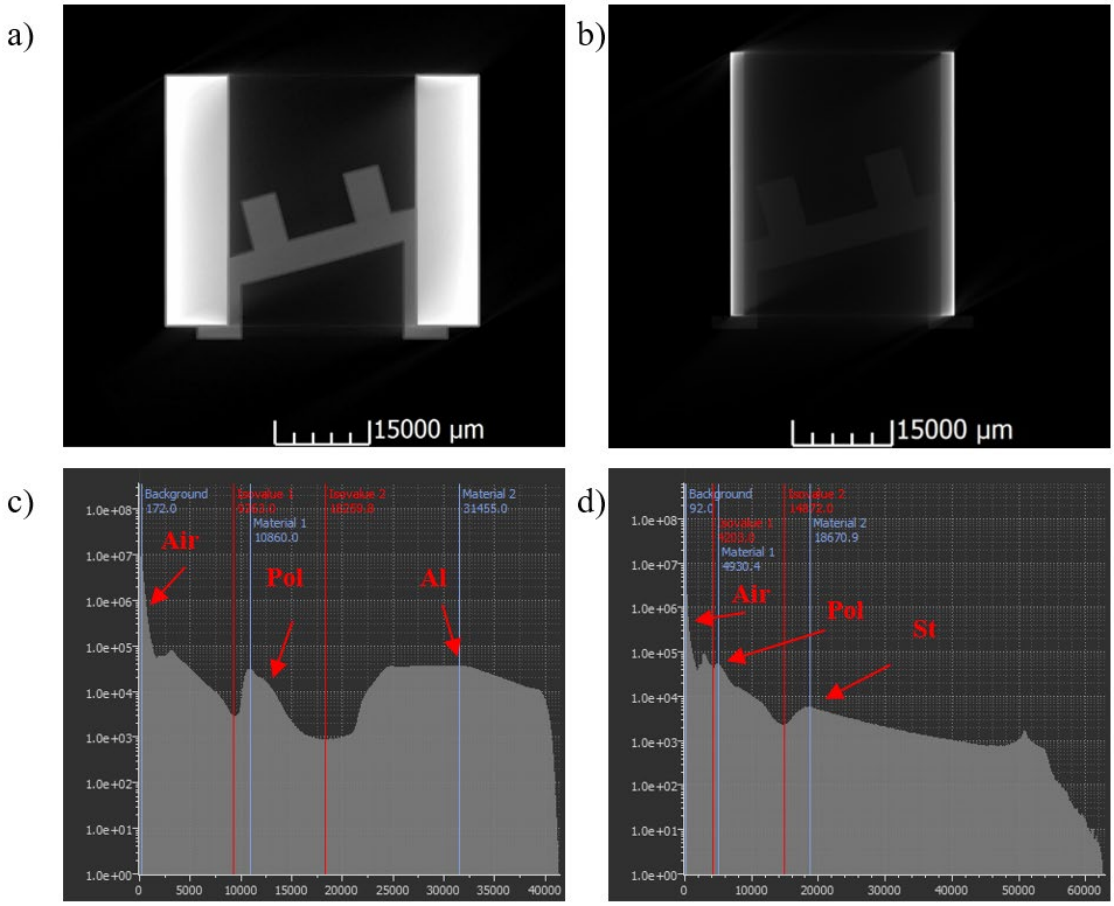

Figure 4.20. Visual comparison of simulated Al and St cases with same I/I_0. (a) Al 20 mm 2D slice. (b) St 4 mm 2D slice. (c) Al 20 mm grey values histogram. (d) St 4 mm grey values histogram.

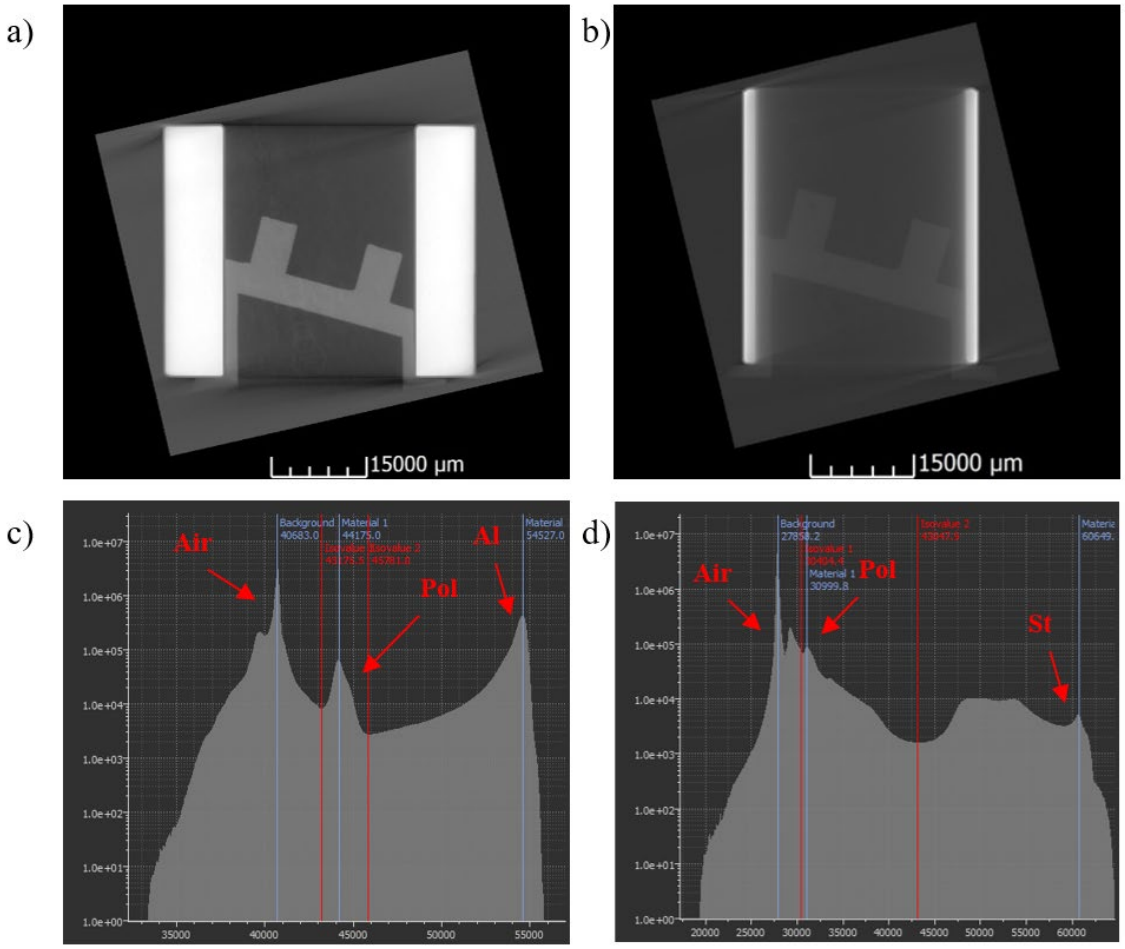

Figure 4.21. Visual comparison of experimental Al and St cases with same I/I_0. (a) Al 20 mm 2D slice. (b) St 4 mm 2D slice. (c) Al 20 mm grey values histogram. (d) St 4 mm grey values histogram.

As confirmed numerically by the CNR calculations, lower contrast is observed in both 2D slice and grey values histogram of St scenario in the polymeric regions, where material definition is less clear. Beam hardening also affects steel cylinders in St scenario, blurring the inner area and creating higher dispersion of grey values. Histogram distribution in simulated tomographies is significantly different; the reason for this phenomena is that in simulations there are several factors that are not possible to model, such as noise, variations in air density, environmental aspects (temperature and humidity variations), etc, which are present in real XCT; however, same trend and similar results are observed, suggesting that accuracy of simulations for this experiment is adequate.

4.2.2.2. Dimensional measurements

Diameters, form errors and distances between elements have been obtained from the measurements of the four cylinders of the polymeric base. As stated before, first XCT measurement of the polymeric base alone (NM scenario) has been used as a reference for an intercomparison with the four experimental cases; same procedure has been done

between simulated NM scenario and the four simulated metal cases. Deviations from NM scenario are displayed in Figure 4.22 for simulations and in Figure 4.23 for experimental XCT.

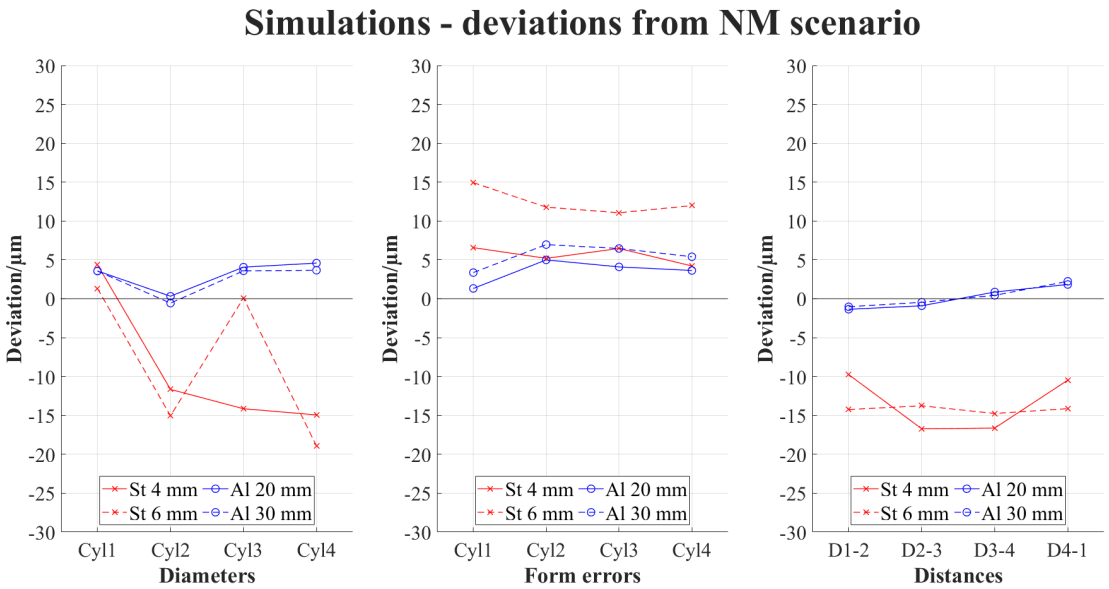

Figure 4.22. Deviations from NM scenario in evaluation of polymeric cylinders (simulations).

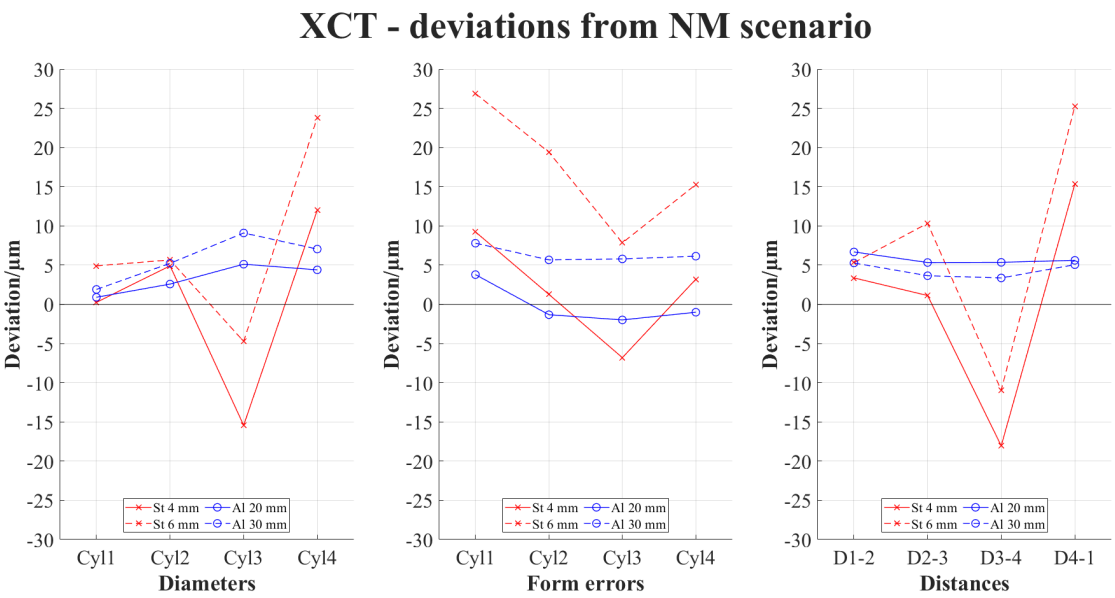

Figure 4.23. Deviations from NM scenario in evaluation of polymeric cylinders (real XCT).

Results show higher stability in all features measured in Al scenarios, where most of the deviations are in the same magnitude. On the other hand, effect of the metal in St scenarios is not equal and varies depending on the position of the cylinder (see Figure 4.17a).

Similar trend is followed both in simulated and experimental measurement, although in real tomographies results are more randomly distributed (mainly in St scenarios) due

to non-modelled factors in simulations as stated in Section 4.2.2.1). The accuracy is slightly better (less deviations from NM scenario) in scenarios with lower metal thickness – higher relative intensity – for both cases (Al and St), following same trends in scenarios with the same material. This is directly related with the results from the CNR analysis, where St scenarios present higher levels of noise and worse contrast both in metal and polymer ROIs. This suggest that, although relative intensity is a relevant factor to consider in metal-polymer assemblies, it cannot be extrapolated from one metal to another as the intrinsic properties of the materials affect differently the quality of the tomography.

Additionally, uncertainty calculations have been performed for the experimental results following standard VDI/VDE 2630-2.1 [67], using Eq. 2 as stated in Section 2.1.4.

Here, u_{drift} has been consider negligible as all measurements has been done with no time lapse. For the calculations of u_{cal}, maximum permissible error (MPE) in a rectangular distribution ($MPE/\sqrt{3}$) has been used, considering MPE = 4 µm for form errors and MPE = 4 + L/100 µm for size and distances measurements, according to datasheet provided by the manufacturer of the XCT device. Results of the uncertainty calculations are shown in Figure 4.24.

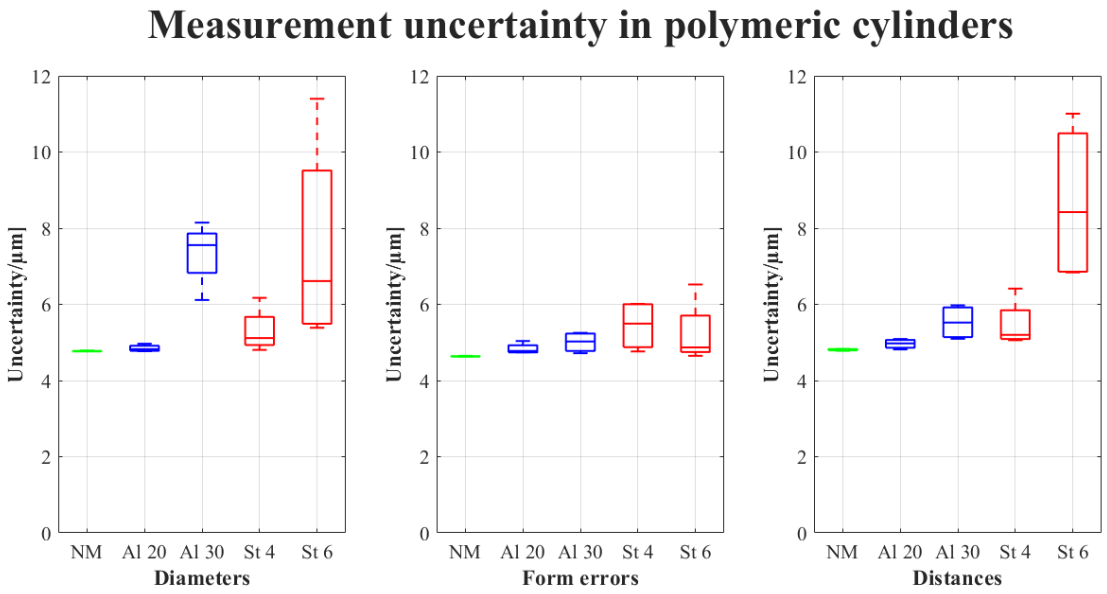

Figure 4.24. Comparison of uncertainty values in experiments for each scenario and each feature type.

Following the same trend as deviations in dimensional measurements, uncertainties increase for scenarios with higher attenuation (lower I/I_0), however, the increment is significantly bigger in St cases. All uncertainty values registered are over 4 µm as two of the main contributors (MPE and resolution of the device) are common for all the measurements. The differential factor here is the repeatability of the process, which is

numerically described as the standard deviation (σ) of the results obtained for each single measurement. Therefore, as measuring repeatability worsen, uncertainties increase.

4.2.2.3. Discussion

Analysis of the level of noise present in the tomographies by the CNR value and dimensional evaluation of the object has confirmed the hypothesis presented in the simulations performed, in which a correlation exists between higher relative intensity and better XCT quality. Uncertainty calculations derived from the diameters, form errors and distances evaluated in the test part (polymeric cylinders) show an increment as the attenuation rises, mainly caused by the worse repeatability registered (numerically evidenced as the standard deviation σ of the results of the same feature); this is a direct consequence of the higher levels of noise, which are randomly present and difficult a correct metrological evaluation.

However, it has been observed that the effect is not the same when the attenuation is produced by different materials; here, results obtained for same I/I_0 values are not the same for steel and for aluminium, as noise and defects are considerably higher in steel scenarios. At first sight, 2D slices of steel scenarios show less contrast between polymeric base and background, and grayscale histograms show i) worse material peak differentiation and ii) higher dispersion on the metal peak (this effect mainly caused by the beam hardening effect on the steel). CNR results confirm this trend, as both metallic and polymeric areas present better results in aluminium scenarios. Dimensionally, results on steel cases are more randomly distributed and with higher deviations, showing lower repeatability and, consequently, higher uncertainty.

To sum up, this study confirms that I/I_0 could be useful for generalization in the adjustment of XCT settings or in the noise expected in XCT measurement of parts and assemblies with the same material configuration, but it cannot be extrapolated for cases with other material configuration. The most probable reason is that there are other factors (e. g. intrinsic material properties, or atomic configuration) that affects the amount of noise created; however, as this study is focused on the effect of the attenuation of the X-rays, it should be investigated in future experiments. Additionally, only scenarios with two metals are evaluated here: for other cases, further experiments should be conducted to properly characterize the behaviour of this parameter in another particular material.

4.2.3. Conclusions

In this study, an analysis of the attenuation ratio, defined by relative intensity, and the effect produced by its variation in the XCT measurement of metal-polymer assemblies is presented. An experimental study has been conducted using an ad hoc designed test object, which includes a polymeric base with four cylinders used as a test element and a series of hollow cylinders made by two metals, aluminium and steel, with different thicknesses. Results of the CNR analysis and dimensional evaluation on the experimental measurements confirm the hypothesis suggested by the simulations, in which there is a correlation between lower attenuation (higher relative intensity) and better XCT quality; however, results differ significantly between aluminium and steel scenarios, suggesting that results cannot be extrapolated from one material to another. In conclusion, relative intensity is a good parameter to consider for noise level and XCT quality predictions but is usage alone should be limited to assemblies in which the material configuration is the same. At this point, it is highly probable that other factors related to the attenuating material (or materials, in case that two or more metals were present in the assembly) would affect to the quality of the tomography, apart from the attenuation ratio registered.

Nevertheless, and as stated before, this study is only performed in two metals and in separated cases, not combining them in the test object. Further experiments should be done in other materials to adequately characterize their behaviour, as well as situations in which two or more dense materials were present in an assembly; alternatively, other factors such as the internal structure of the material could be investigated, to determine other causes that can affect the XCT quality.

4.3. Closing remarks and future work

In this chapter, an investigation of the attenuation in metal-polymer assemblies is done, divided into two experiments which, although are independent, similar outputs from both can be obtained. Main conclusions and contributions are summarised as follows:

- It has been seen that dimensional evaluation of polymeric macro geometries with an acceptable accuracy is possible in metal-polymer assemblies, even including high-density metals (in this case, steel). It is true that the denser is the material, the more artifacts are found in the polymer; however, low deviations are found in the measurement of spheres' diameters and distances, which are not dependant on surface determination of the part and therefore are

less affected by external noise and artifacts. This should be taken with caution in form error and roughness measurement, as both are highly dependent on the surface, and higher distortions are found.

- Considering optimized XCT settings for metal-polymer assemblies, relative intensity (I/I_0) could be used as an indicator of the expected XCT accuracy when measuring this type of assemblies, as it is directly related to the attenuation of the X-rays. Consequently, there is a correlation with the noise levels and artifacts in the tomographies. However, not only I/I_0 can be used for the evaluation of XCT quality, and more parameters should be considered together, as results cannot be automatically extrapolated. Nevertheless, these results can be used as a reference in assemblies with similar material configurations.

Knowledge obtained from these two experiments allow to better understand the behaviour of XCT when evaluating metal-polymer assemblies, which are commonly present in most products and therefore industry have a high interest in its quality control. Considering that relative intensity is an interesting parameter and which has been useful in the estimation of noise and defects in the XCT measurements, further investigation on the usage of this value as an indicator for a wider range of metals and in different situations is needed.

Investigation carried out in chapters 3 and 4 uses conventional macro and micro geometries for the evaluation of XCT capabilities; however, one of the main advantages of this technology is the characterization of complex geometries. In the next chapter, experiments are focused on the evaluation of lattice structures, a type of complex features which are interesting for industry as they reduce the material usage without a loss of functionality.

5. Polymeric lattice structures. Accuracy of XCT measurements

Additive manufacturing (AM) has become an innovative manufacturing technique, as it is capable to produce complex geometries which are challenging or impossible for traditional manufacturing technologies, such as subtractive methods (milling, turning, etc). Lattice structures are one of these complex forms that AM is capable of produce; they suppose an advantage in cost-effective design, as there is a significant save in material while conserving same mechanical properties compared to solid elements with the same shape.

Here, XCT is the most optimal metrological technique for the complete evaluation of lattices, as it is able to characterize internal and hidden features. However, the biggest challenge for XCT is the traceability of the measurements. Uncertainty estimation of XCT is still in development, and studies typically use high-resolution calibrated devices such as focal variation microscopes (FVMs) or CMMs as a reference, focusing on certain parts of the lattice but not the whole structure.

In this chapter, the accuracy of XCT when measuring a realistic lattice structure through an intercomparison with a surface characterization reference device is presented. FVM, the instrument used for this study, is able to obtain high-quality 3D surfaces but has the limitation of the range of evaluation; here, an experiment is made using a test object adapted for the measurement by both FVM and XCT, simulating a 4 × 4 × 4 cubic lattice.

Polymeric additive manufacturing has been selected for the manufacturing of the parts. Typically, studies are based on metal lattice structures; however, polymeric lattice structures also have a great interest in industry as they are more cost-effectively produced. Additionally, the evaluation of polymers by XCT requires different machine settings, and therefore, the results of measurements performed on metal parts cannot be extrapolated.

This chapter is a description of the work published in the article “Progress toward the definition of X-ray computed tomography accuracy in the characterization of polymer-based lattice structures” [149]; therefore, this chapter has been organized according to the sections and subsections present in the paper.

5.1. Materials and methods

In this section, a description of the test objects designed to carry out the experiments and the methodology followed to support their evaluation is presented.

5.1.1. Design of test objects

Test objects were designed for the optimization of the measurements both in XCT and FVM. Three lattice configurations were used for the design of the probes, according to the most common typologies and the most suitable for the experiment: body-centered (BCC), face-centered (FCC), and body-centered with additional vertical struts (BCCZ). Each individual probe included 4 cubic cells of 5 mm length and 1 mm diameter struts. Criteria for the selection of cell size and strut diameter were used to obtain a proper diameter/length ratio in the struts: here, 1:5 ratio was considered appropriate. With this ratio, amount of material is significantly reduced in comparison to a solid cube, and the post-processing of the parts is facilitated. Higher ratio would not be realistic for a lattice structure, as mechanical characteristics of the part would have been considerably affected because of manufacturing limitations.

An assembly was designed for each typology, which included several individual probes, connected by a solid base (Figure 5.1). The intention of this assembly is to simulate a 4 × 4 × 4 lattice structure for the measurements in XCT; however, in this configuration, it was not possible to reach the inner cells using FVM, so the solid base was removed after the XCT evaluations to measure each probe individually in the microscope.

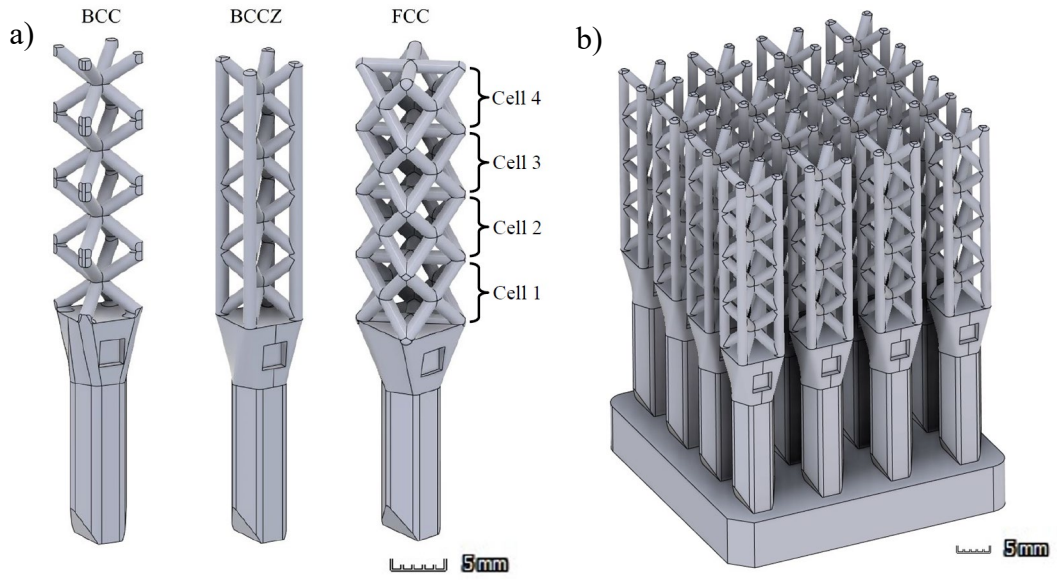

Figure 5.1. CAD models of test objects. a) Individual probes of each cell typology: BCC, BCCZ, FCC. b) 4x4x4 assembly (BCCZ).

Manufacturing of the test objects was carried out using SLS device (Lisa Pro, Sinterit, Kraków, Poland) in polymer polyamide 12 (PA12). Post-processing was applied after the manufacturing by cleaning the parts with compressed air and abrasive dust, as recommended by Sinterit, to remove unfused particles in the surface.

5.1.2. Methodology

First evaluation of the assemblies was performed by XCT Zeiss Metrotom 800 G3/225 kV, using integrated software Metrotom OS 3.12 (Zeiss, Oberkochen, Germany). A total of 5 iterations were taken for each assembly. After XCT evaluation, individual probes were separated from the solid base and measured by focal variation microscope—InfiniteFocusSL, from Alicona—using an incorporated rotary plate that allows obtaining a 360° scan along a horizontal axis and integrated software IfMeasureSuite 5.3.6 (Alicona Imaging). Disposition of the test objects for the evaluation in XCT and FVM is displayed in Figure 5.2.

Settings used for the evaluation in XCT and FVM are displayed in Table 5.1. Same settings were used for all parts.

Table 5.1. Settings and parameters of the evaluation in each device.

	XCT	**FVM**
Voltage/kV	70	-
Current/µA	478	-
Physical filter	No	-
Projections	1700	-
Exposure time/ms	667	27.5
Contrast [1]	-	0.45
Magnification	4.0	4x AX (Lens)
Resolution/µm	34.26 (Voxel size)	0.13 (Vertical), 8.5 (Lateral)
Time elapsed/min	14–16	70–75 (each probe)

[1] non-dimensional contrast coefficient provided by software IfMeasure.

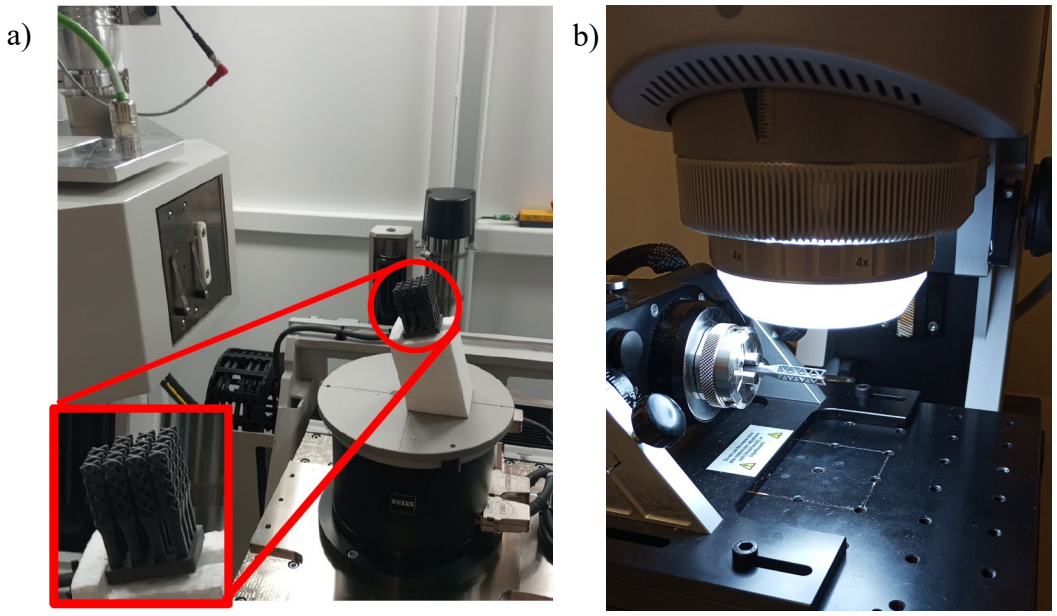

Figure 5.2. Disposition of test objects in the evaluation devices. a) XCT. b) FVM.

Resolution and time elapsed are the two parameters resulting from the adjustment of the process settings of each method. For FVM, sampling resolution is inversely proportional to time elapsed, while in XCT, the resolution obtained is the minimum achievable for the complete characterization of the test object. This depends on the geometrical magnification, a property resultant from the source-to-object distance (SOD) and source-to-detector distance (SDD). Magnification in this case could have been improved by local tomographies; however, time elapsed would have increased exponentially with no significant accuracy gains.

STL files were extracted for each probe for dimensional evaluation and intercomparison XCT-FVM using software Zeiss Inspect X-Ray Pro 2023.3.0 and VG Studio Max 3.4.2. In XCT evaluation, surface determination of the parts was performed in software VG Studio Max 3.4.2, in Advanced mode, selecting a local gradient threshold with a search distance of 4 voxels, with no extra post-processing. Geometry and material of the test objects do not imply a challenge in terms of XCT process settings adjustments or surface determination; therefore, the aim was to automate as much as possible the surface-determination process in order not to have any influence on the dimensional results.

5.2. Results

In this section, details of the results obtained in the evaluation of the test objects are shown, including a first qualitative comparison of the STL obtained (Section 5.2.1) and various analyses of the dimensional measurements of the lattice struts (Section 5.2.2).

5.2.1. STL quality comparison

The first qualitative analysis of the lattice surfaces obtained by FVM and XCT was performed. STL files were extracted from each FVM and XCT measurement and imported using the software VG Studio Max 3.4.2 for the evaluation.

In Figure 5.3, STL files of a single probe from each lattice typology in FVM measurements are shown.

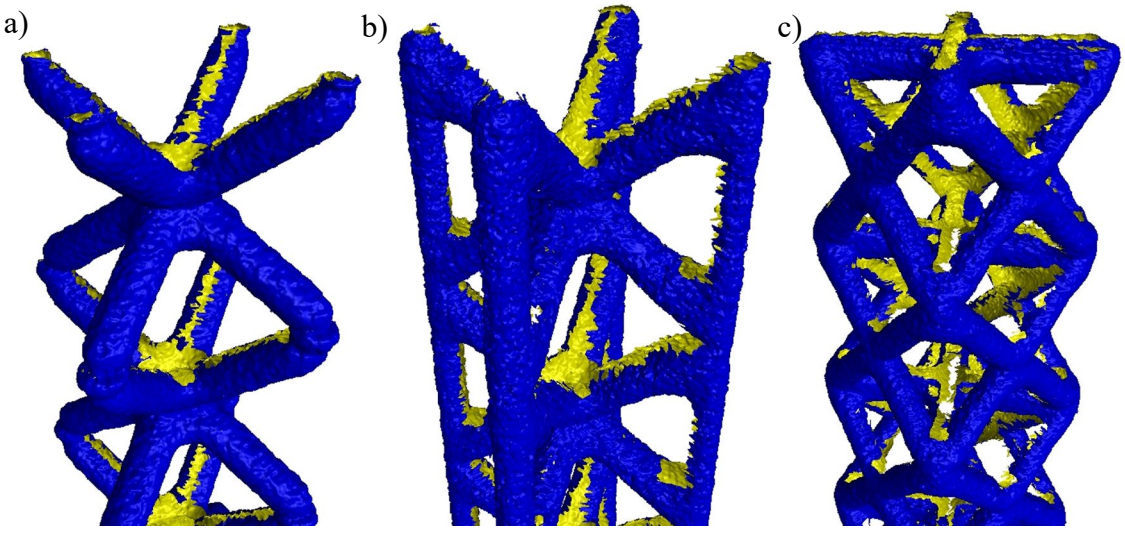

Figure 5.3. STL files obtained for each lattice typology in FVM measurements. Outer surface (blue) and holes (yellow) are displayed. a) BCC. b) BCCZ. c) FCC.

The first visual observation indicates that the reconstructed 3D files are not complete in all cases; however, BCC probes show considerably fewer holes. These errors are located mainly in internal zones, which are not possible to characterize by FVM as remaining “hidden” by outer elements. Areas with no data have registered artifacts and deformations in the edges.

In Figure 5.4, STL files of the XCT reconstruction of single probes for each typology are displayed.

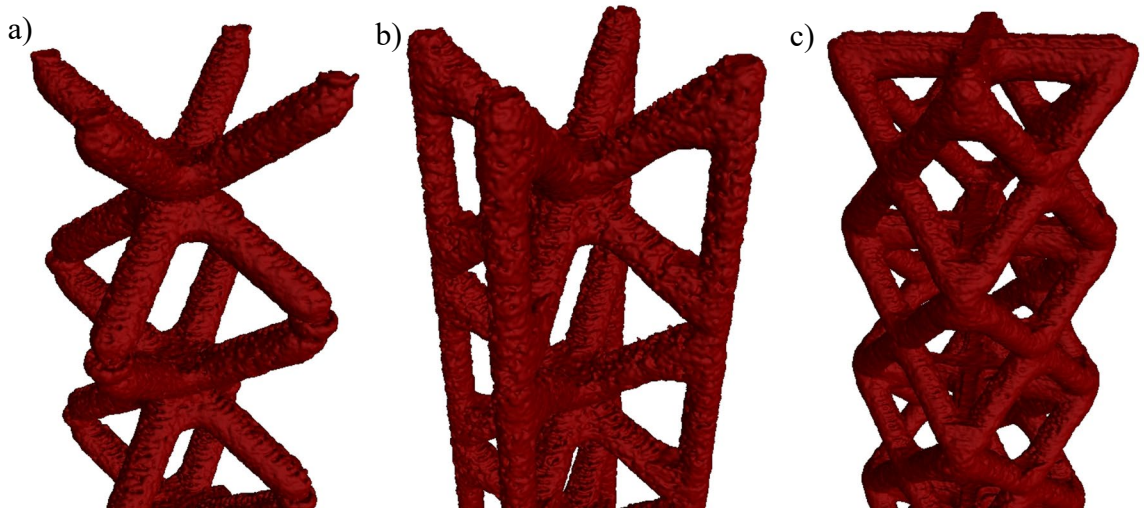

Figure 5.4. STL files obtained for each lattice typology in XCT measurements. a) BCC. b) BCCZ. c) FCC.

The XCT evaluation allowed us, as expected, to obtain complete STL files without holes in the inner areas; as stated before, this technique allows us to inspect hidden elements and inner features. Therefore, it has been able to reach zones that FVM is not capable of characterizing. However, this first look does not allow us to fully understand the level of detail of both devices. A close-up evaluation through 2D sections was performed. In Figure 5.5, examples of 2D slices of both XCT and FVM surfaces with a grayscale XCT background are shown, along with 3D details of the surfaces.

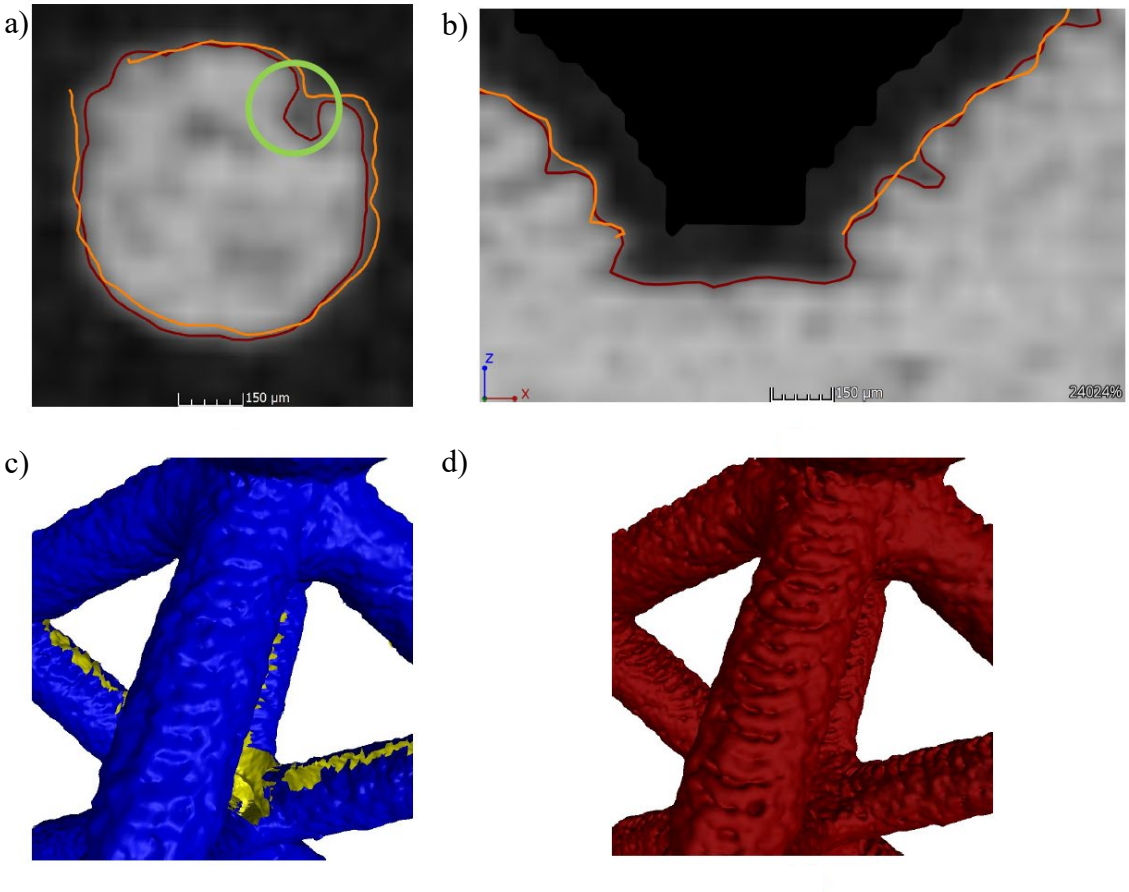

Figure 5.5. 2D slice comparison of FVM (orange) and XCT (red) surface reconstruction over grayscale map. a) BCCZ vertical strut. b) FCC transversal cut of a node. c) 3D FVM surface details. d) 3D XCT surface details.

In these 2D slices and 3D details, it is possible to see that the XCT surface has more microscopical details at a surface roughness level and at some features that, even though they are not internal elements, are not directly on sight; these elements are called re-entrant features (circled in green in Figure 5.5a) and are only possible to be measured by XCT [39]. Holes in the surface and the edge defects are evident, as seen in Figure 5.3.

The first visual analysis suggests that the quality of the 3D data obtained by XCT is higher than by FMV. Inner areas are not adequately characterized by FVM, showing errors in the edges of the holes that could affect the measurements of the struts. Also, some microscopic details and re-entrant features are only possible to be obtained by XCT; although having better resolution, it is possible that problems have occurred in FVM results due to the 360° reconstruction. Here, it has been shown that the cell type was relevant in FVM evaluation, as cell types with a higher amount of surface area that is not in direct sight have bigger reconstruction errors. In XCT, as this technology is able to characterize internal and hidden elements, this problem is not observed. To confirm the

suggestions obtained in this analysis, a quantitative evaluation was performed through dimensional measurements of the lattice struts.

5.2.2. Dimensional measurements

The results were obtained from the dimensional measurements of the individual struts of the lattices. The mean values of each cell were intercompared for each lattice typology (Section 5.2.2.1) and according to the cell position (Section 5.2.2.2). For this purpose, the software Zeiss Inspect X-Ray Pro 2023.3.0 was used.

5.2.2.1. Single probe

The first analysis was performed by comparing the evaluation of a single probe of each lattice typology using both devices. The mean values of the struts' diameters were grouped by cell unit, following the scheme shown in Figure 5.1a. A comparison of the mean values obtained from the XCT and FVM evaluation for each lattice typology are displayed in Figure 5.6, including standard deviations of the results (error bars).

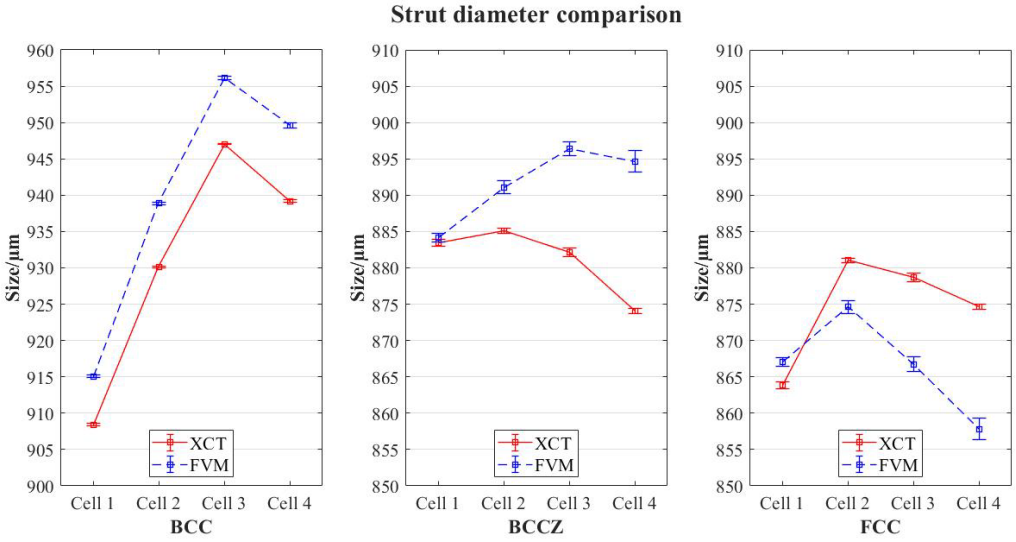

Figure 5.6. Strut diameter comparison for each lattice typology with standard deviations.

The results show an increase in the deviation of the values between both devices for cells located in higher positions; this becomes more evident for BCCZ and FCC, but the affection is different (diameters in FVM evaluation for FCC are smaller, while those for BCCZ are bigger). The standard deviation (σ) of the mean results is summarized in Table 5.2.

Table 5.2. Standard deviation (σ) of mean results of strut diameter evaluation for each case.

	Cell 1		**Cell 2**		**Cell 3**		**Cell 4**	
	XCT	FVM	XCT	FVM	XCT	FVM	XCT	FVM
σ_{BCC} *(µm)*	0.32	0.37	0.28	0.35	0.23	0.49	0.33	0.72
σ_{BCCZ} *(µm)*	0.97	1.26	0.62	1.76	1.23	1.99	0.79	2.97
σ_{FCC} *(µm)*	0.36	3.52	0.39	3.34	0.37	2.79	0.42	4.57

Additionally, expanded uncertainty calculations were made according to the procedures indicated in the specific standards for each device:

- ISO 15530-3:2011 [91] for FVM measurements. ISO 15530-3:2011 defines general calculations for the uncertainty estimation of a metrological device.
- VDI/VDE 2630-2.1 [67] for XCT measurements. As stated before, there is still no standard for the determination of the uncertainties in XCT evaluation; however, this directive has good explanations of the factors to consider. Also, recommendations suggested in [139] are followed. It is also worth mentioning that, for XCT uncertainty calculations, a maximum permissible error (MPE) = 4 µm, considering a rectangular distribution, was used as it was provided by the manufacturer of the XCT device.

The results of the uncertainty calculations registered for the strut diameter measurements are shown in Figure 5.7.

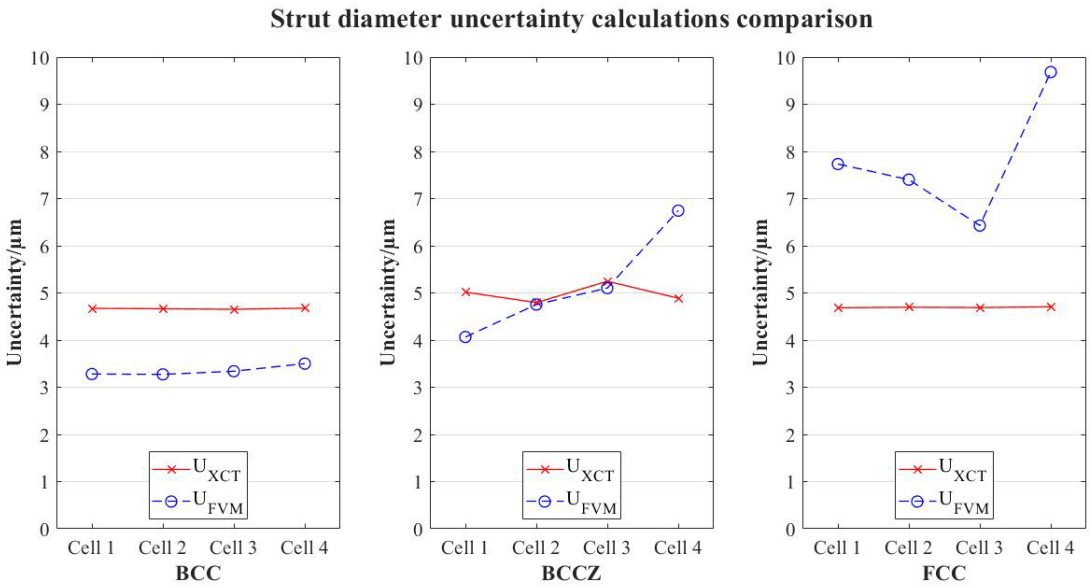

Figure 5.7. Comparison of uncertainties in strut diameters for each lattice typology.

The standard deviations registered are considerably higher for FVM measurements; also, it is shown that, even with considerably lower resolution, uncertainty of the results is similar or even lower for XCT measurements. This, combined with trends observed in Figure 5.4, suggest that (i) repeatability of XCT results is higher and (ii) reconstruction problems occur in FVM characterization. FVM measurements are taken along a horizontal axis in which the single probe is aligned. As the alignment is not perfect, rotation of the probe is not totally symmetric; therefore, the suggestion is that the further the cell is from the clamping of the probe, the higher the asymmetry, as it is possible that a "cone effect" could be created. The numerical results confirm that this may affect the reconstruction of the volume for FVM, as deviations are higher in the upper cells. In XCT, however, this effect does not happen, as the standard deviations and the uncertainties are similar regardless of the position of the cell in the probe.

This reconstruction problem in FVM affects differently depending on the geometry of the lattice. For cell typologies that has less hidden elements (BCC mainly), smaller deviations FVM-XCT are found. This suggests that the more surface reachable by the microscope, the higher the correlation with XCT results. However, the suggested "cone-effect" is common in all the typologies, as it is still present in upper BCC cells.

5.2.2.2. Cell position – 4x4x4 structure

A second analysis was performed regarding strut diameter evaluation. In a complete lattice, cells were divided according to their location in the 4 × 4 × 4 structure, as it is shown in Figure 5.8, and grouped in 4 different positions: corners, faces, edges, and centres.

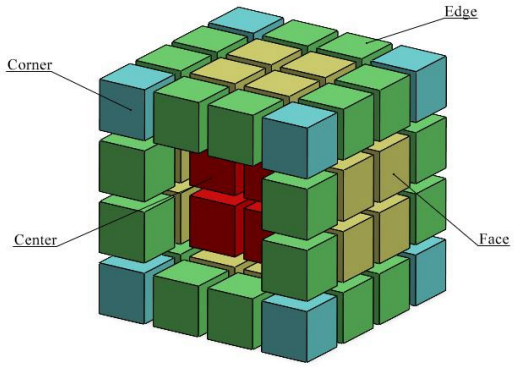

Figure 5.8. Cell position groups divided by colours.

The objective was to check for different trends in the deviations XCT-FVM in contrast to the results of the single-probe evaluation. The BCCZ lattice was chosen for this

analysis, as the lattice density is higher, and it can create higher noise levels in the measurement of inner cells. The results are shown in Figure 5.9.

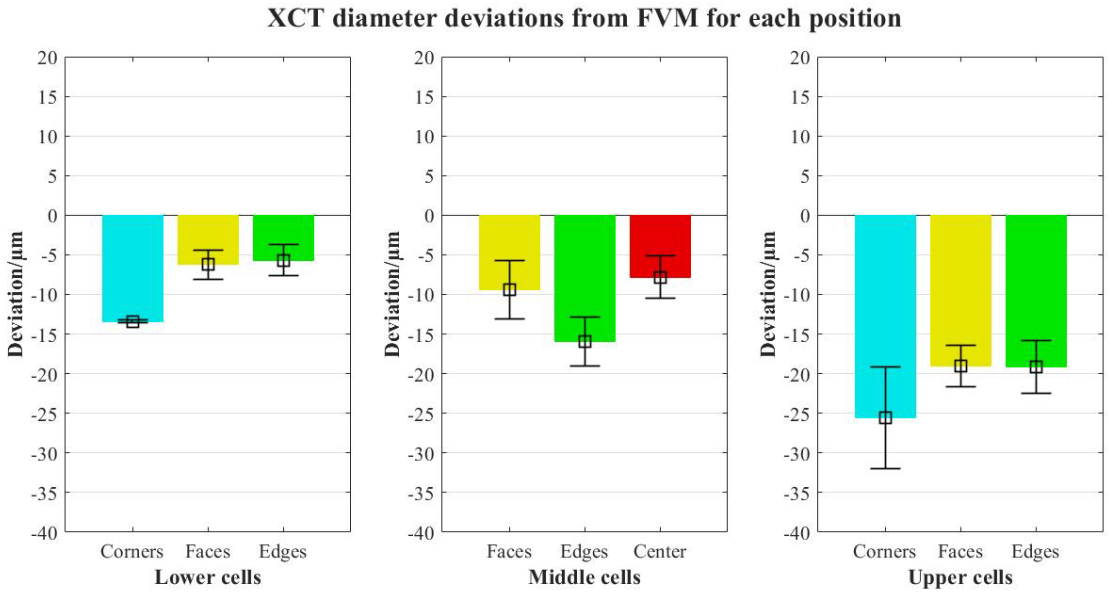

Figure 5.9. Comparison of XCT deviations of the struts' diameters from FVM for each cell location along the structure.

The results are divided into lower, middle, and upper cells considering single-probe analysis segmentation. The values obtained show similar trends as previously, with higher deviations in upper cells. Regarding positions, outer cells have higher errors (also worse repeatability in terms of the standard deviation of results) than inner cells; this is an important point, as it suggests that no additional measurement errors are found in inner cells, and therefore in the case that reference measurements are required for any metrological analysis (accuracy, uncertainties, etc.), outer cell characterization is representative enough for the whole structure.

5.3. Discussion

The analysis of the measurements taken shows, as expected, better results for XCT in all aspects. Although a 3D reconstruction of the single probes by the microscope is possible with acceptable accuracy, the better repeatability of the XCT surfaces obtained is demonstrated by smaller standard deviations and better uncertainties in strut diameter evaluation and higher-quality STL files. Although having better resolution, FVM is not capable of characterizing certain details, such as re-entrant features, due to its limiting optical measuring principle; in XCT, however, these non-visible elements are reachable, therefore obtaining surfaces closer to the real part. Of course, the aim of this experiment is not to evaluate the precision of FVM in lattice structure evaluation as it is not the most

suitable device for this purpose. Still, it is worth pointing out that compared to the reference instrument, which had a remarkably better resolution (up to hundreds of nanometres) when acquiring surface data, XCT obtained more repeatable results, which leads to the suggestion of better precision. In addition, it is confirmed that cell type influences the accuracy of the FVM evaluation method as the area proportion which is directly visible by the microscope is not equal for all typologies; however, in XCT, there is no such problem, as this technique is able to characterize hidden surfaces.

Another aspect to consider is the non-variability of the XCT results no matter the position of the cell in the 4 × 4 × 4 structure, apart from the deviations found caused by the reconstruction errors in FVM. As stated in previous studies [68], it is challenging to compare inner cell results with reference devices because XCT is the only non-destructive method able to characterize hidden parts. Thus, it is relevant that the XCT accuracy does not decrease for inner cells; this suggests that a reference measurement of external lattice elements by a reference device is enough for a performance evaluation of a complete XCT lattice inspection. This must be taken with caution, as this experiment is performed in a single material (polymer) and with a particular methodology; for other materials or reference devices, further experiments should be required.

5.4. Conclusions

In this study, an approach to the precision estimation in X-ray computed tomography (XCT) characterization of polymeric lattice structures through a metrological evaluation is presented. An experimental framework is settled, using a focal variation microscope (FVM) as a calibrated reference device for the intercomparison with the XCT measurements; this instrument was selected due to its higher resolution and its common usage in surface 3D data acquisition. Ad hoc test objects were designed for the optimization of measurements by both devices, simulating 4 × 4 × 4 structures composed of cubic-based lattice cells organized in three typical configurations: body-centred cubic (BCC), body-centred cubic with vertical struts (BCCZ), and face-centred cubic (FCC). A first qualitative analysis of the surface obtained from the probes was performed, along with a metrological evaluation of the diameters of the struts considering single-probe evaluation (Section 5.2.2.1) and the complete structure for cell position error analysis (Section 5.2.2.2).

The results show higher repeatability of the values obtained in XCT measurements of the diameter of the struts, with significantly lower standard deviations and good

uncertainty values. A trend was observed in FVM evaluation, as higher deviations from XCT as well as lower repeatability were registered for upper cells. Errors are most likely caused by reconstruction of the volume, as the rotation axis is not totally aligned with the horizontal axis; this “cone-effect” is less evident in the BCC lattice, matching with the higher amount of data obtained in the characterization.

Analysis of the deviations according to cell position along the 4 × 4 × 4 structure has revealed similar trends, with no additional differences apart from reconstruction errors in FVM mentioned before. This shows that no higher dimensional errors are found in the XCT evaluation of inner cells of the lattice, therefore suggesting that the accuracy of inner cell XCT measurement does not decrease, and reference measurements taken in outer cells may be representative of all of the structure. However, this must be taken with caution, as this experiment was performed with a particular methodology and for polymers.

As future work, further research should be performed for other materials (such as metals) to complement this knowledge and to find out if these conclusions obtained could be generalized for all cases. Additionally, studies could be expanded to other lattice types, such as gyroids, diamond shapes, or organic forms, to verify the methodology.

5.5. Closing remarks and future work

In this chapter, research has been focused on the estimation of XCT accuracy in the evaluation of polymeric AM lattice structures, in comparison to a high-quality reference device (FVM) typically used for the characterization of high-resolution surfaces and micro-geometries. Research has confirmed that XCT accuracy is higher, even though its resolution is lower; higher quality 3D files have been obtained, as well as higher repeatability in the dimensional evaluation. Additionally, it has been seen that cell position does not have a significant influence in the evaluation, suggesting that accuracy on the measurement of external cells could be representative of the whole structure.

In summary, with the investigation carried out in this chapter, a deeper knowledge about the accuracy and traceability of XCT measurements of polymeric lattice structures is obtained. These features are an innovative advance in product design, as they could replace solid parts with similar mechanical characteristics and considerably lower usage of material; as stated before, XCT is the most optimal method for the evaluation of this geometries, therefore traceability of its evaluation is critical.

This particular research is focused, as mentioned before, in polymeric lattice structures and in certain lattice shapes; however, results cannot be extrapolated to other materials, and further investigation could be done in different materials and composites to verify the hypothesis here presented.

The three fields of investigation in this thesis have led to improvements in the evaluation of micro geometries, metal-polymer assemblies and polymeric lattice structures. This knowledge has been applied in chapter 6 to the methodology designed for the optimization of uncertainties evaluation through a multi-geometry test object. Studies performed on the next chapter have been developed in parallel to the rest of the experiments, introducing this newly acquired knowledge for the modification and improvement of the procedures and the workpieces.

6. XCT uncertainty estimation for polymeric AM objects

X-ray computed tomography (XCT), as an innovative technique in industrial metrology, has in its versatility its major advantage in comparison with other devices. It is capable of the evaluation of macro and micro geometries, in external and internal features, using a non-destructive technique based on the reconstruction of 3D volumes through the acquisition of a series of 2D X-ray images along a 360º rotation of the workpiece.

However, traceability of the results obtained is still a challenge in metrology: i) contrary to simpler technologies, there are a high number of factors to consider when calculating uncertainties, and some of them are difficult to correctly estimate; ii) consequently, standards which regulates uncertainty definition and calculation for XCT are still in development; therefore, there is a lack of agreement in the uncertainty calculation procedure.

At this stage, directive VDI/VDE 2630 [60,67,150–152] is the commonly used procedure for the definition of factors and for the uncertainty estimation in XCT, which is based on the application of standard ISO 15530:3-2011 [91]. Here, the substitution method is widely applied, in which a series of measurements of a calibrated workpiece are done by a reference device.

One of the requirements for the reference calibrated workpiece in the substitution method is the similarity with the real part, in terms of geometries, material and manufacturing process. It is more critical in XCT, as material and penetration length are the main components of the attenuation of the X-rays (as stated and described in Chapter 4); therefore, reference standards or test objects used in the calibration of XCT should be adapted to the parts that will be evaluated.

With this premise, the objective of the work presented in this chapter is to obtain a precise uncertainty estimation in the evaluation of parts made by polymeric AM, through the definition of a procedure for this uncertainty estimation with a proper AM-based test object. In contrast with studies presented in chapters 3, 4 and 5, which have been performed sequentially, this has been an investigation developed in parallel with the rest of them. Along this chapter, some of the advances and issues found are common to the other individual studies, contributing to the development of the part designed for the

uncertainty estimation. Initial work related to this topic was published in the article "Reference standard for the uncertainty estimation of X–ray Computed Tomography measurements of complex macro- and micro-geometries" [153], which has served as a starting point. Also, the investigation regarding the evaluation of polymeric precision spheres [154] were published as well in conference proceedings.

6.1. Multi-geometry test object – first approach

6.1.1. Design and manufacturing

The target of the study is to design an AM produced artefact which can be used as reference object for the uncertainty estimation of XCT systems, through the application of current standard (ISO 15530-3:2011) [91]. In this section, the initial design constrains are expounded and then, the design of the novel test part is explained and described.

6.1.1.1. Initial constraints

The manufacturing technology that has been selected to build the test object is AM. AM and XCT have a direct relationship: AM enables the production of complex hidden geometries and internal structures such as scaffolds, whereas the ability of XCT to measure internal and hidden surfaces makes it the only suitable instrument when sectioning the part is not desired.

Although in the last years many artefacts for testing AM processes have been designed, they lack a design optimization for the use in XCT [155]. The artefact design must not only comply with AM design rules, but also it must minimize aspects which negatively affect the XCT measurements [156]. For this reason, polymers have been selected, even though AM is able to work with different types of materials, from ceramic to metals. In this first phase of the study, the choice of plastic is justified by the fact that X-rays weaken when they penetrate dense materials; in addition, polymeric AM is more cost-effective for prototypes and several iterations and re-designs could be performed. In future works, the effect of measuring the same reference object manufactured in denser materials could be studied. In addition, since the calibration is going to be performed by the substitution method, its features must also be measurable by other metrology instruments such as a coordinate measuring machine (CMM) and a Focus Variation Microscope (FVM). The initial constraints that the design must fulfil are summarized below:

- Limited thickness of the walls: The maximum wall thickness depends on the XCT system voltage and the scanned material. For polymers, it should be under 90 mm for a low voltage (130 kV) [156].
- Avoid thin layers and sharp edges: When the X-rays are perpendicular to the thin wall, just a small portion of them will pierce the material. Similarly, sharp edges should also be avoided because they cause scatter of the X-rays, causing a lack of definition of the edge [156].
- Measurable by other existing techniques: The measuring features must be physically accessible; dimensions larger than 2 mm will be measured by a CMM while dimensions smaller than 4 mm will be measured by an FVM. The main issue are the hidden geometries, which need to be made accessible.
- Features and geometries must be compliable with applicable norms for the expression and estimation of uncertainty with calibrated workpieces [67,91].
- Avoid cantilever features in order not to need support structures which would affect the surface finish of the part.

It is worth mentioning that the characteristics and settings of the XCT system are not considered in this investigation, as the intention for this test part is to be used in any industrial XCT system.

6.1.1.2. Geometries and dimensions

The initial test object has been designed considering the above mentioned constrains and the state-of-the-art previously studied. Most of the reviewed test objects consist of simple geometries with limited types of dimensions [99–101,157] that often serve for calibration [99,134]. The novel design proposed in this article aims to allow the characterization of XCT systems when measuring micro and macro geometries, dimensions and roughness profiles, in visible and hidden parts.

The final design is shown in Figure 6.1. The hidden parts are made accessible to the measuring instruments by removable parts. The assembly with the covers attached is shown in Figure 6.1a, the main body is shown in Figure 6.1b and the covers are shown in Figure 6.1c and Figure 6.1d.

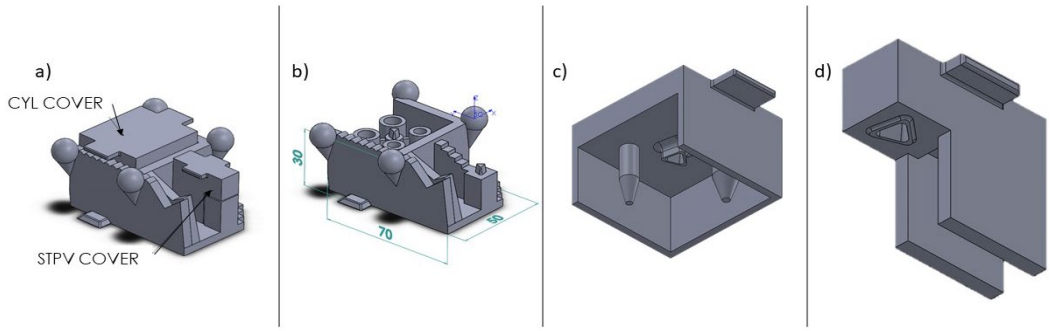

Figure 6.1. Element disposition in the test object. a) General assembly. b) Base general dimensions. c) Cylinder cover. d) Step cover.

The geometrical features that have been included in the model are based on the test parts previously reviewed, namely: reference spheres [99,134], cylinders and stepped stairs [101,103,157], distances [99,134], different profiles for roughness measurement [158] and internal cavities [102]. Having these geometrical features in one artefact leverages the XCT systems capability of characterizing all of them in just one measurement without sectioning or dismounting the artefact. As shown in the Figure 6.1b, the dimensions of the artefact are approximately 70 mm × 50 mm × 30 mm, which is within the range of the state-of-the-art designs. The removable covers allow to create hidden geometries which can be measured by XCT. These geometries are accessible to the CMM and the focus variation microscope by removing the covers.

Test object has been manufactured by two polymeric AM technologies: FDM, using PLA filament, and Polyjet, employing photopolymer Rigur™ RGD450. Nominal layer thicknesses selected are the finest possible for each device: 100 µm in FDM and 16 µm in Polyjet.

6.1.2. Experimental measurements/calibration

This section presents the results of the inspection of the first prototype. Measurements have been performed with a CMM ZEISS PMC-876 CNC and a FVM InfiniteFocusSL of Alicona.

6.1.2.1. Measuring features

First, a reference system is created with three of the reference spheres (S1, S2 and S3). A XY plane is built by the centres of the reference spheres, setting the origin in S1 as shown in Figure 6.2.

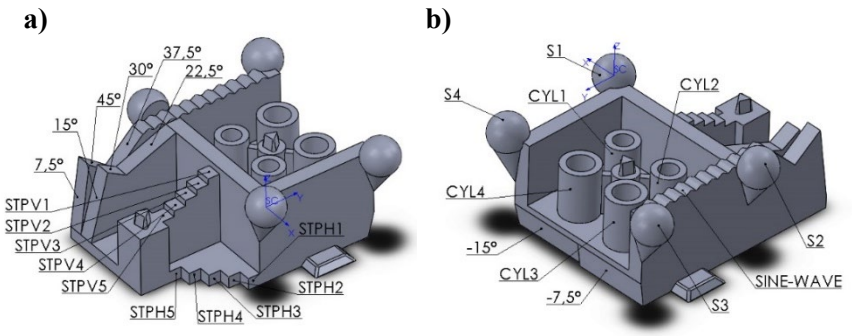

Figure 6.2. Geometries included for the dimensional evaluation. a) Positive inclined ramps and steps. b) Spheres, cylinders and negative ramps.

The geometries that have been evaluated with the CMM are the diameters of the reference features and the distances between these elements, while the FVM has been used to characterize the horizontal dimensions due to the limitations of the instrument. A total of three measurements of each geometry have been taken, considering the average as the reference result. The measured features are shown in Figure 6.2a and Figure 6.2b.

The leaning walls (ramps from -15º to 45º) and the sinusoidal profile of the artefact have been used to generate roughness profiles. The instrument used to measure these profiles is the FVM InfiniteFocusSL of Alicona.

6.1.2.2. Uncertainty calculations

The evaluation of the expanded measuring uncertainty of the measurements obtained by the reference instruments (CMM and FVM) has been done according to the standard ISO 15530-3:2011 [91], following Eq. 1 described in Section 2.1.4.

To verify the results the parameter E_N is calculated. This value relates the deviations measured by different instruments in the same dimension. A value of $E_N < 1$ indicates that results can be comparable. Calculations are done following standard ISO/IEC 17043:2023 [98] described in Eq. 3 as stated in Section 2.1.4.

6.1.3. XCT evaluation. Issues found and improvements.

First XCT evaluation is done in an external laboratory with a GE SEIFERT X-CUBE Compac 195kV device. During the development of this first experimental approach, the XCT device present in the University of Zaragoza was not yet available; therefore, XCT measurements had to be externalized. Settings used for the measurements are listed in Table 6.1.

Table 6.1. XCT settings used for first evaluation.

Voltage (kV)	181 kV
Voxel size (µm)	155
Exposure time (ms)	70
Physical filter	Cu 1 mm
Projections	720

Post processing of the volume was carried out by software VG Studio Max 3.4.2. After the analysis of the volume and the dimensional results obtained, several issues were found:

i. Resolution of the XCT measurements was inadequate for the proper evaluation of surface roughness. XCT is able to obtain sub-voxel characterization (up to 1/10 Vx); however, 155 µm were not enough precise to properly distinguish expected roughness values (see Section 6.1.2.1). In Figure 6.3, an example of an extracted ramp from the obtained surface is shown.

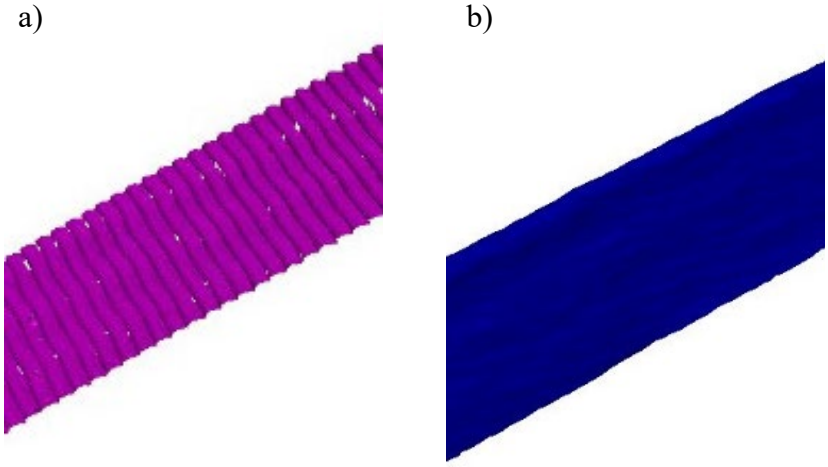

Figure 6.3. Inclined ramp surface comparison from both devices. a) FDM. b) XCT.

ii. Deviations in diameters and distances between XCT and reference measurements are excessively high (up to 200 µm) and do not follow a trend. This, combined with the bad repeatability of results (both in tomographies and repeated reference evaluations) does not allow to properly estimate uncertainties.

iii. As XCT evaluation is externalized, the environmental conditions during the transportation of the test object cannot be tracked adequately. This requires the estimation of the component u_{drift} to the uncertainty calculations in Eq. 2, which

could not be negligible in this case, so the uncertainties increase significantly. Additionally, as it is stated before, no systematic errors are found as deviations in dimensions are randomly distributed.

After the identification of the problems found, a series of improvements have been proposed:

- As stated before, the deviations found are randomly distributed for all geometries included in the test object. However, its importance is not the same for all; spheres, which are defined as reference elements, should provide more repeatable measurements and therefore their quality must be higher. Stepped stair effect found in the spheres is more evident due to their shape and compromises the quality of the geometry; this is more evident in the FDM test object, as layer thickness is higher than in Polyjet, (100 μm in FDM, 16 μm in Polyjet). To solve this problem, precision polymeric spheres have been proposed to replace printed AM spheres. An experiment to test their viability was planned, and its results are presented in Section 6.2.
- Resolution of the XCT evaluation was not adequate for the measurement of ramps proposed, mainly in Polyjet prototype as nominal surface roughness is significantly lower than voxel size achievable. In parallel, experiments presented in Section 3 were developed to i) improve evaluation settings (geometrical magnification mainly), ii) design workpieces suitable for the roughness measurements in XCT and consequently iii) evaluate the capabilities of XCT for the accurate characterization of these roughness parameters.
- Improvements in the evaluation methodology and measuring plan are proposed. One of the issues found is the different amount of information obtained from CMM and XCT; while an average of 15 points were measured in CMM for each geometry, up to 10000 points were registered in XCT. To solve it, the implementation of normalized procedures to for the verification of devices are proposed, such as E-test and P-test [87–89] for the correct comparison of the results. This is strongly related to the substitution of printed spheres by precision ones, as P-test is designed specifically for the measurement of high quality elements: their low shape error ensures the higher repeatability of the results.

This improvements proposed and outputs obtained from parallel studies are applied to a new optimized test object in the study presented in Section 6.3.

6.2. High precision polymeric spheres – additional study

In this study, an evaluation of various polymeric features by means of XCT has been carried out. The target is to evaluate the capabilities of XCT when measuring polymers with slight differences in density, and the effect of manufacturing surface quality of the part in the measurement process. An ad hoc assembly made of various polymers has been designed, in which a base with AM spheres and hollow cylinders, and precision polymeric spheres are included for metrological evaluation and comparison. Reference measurements were taken before and after XCT evaluation to calibrate the part and to ensure no significant deformation occurred over time.

6.2.1. Design and materials

Precision spheres with nominal value of Ø12 mm have been selected to be compared with AM spheres and cylinders, with a tolerance of 25 µm in diameter and 12 µm in form error. Distances between centres of spheres are solid dimensions because they are not as dependant on determined surface as plane-to-plane measurements. Also, diameters of spheres offer good stability.

Four materials have been selected for the precision spheres: PTFE, POM, PP and PA6. A base is designed and manufactured by Polyjet technology, printed in photopolymer Rigur™ RGD450, where four spheres of each material were distributed in four groups along the base. Five AM printed spheres (Ø12 mm) and eight hollow cylinders (Ø8 mm) are included in the base. CAD model of the assembly with general dimensions and the distribution of the elements is shown in Figure 6.4.

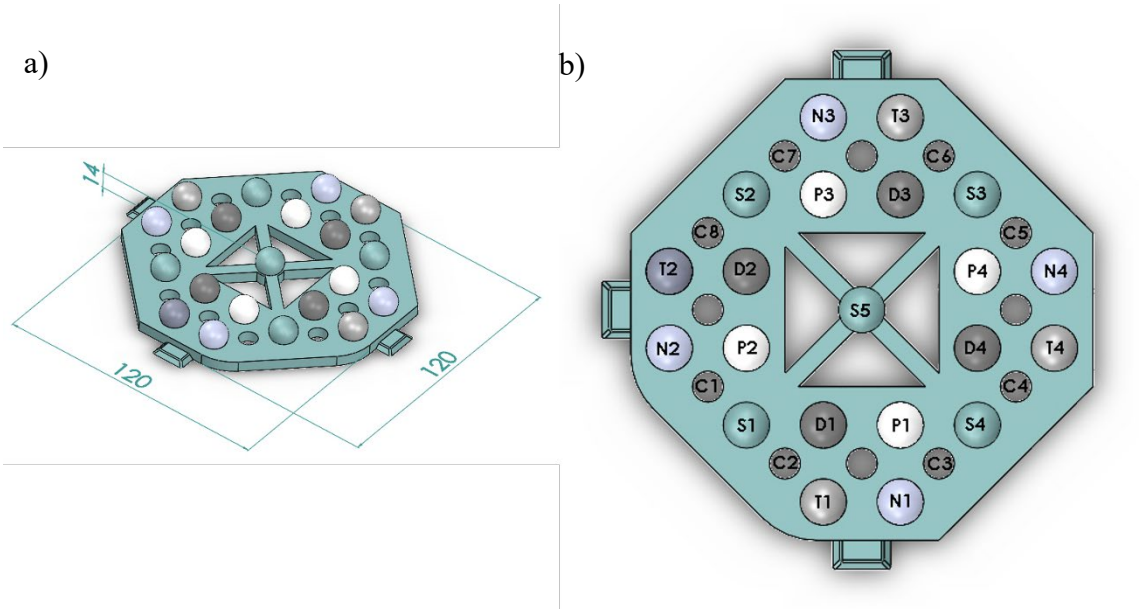

Figure 6.4. Test object design. a) General dimensions. b) Element distribution.

Each group has one sphere of each material. Nomenclature: D – POM, P – PP, T – PTFE (Teflon), N – PA6 (Nylon), S – AM printed spheres and C – hollow cylinders.

6.2.2. Methodology

Three XCT measurements have been taken using a Zeiss Metrotom 1500/225 kV device. Settings are listed in Table 6.2.

Table 6.2. XCT settings selected.

XCT Settings	**Value**
Voltage [kV]	120
Current [µA]	837
Physical filter	Al 1mm
Nº of projections	3000
Exposure time [ms]	500
Voxel size [µm]	58

As deformations may occur, reference measurements were taken with a coordinate measuring machine (CMM) Zeiss PMC-876 CNC before and after XCT characterisation. CMM evaluation before and after XCT is critical for artefact calibration, for XCT deviation comparison and for stability check along time.

Geometries evaluated are features' diameters and form error, and distances between similar elements (same-material spheres, cylinders). AM spheres S1, S2 and S4 were used

as references for alignment. Software Calypso has been used for CMM reference measurements, and VG Studio Max 3.4.2 for XCT post process. Initial surface determination (SD) in Advanced mode (search distance of 4 voxels) and second ROI local SD of each element have been performed.

6.2.3. Results

6.2.3.1. Material differentiation

In the first qualitative inspection of the results, histogram of grey values (see Figure 6.5) shows that 4 different peaks can be distinguished apart from the background/air peak (displayed on the left).

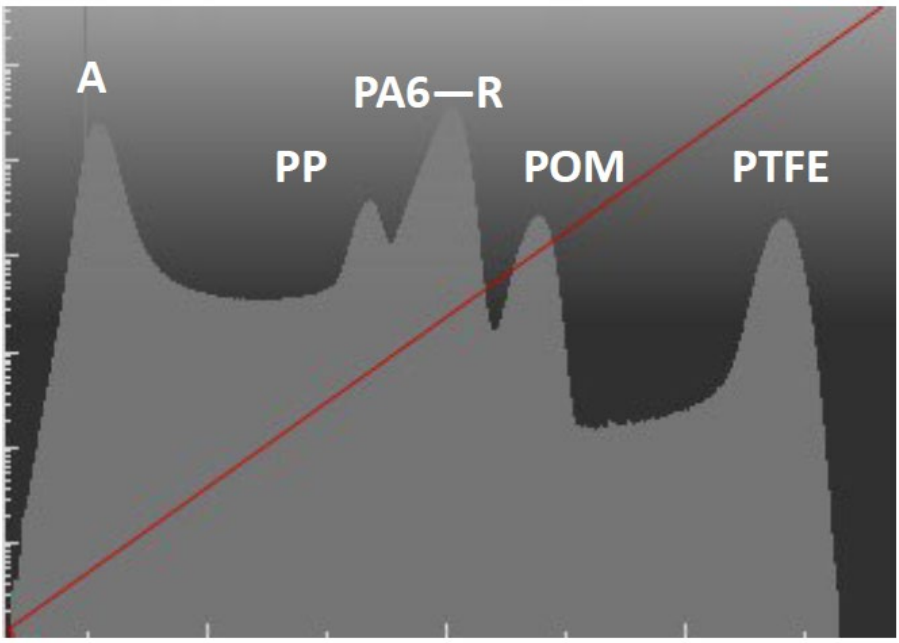

Figure 6.5. XCT histogram of grey values.

Through an Advanced - Multi Material surface determination, each peak has been separated into an independent volume. In Table 6.3, density of each material and its corresponding approximate grey value (according to its peak) is shown.

As XCT data is acquired in 16 bits, complete spectrum of grey values goes from 0 (white) to 65535 (black). Theoretically, denser materials should have higher grey values.

Table 6.3. Material density and corresponding XCT grey value.

Material	Density [g/cm^3]	Grey value
PP	0.87	8300
PA6	1.11	10100
Rigur™ RGD450	1.21	10100
POM	1.37	11900
PTFE	2.16	17000

Results show a correlation between density and grey value, and a differentiation between almost all materials. Only, it is not possible to distinguish Rigur™ RGD450 and PA6 due to its very similar density (0.1 g/cm^3 difference). However, a differentiation between Rigur™ RGD450 and POM is possible, with a slightly higher density difference (0.16 g/cm^3).

6.2.3.2. Dimensional results

A summary of XCT deviations from CMM measurements is presented in this section. Mean values of each type of geometry have been considered. As distance nominal values are unequal for all features, µm/mm coefficient has been used for comparison, considering the division between deviation (in µm) and the nominal value of the distance (in mm). Results are displayed in Table 6.4.

Table 6.4. XCT deviations from reference CMM measurements.

Geometry	Diameter [µm]	Form error [µm]	Distance [µm/mm]
AM spheres	-30.9	45.3	0.39
AM cylinders	43.5	29.6	0.41
Prec. spheres	4.8	3.9	0.28

Negative values of diameter deviation on AM spheres are related to the layer-by-layer AM technology: only surface peaks are reachable by CMM while XCT device is able to characterise the complete topography. Same effect in the opposite direction occurs to AM hollow cylinders. AM diameter and error form deviations are 700%-900% higher than precision spheres deviations, while values of distances deviations are around 30% higher for AM features. Precision spheres' distances are strongly influenced by the AM base

where they are placed; however, deviations remain lower. Further studies are necessary to evaluate each contribution in deviations.

6.2.4. Conclusions

A polymeric multi-material XCT evaluation, focused on AM comparison to precision features, is presented in this section. Research have shown that differentiation between polymers with similar density is possible, with good threshold results for variations of 0.16 g/cm^3 or higher. For multi material part evaluation, this could be interesting in order to ensure proper polymer differentiation in presence of other types of materials. AM features show higher deviations from CMM measurements in terms of diameter and form error as expected. Distances, strongly influenced by AM base, are still higher for AM features, which indicates a contribution of AM surface in distance errors.

The main output obtained from this experiment is the suitability of the introduction of polymeric precision spheres in the multi-geometry test object, as deviations found in diameter and shape with the measurements by calibrated reference device (CMM) are significantly lower. The purpose of these elements is to be used as reference geometries (mainly for the alignment of the part), as dimensions obtained in spheres are more solid than in other geometries. Therefore, a minimum quality is required, and AM spheres could not provide it.

6.3. Multi-geometry test object – new proposal

After performing parallel studies and to apply the improvements proposed, a new experiment has been conducted, in which it has been included:

- An optimization of the design, eliminating duplicated and redundant elements and re-organizing shape and features in the main base. Also, printed spheres have been replaced by precision polymeric spheres as proposed in Section 6.1.3 and after the results obtained in the parallel study (Section 6.2).
- An improvement of the measurement plan, applying normalized procedures for the evaluation of reference elements and simplifying the procedure. The acquisition of an XCT device by the University has supposed a huge advance in the experiments: transportation of the test objects could be avoided and, consequently, measurement uncertainties derived from drift between calibrations and XCT evaluation are reduced.

6.3.1. Test object design

As stated before, a new concept of test object has been developed for the optimization of the measurements, avoiding redundant elements. In Figure 6.6, main dimensions of the artefact and distribution of elements is shown.

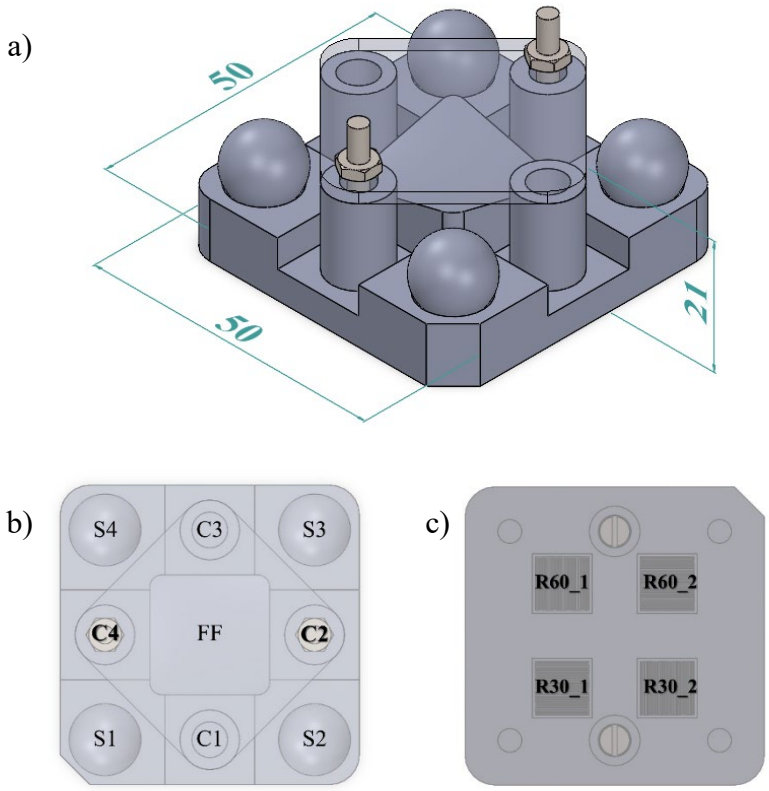

Figure 6.6. Test object improved design. a) Assembly and general dimensions. b) Upper elements. c) Lower elements.

Test object is composed by a main base in which the features are settled, including four inserted precision polymeric spheres (Ø12 mm diameter), four hollow cylinders (Ø12 mm external cylinder, Ø6 mm internal cylinder), a hyperbolic paraboloid surface contained in a 20x20x5 mm box and four inserted ramps with dimensions 9x9x1 mm in the lower part for roughness evaluation. A squared-shape covering is included and fixed with polymeric bolts and screws (material: PA6.6) with the aim to create artificial hidden elements (in this case, the four internal cylinders here mentioned). With this distribution, macro geometries, micro geometries and a freeform are included in the design. A summary of the dimensions evaluated is done in Table 6.5.

Table 6.5. Dimensions and geometries evaluated.

Geometry	**Dimension evaluated**	**Value (mm)**
Spheres	Diameters	Ø12
	Distances (centre-to-centre)	35 (short), 49.5 (diag.)
Cylinders	Diameters	Ø12 (ext.), Ø6 (int)
	Distances (centre-to-centre)	24.75 (short), 35 (diag.)
Planes	Distances	5 (Z axis), 15 (X and Y axis)
Ramps	Surface roughness (Ra)	15.00 - 25.98 (µm)
Hyperbolic paraboloid	Freeform surface	-

Main base is manufactured in Polyjet printer Objet Eden 350V (Stratasys, USA), material Rigur^{TM} RGD450, while roughness ramps are produced in FDM Ultimaker S5 (Ultimaker, Netherlands), material PLA. Selection of the manufacturing process of the ramps has been done according to its resolution. Nominal layer thickness of Polyjet is 16 µm, which creates roughness profiles that are not suitable for its measurement by XCT (as its resolution is not small enough). On the other hand, with FDM technology, it is possible to naturally create roughness profiles of ≈ 15-26 µm, through layer thicknesses between 100 – 200 µm, which XCT is able to characterize. Complete manufactured assembly is displayed in Figure 6.7.

a) b)

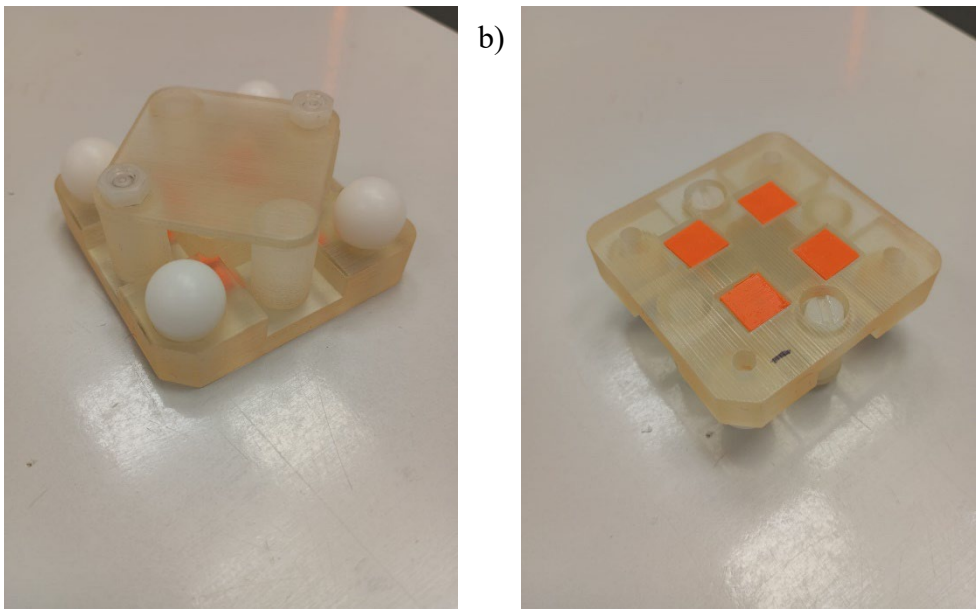

Figure 6.7. Manufactured test object. a) Upper part. b) Lower part.

6.3.2. Methodology

In this section, the methodology proposed for the calibration and XCT evaluation of the test object and the instruments selected are described.

6.3.2.1. E-test and P-test

One of the issues addressed in Section 6.1.3 is the different amount of information obtained from XCT and CMM in terms of number of points used to reconstruct macro geometries. Although the number of points registered in CMM measurements is lower, their quality is supposed to be higher due to the higher accuracy of the device and, consequently, the lower uncertainty associated.

To evaluate the quality of points acquired by XCT, principles used in two acceptance tests defined in standards will be applied. Procedure is described in ISO 10360 [87–89] which have been adapted for the usage in XCT in directive VDI/VDE 2630-1.3 [60], for the measurement of certain geometries of the test object. These tests are commonly used for the general performance evaluation of a coordinate measuring system (CMS), considering almost all components and factors of the device that could be involved in measuring errors.

Length measuring error test (E-test) is used for the characterization of global errors, normally using reference standards designed to evaluate lengths (distances between spheres, steps, etc). Two different length types are evaluated: bi-directional and uni-directional (as shown in Figure 6.8).

Probe error test (P-test) evaluate local errors in feature size, form errors and surface positions. Typically, is performed using least-squares fitting points measured on a calibrated sphere, which are distributed along its upper hemisphere (Figure 6.8). Dimensional data obtained from the reconstruction of the sphere using these points is compared with the calibrated data. Here, precision spheres play an important role, as this test is specifically designed to be performed in elements with high manufacturing quality and narrow tolerances. P-test would have provided unsuccessful results on AM spheres, as their surface finish is not optimal for this purpose and the points obtained would have low repeatability.

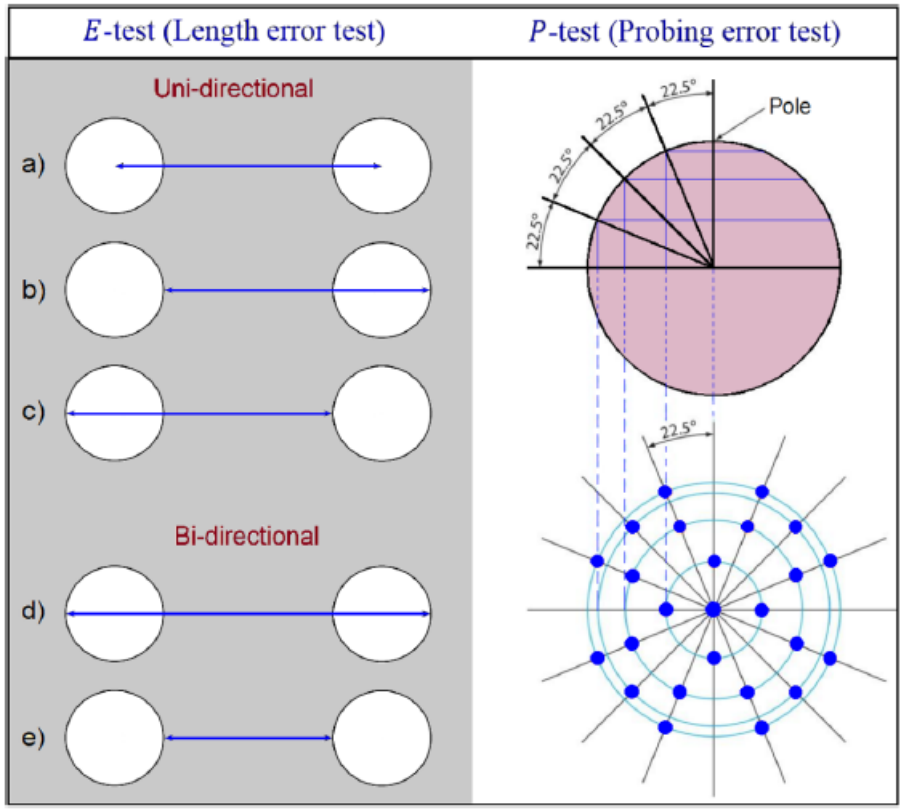

Figure 6.8. Graphic description of the E-test and P-test procedures [6].

E-test has been proposed to its application on external hollow cylinders, while P-test has been planned for precision spheres.

6.3.2.2. Uncertainty estimation methods

Two uncertainty estimation methods have been proposed for the verification of the test object:

- Substitution method is widely applied in the uncertainty estimation of CMS (standard ISO 15530-3:2011 [91]), and adapted for the usage in XCT (directive VDI/VDE 2630-2.1 [67]) The procedure for the calculations is described in Section 2.1.4, Eq. 1 for general calculations and Eq. 2 for its adaptation to XCT uncertainties estimation. This procedure involves the usage of a reference device; in this case, as in the first experiment described in Section 6.1, a CMM will be used for the calibration of macro geometries and a FVM for surface roughness and freeform surface comparison. Here, in addition, normalized error (E_N) parameter will be calculated according to standard ISO/IEC 17043:2023 [98] following Eq. 3 in Section 2.1.4 for the evaluation of result comparability.

- Multiple measurements approach, which is a recently developed method and was earlier proposed for its application in tactile CMMs uncertainty calculations and was firstly used in XCT measurement of lattice structures by Zanini et. al. [68]. It consists in the repetition of XCT measurements of the test object in multiple orientations (at least 4) with the objective of randomize systematic errors to reduce them by averaging results obtained. With this method, it is possible to determine uncertainties by the variance of the results. Here, some orientations of the workpiece have to be avoided in the experiment, not to obtain inadequate measuring conditions and higher errors.

  Calculations for the determination of the expanded uncertainty (U_{MMA}) in this procedure, based on [68,159,160] are described in Eq. 9:

$$U_{MMA} = k * \sqrt{\frac{u_{rep}^2}{n_1} + \frac{u_{geo}^2}{n_2} + u_L^2 + u_D^2 + u_{temp}^2} \quad (9)$$

  where k is the coverage factor (k=2 for a level of confidence of approximately 95%), u_{rep} is the standard uncertainty contribution originating from repeatability, n_1 is the number of repeated measurements, u_{geo} is the standard uncertainty contribution originating from the errors of the XCT system geometry, n_2 is the number of the sample orientations, u_L is the standard uncertainty contribution connected to the computation of the scale error (E_L), u_D is the standard uncertainty contribution related to the computation of the probing error of size (E_D) and u_{temp} the standard uncertainty contribution from temperature related effects.

6.3.2.3. Reference devices and XCT settings

As stated before, two devices are selected for the reference measurements for XCT intercomparison, depending on the feature evaluated:

- For macro geometries, a coordinate measuring machine (CMM) ZEISS PMC-876 CNC, is selected, with a 3 mm in diameter spherical ruby probe. Software Zeiss Calypso 3.6 is used for the planning and post processing of the results.
- A focus variation microscope InfiniteFocusSL of Alicona (Graz, Austria) is selected for surface roughness of the ramps and freeform surface, using integrated software LaboratoryMeasurementModule 6.6.12. A 10× magnification lens is used, with a lateral resolution of 8 μm and a vertical resolution of 130 nm. STL

files are exported for each ramp, using software Gwyddion 2.60 for the obtention of areal and linear roughness parameters.

XCT evaluation is performed by device Zeiss Metrotom 800 G3/225 kV, using integrated software Metrotom OS 3.12 (Zeiss, Oberkochen, Germany). Post processing of the volumes is done by software Zeiss Inspect X-Ray Pro 2023.3.0.

6.3.3. Preliminary results and discussion

For the first evaluation, multiple measurements approach has been selected for the uncertainty estimations due to its novelty and practical application (as no other reference device is required). In future evaluations, substitution method will be also applied as stated in Section 6.3.2.2.

To follow the procedure for the uncertainty estimation by multiple measurements approach, four orientations have been planned with different angles of inclination from the horizontal plane. Orientations are displayed in Figure 6.9.

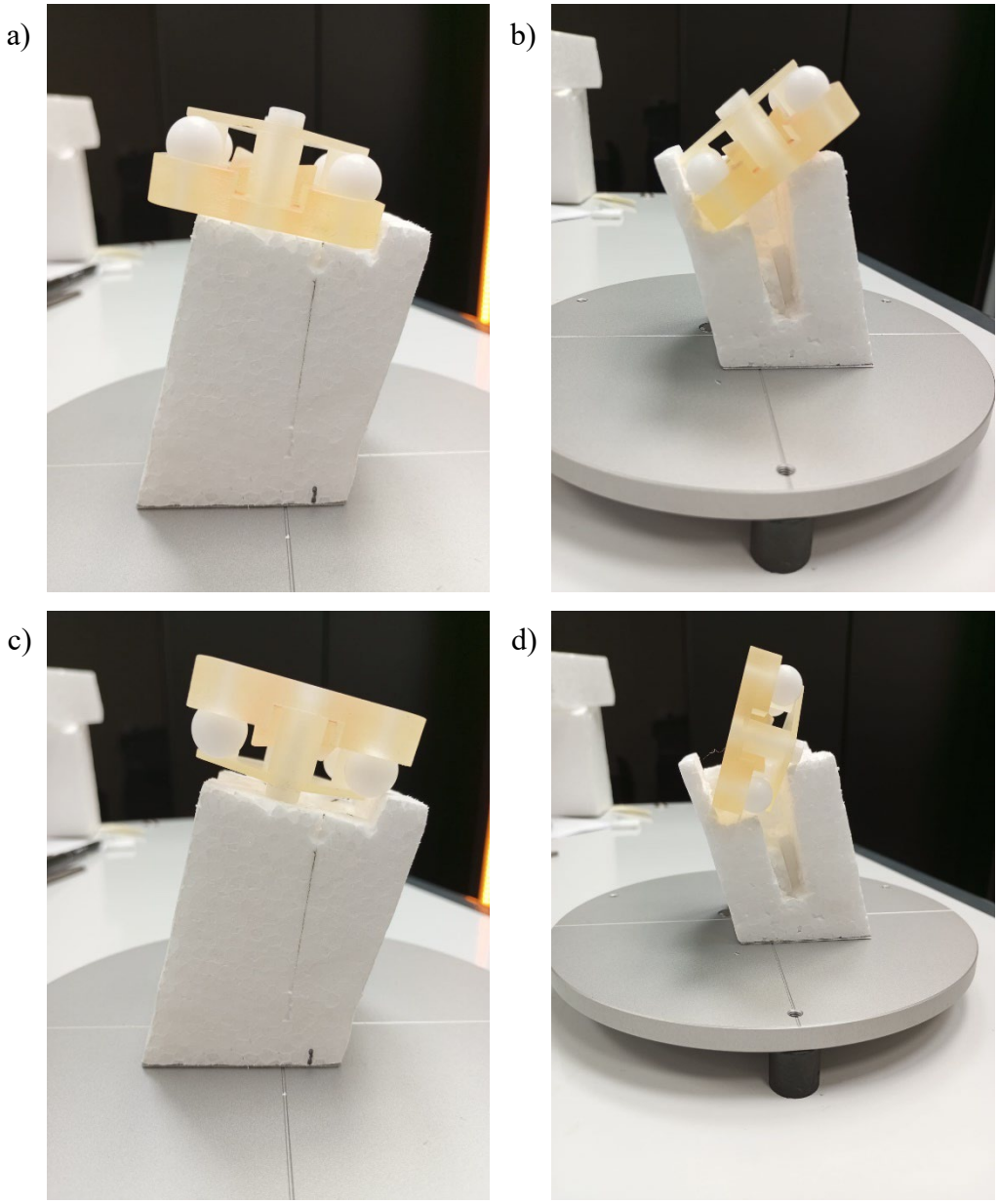

Figure 6.9. Test object orientations. a) 20º. b) 45º. c) 160º. d) 105º.

First preliminary measurements have been done to test the suitability of the part designed and the methodology, as well as to obtain repeatability results.

Following the orientations selected for the multiple measurement approach evaluation, 20º orientation (position 1) has been considered for the XCT measurements. Position 1 is shown in Figure 6.9a. Settings used in the device are displayed in Table 6.6.

Table 6.6. XCT settings used for first evaluation.

	XCT
Voltage/kV	100
Current/µA	564
Physical filter	No
Projections	1850
Exposure time/ms	500
Magnification	3.48
Resolution/µm	39.00 (Voxel size)
Time elapsed/min	14–16

Macro geometries have been evaluated, in terms of diameters and distances, using normalized acceptance tests (as described in Section 6.3.2.1) if applicable. Standard deviations (σ) of the results is shown in Figure 6.10.

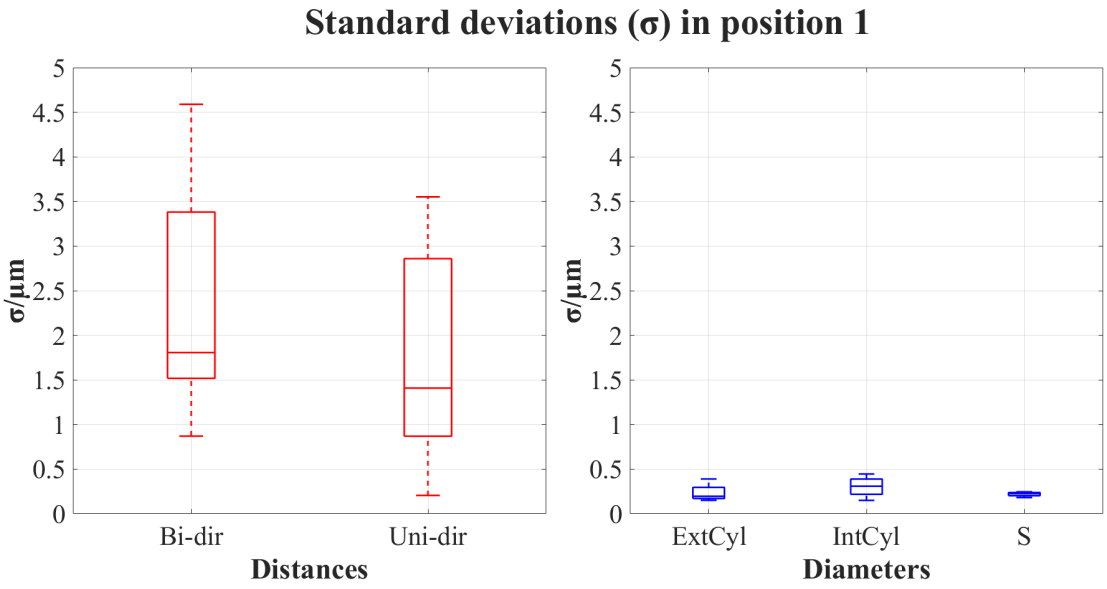

Figure 6.10. Standard deviations of diameters and distances in position 1.

Standard deviations found are significantly low, mainly for diameters as values are below 0.5 µm in all features. It has been observed that σ in uni-directional distances is lower than bi-directional features, which is common as bi-directional dimensions are more sensible to variations in surface determination. Nevertheless, both results in diameters and distances are considered acceptable as standard deviations are in general lower than the MPE for the device used (MPE = 4 + L/100 µm for size and distances measurements, according to datasheet provided by the manufacturer of the XCT device.).

This, as a first evaluation of the test objects, is promising as results have improved considerably the values obtained in previous experiments.

6.3.4. Conclusions

In this study, a newly developed multi geometrical test artefact for the uncertainty estimation of XCT measurements of polymeric AM parts is proposed, together with a methodology for the adequate evaluation, calibration and traceability calculations.

With the starting point described in Section 6.1, the knowledge obtained in parallel studies and the improvements planned, the complete procedure has been optimized; first results are promising, as they show significantly lower standard deviations and therefore more stability. Evaluation process has allowed to increase the quality of XCT evaluations, optimizing device settings and improving magnification (thus, obtaining better resolution), which is a key aspect in micro geometries characterization.

Inclusion of polymeric precision spheres has a positive impact as reference features, as high quality results and better alignment system is reached, while normalized procedures based on acceptance tests (E-test and P-test) will allow to obtain more comparable measurements with calibrated devices.

However, as the experiment is still in process, first positive results should be confirmed with the calibration of the test object by reference devices, a good uncertainty estimation by both procedures mentioned in Section 6.3.2.2 and a stability study along time.

6.4. Closing remarks and future work

In this chapter, investigation is focused on the uncertainty estimation of XCT measurements of polymeric AM parts. An experimental approach is settled, based on an ad hoc multi geometry test object which covers a wide range of typical macro and micro features found on polymeric AM industrial products. A first approach was done, and after negative results, certain improvements were planned. Experiments developed in parallel with this study have allowed to optimize the measurement process and to modify the workpiece, introducing new elements (such as precision spheres). Normalized procedures for the evaluation (see Section 6.3.2.1) and the uncertainty estimation (see Section 6.3.2.2) have been introduced to improve the measurement methodology. Main conclusions and contributions of this work are described below:

- Evaluation of AM spheres in XCT is strongly dependant on the surface determination, as the roughness profile differs severely in high and low

resolution measurements; it also affects the evaluation in CMM, as repeatability of the surface points registered is very low. Consequently, introduction of high quality spheres in a test object for the uncertainty calculations is adequate, as this repeatability due to the measuring process will improve significantly. As stated in the rest of experiments concerning polymeric features, this conclusion should be limited to polymers, and different materials could obtain different results and further experiments would be required.

- Optimization of the measuring process and introduction of normalized procedures have highly improved repeatability of the XCT measurements in the first preliminary evaluation. The study is still in development, but first results are promising, and it suggests that this modification of the methodology is positive to reach the final objective of the project (uncertainty estimation in XCT measurements of polymeric AM parts).

To sum up, although the study is still in progress and several issues have been found in first stages of the experiment, preliminary results of the optimized test object with improved methodology are promising and suggest a positive effect on the final results. As the study continues, further work consist of a consolidation of the methodology and a verification of the repeatability through the uncertainty calculation methods proposed.

7. Summary and conclusions

This chapter is dedicated to the closing remarks of the thesis, including the contributions done with the research conducted, key findings related to the objectives planned at the beginning of the project and future work programmed as a result of this dissertation.

7.1. Key findings and contributions

As stated in Section 1.2, the main aim of this thesis is the development of an experimental methodology for the analysis of the XCT precision in the evaluation of polymeric additively manufactured parts. With this methodology, the goal is to provide deeper understanding of this type of XCT evaluations, being able to apply the developed process and guidelines to future measurements, improving their traceability and uncertainty estimation procedures.

In relation to the objectives planned for this thesis, a list of general milestones obtained, common for all the individual experiments, is shown below.

i. First literature review has allowed the author to identify the most promising research topics in the field of XCT evaluation of polymeric AM. With this base knowledge, a series of experiments have been planned to cover four gaps found: surface characterization of different polymeric AM parts by means of XCT, evaluation of attenuation effect on the XCT measurement of metal-polymer assemblies, accuracy estimation of XCT characterization of polymeric AM lattice structures and uncertainty estimation of XCT evaluation of polymeric AM parts.

ii. Common procedures used in XCT evaluation have been studied and applied (or modified) for the experiments planned: settings adjustments depending on the workpiece, selection of reference devices for the calibration of the workpieces (CMM for macro geometries, FVM for micro geometries) and uncertainty calculations adapted to the measurement conditions. For this purpose, the substitution method and the multiple measurement approach (when applicable) were employed. Good practices have been developed and improved along this thesis, implementing these optimizations to the new experiments. As a consequence, results with higher quality and fidelity have been obtained.

iii. Methodologies used for the evaluation and calibration of polymeric AM test objects have been studied and adapted for each case. Methods investigated are: orientation of the surface evaluated in FVM, alignment of the parts in CMM, number of repetitions for each measure to obtain adequate repeatability data, etc. This methodology has been used for the evaluation of the artefacts developed, with successful results.

iv. Guidelines for the design of the test objects for each experiment have been studied and developed. A design-manufacturing-measurement cycle is created, in which it has been possible to evaluate design errors and improvement opportunities. As a result, workpieces used for the studies have been improved along the research. It has served to obtain better results and amplify the knowledge on the design of parts and assemblies with similar characteristics. This will serve in the future for further investigation.

v. XCT methodologies designed and planned have been refined together with the test objects, as a consequence of the design-manufacturing-measurement cycle created. A high level of quality has been reached, in terms of part evaluation and adaptation to the object measured, allowing to extrapolate procedures from one experiment to another as knowledge obtained remains transversal.

vi. Uncertainty calculation procedures have verified and validated the methodologies proposed, as they have reached an adequate level of traceability and repeatability along the experiments.

Focusing on each individual research opportunity and as described at the end of each chapter, several contributions have been made in this thesis and summarized below.

Concerning the surface characterization in polymer-based AM (chapter 3):

- It has been found that a minimum ratio of Ra'/Vx ≈ 0.75 (coefficient between average roughness and voxel size) is desirable for an adequate evaluation of surface roughness by XCT. Of course, higher resolution (consequently, lower voxel size) will result in higher accuracy when evaluating micro geometries. However, in cases where test objects are big enough, excessively high magnification could result in non-complete XCT evaluation and therefore more time-consuming measuring process. With this relationship, an estimation of the adequate magnification for each part and each micro feature could be done. Nevertheless, this experiment is focused on polymeric AM parts, and further

considerations should be taken for the measurement of other types of materials and processes.

- Regarding evaluation of surface roughness in different polymeric AM technologies, it has been found that linear roughness parameters are suitable for fused deposition modelling (FDM) and Polyjet, but areal parameters are required for a correct characterization of selective laser sintering (SLS). Same conclusion has been obtained for the real roughness estimation by the two studied predictive models [37,38]. Main reason is the post process necessary for the cleaning of the surfaces: SLS uses compressed air to remove the unfused dust present after the manufacturing; however, a significant percentage of the powder remain trapped between the stairsteps. Additionally, not all powder on the surface is completely fused, which creates re-entrant features that only are possible to evaluate by XCT. In contrast, FDM does not require any post processing of the surface, while Polyjet parts are cleaned by pressurized water; it eliminates almost all support material, with low effect on the surface roughness. Here, it is worth to mention that, in case of Polyjet parts, as nominal layer thickness is significantly smaller, false stairsteps have been designed to equalize roughness values with FDM and SLS.

Related to the attenuation in XCT evaluation of metal-polymer assemblies (chapter 4):

- It has been shown that dimensional evaluation of polymeric macro geometries is possible in metal-polymer assemblies, with an acceptable accuracy, even including high-density metals (in this case, steel). It is true that the denser is the material, the more artifacts are found in the polymer. However, low deviations are found in the measurement of spheres' diameters and distances. These features are not dependant on surface determination and therefore are less affected by external noise. This should be taken with caution in form error and roughness measurement, as both are highly dependent on the surface, and higher distortions are found.
- Considering optimized XCT settings for metal-polymer assemblies, relative intensity (I/I_0) could be used as an indicator of the expected XCT accuracy when measuring this type of assemblies, as it is directly related to the attenuation of the X-rays. Consequently, there is a correlation with the noise levels and artifacts in the tomographies. However, not only I/I_0 can be used for

the evaluation of XCT quality, and more parameters should be considered together, as results cannot be automatically extrapolated. However, these results can be used as a reference in assemblies with similar material configurations.

About the accuracy of XCT measurements of polymeric lattice structures (chapter 5):

- It has been seen that, even with lower resolution, repeatability of XCT when dimensioning lattice structures' features is higher than FVM, a device able to obtain high quality surfaces. Main reason is its ability to characterize internal and hidden elements, which are not in direct sight, in contrast to FVM that is capable only of reaching outer elements. Although XCT is typically used for lattice evaluation, traceability of measurements is still challenging and therefore a comparison with other devices was a need. With this investigation, deeper knowledge about the precision of this technology (XCT) for this purpose (lattices) is obtained. However, here the study is limited to polymeric AM lattices made by SLS; further investigation could be done for other materials with interest in industry, such as metals or composites.
- It has been observed that cell position does not affect the XCT accuracy in the dimensioning of the struts in a full lattice, as inner cells has similar deviation as outer cells. This is an important aspect, for two reasons: i) attenuation does not significantly affect the characterization of struts. Thickness of these elements is usually very thin; any disruption could cause high differences in surface determination and, therefore, worse measurement accuracy. ii) If reference measurements are required for an intercomparison with XCT (e.g. for the verification of XCT measurements), outer cells could be representative enough of the whole structure. This could allow devices such as FVM (which are not able to characterize the internal parts) to perform this quality control.

Finally, regarding studies for XCT uncertainty estimation for polymeric AM objects (chapter 6):

- Evaluation of AM spheres in XCT is strongly dependant on the surface determination, as the roughness profile differs severely in high and low resolution measurements. It also affects the evaluation in CMM, as repeatability of the surface points registered is very low. Consequently, introduction of high quality spheres in a test object for the uncertainty

calculations is adequate, as this repeatability due to the measuring process will improve significantly. As stated in the rest of experiments concerning polymeric features, this conclusion should be limited to polymers. Different materials could obtain different results and further experiments would be required.

- Optimization of the measuring process and introduction of normalized procedures have highly improved repeatability of the XCT measurements in the first preliminary evaluation. The study is still in development, but first results are promising, and it suggests that this modification of the methodology is positive to reach the final objective of the project (uncertainty estimation in XCT measurements of polymeric AM parts).

7.2. Future work

As stated in previous chapters, further research is programmed in relation with the results obtained in each field of investigation, in order to continue to provide deeper understanding of XCT measurements of polymeric AM parts. A summary of this future work is shown below.

Regarding XCT surface characterization of different polymeric AM technologies, experiments here presented have been limited to planar surfaces. However, surface roughness is present in all shapes produced by AM; therefore, further investigation could be focused on the evaluation of non-planar test objects. For this purpose, a first approach has been done in the design of workpieces which include parametrical surfaces. Some of them are a hyperbolic paraboloid, a sinusoidal wave and different surfaces defined by Chirp profiles (wavy functions in which frequency is variable depending on the position). Here, theoretical models described in Section 3.1.1 should be adapted, as they are only defined for straight profiles. Advances in this field could lead to a complete roughness characterization on polymeric AM parts by means of XCT, no matter the shape evaluated, which is currently limited.

In the field of multi material XCT measurements, precisely in metal-polymer assemblies, relevant advances have been done in this thesis to generalize settings definition and expected accuracy, based on the attenuation of the X-rays and relative intensity (I/I_0). However, experiments have been limited to two metals: aluminium and steel, and results found in Section 4.2 show that tendencies vary depending on the material of the test object. Therefore, further work should be focused on the amplification of the

experiments to other types of materials. Here, simulations done in software aRTist 2.12 have obtained acceptably accurate results comparing to experimental data. This provides an important design freedom in the experiments, as no manufacturing constraints are found to test scenarios with different materials.

Concerning accuracy definition on XCT evaluation of polymeric AM lattices, a good experimental approach has been done in the study conducted; however, as indicated before, it is limited to polymeric materials and for a certain type of lattices (strut and cell based). Here, investigation on other shapes and lattice distribution could be interesting, considering organic forms (such as gyroids or free forms). Additionally, as the research have advanced in the precision estimation of XCT, the aim is to use it as a tool for further investigation in the usage of realistic 3D models for the finite model method analysis, to study mechanical effect on real cases of lattice structures. In this terms, observations made in the porosity of the printed test objects used for the experiments presented in this thesis could be an interesting aspect to characterize, due to its effect on the mechanical properties of the part.

Lastly, in the field of uncertainty estimation of XCT measurements of polymeric AM parts, study is still in development as stated in Section 6.4. In this aspect, all the previous points have contributed to the improvement of the methodology applied. First step in the future work, thus, is to further analyse the results obtained and evaluate the accuracy and adequacy of the methodology proposed. This procedures could help in the efforts done previously by other academics to improve the standards currently used for the estimation of uncertainties and traceability procedures, as the research group has acquired a valuable knowledge during the experiments performed.

8. Versión en castellano

En esta sección se hace una traducción al castellano de la introducción, campo de investigación, estructura y objetivos propuestos para la tesis explicados en el capítulo 1, y de las conclusiones y trabajo futuro descritos en el capítulo 7.

8.1. Introducción

La aplicación de la tomografía computarizada de rayos X (XCT) en el campo de la metrología industrial ha tenido un impacto significativo en la evaluación no destructiva de piezas y ensamblajes. Su capacidad para caracterizar no solo superficies externas, sino también el interior del objeto a medir permite inspecciones mucho más completas. La XCT comúnmente se basa en la adquisición de imágenes 2D de rayos X en torno a una rotación completa de la pieza en su eje vertical, obteniendo una reconstrucción 3D del objeto. Esto incluye la medición de elementos (superficies libres, cavidades internas, celosías, etc.) los cuales no son accesibles mediante métodos e instrumentos metrológicos tradicionales. Además, con una única tomografía es posible medir macro geometrías (diámetros, distancias entre elementos, errores de forma, etc.) y micro geometrías (rugosidad superficial, porosidades, etc.).

Sin embargo, esta tecnología innovadora presenta desventajas. La XCT depende de la capacidad de penetración del objeto por parte de los rayos X; por tanto, una adquisición adecuada de las radiografías está determinada por una correcta selección de los parámetros de la fuente de rayos X. En este punto, una serie de aspectos deben ser considerados: tamaño de la pieza, densidad del material, espesores máximos, elementos a medir, etc. Como cada objeto posee diferentes características, generalizar en cuanto a parámetros de medición resulta extremadamente difícil, principalmente cuando las condiciones de medida no son las óptimas (por ejemplo, ensamblajes multimaterial con grandes diferencias en radiopacidad). Esto tiene como resultado no solo la necesidad del estudio de casos puntuales para cada medición, sino también un déficit de normativa general para obtener estimaciones de incertidumbre de medida para mediciones por XCT.

El objetivo de esta tesis es profundizar en el conocimiento de las mediciones de piezas mediante XCT y en la mejora de la estimación de la incertidumbre de medida mediante un marco de carácter experimental. En base a la literatura estudiada, se han investigado las tipologías de piezas más relevantes con aplicación industrial y se han diseñado una

serie de objetos de test para realizar los experimentos. En dichos experimentos se ha aplicado un ciclo diseño-fabricación-evaluación para obtener una cantidad suficiente de datos con los cuales generar directrices específicas para cada caso y extrapolarlas al proceso general de medición por XCT. La investigación se ha centrado en materiales poliméricos y fabricación aditiva (AM). Los polímeros presentan un comportamiento diferente (en comparación con los metales) en su caracterización por XCT en términos de atenuación de los rayos X, y resultan interesantes en el ámbito industrial (normalmente más sencillos y menos costosos de fabricar en AM en comparación con otros materiales). Por otra parte, la AM permite producir geometrías complejas que no son posibles de fabricar mediante otras tecnologías.

En esta sección se presenta un resumen del marco teórico en relación con campos de estudio relevantes a esta tesis, junto con los objetivos planteados para esta investigación.

8.1.1. Contexto

Desde los inicios de la producción en masa en el ámbito industrial, los controles de calidad han sido necesarios para asegurar la precisión adecuada de los productos fabricados. Este control de calidad normalmente incluye una serie de pruebas y protocolos realizados mediante instrumentos específicos para verificar ciertos aspectos clave de las piezas y comprobar su correcta funcionalidad. El constante aumento de los requisitos de calidad ha dado como resultado un desarrollo de una ciencia que regula la calibración y verificación de los instrumentos de medición para asegurar la precisión de sus medidas: la metrología industrial [1,2].

Uno de los principales aspectos considerados en el control de calidad es la precisión dimensional: en cualquier mecanismo o ensamblaje, una desviación dimensional o de forma en alguna de sus piezas puede provocar ajustes incorrectos, desequilibrios y otros defectos que conllevan a fallos críticos. Para mediciones simples, esta tarea se puede realizar mediante herramientas manuales como micrómetros, goniómetros, galgas de precisión, etc., que permiten una evaluación rápida sin necesidad de post procesar datos. Sin embargo, estas herramientas no son adecuadas para inspecciones más complejas o mediciones de alta precisión. Para ello, se han desarrollado una serie de dispositivos y máquinas a lo largo de la historia.

Existen dos aspectos de gran importancia en la metrología dimensional a la hora de escoger el instrumento de medición más apropiado: el rango de medición (área o volumen máximos que el instrumento es capaz de alcanzar) y la resolución (tamaño mínimo de

elemento que es capaz de medir). Ambas propiedades están inversamente relacionadas; teóricamente, para obtener una muy alta resolución en un área muy extensa es necesario un tiempo de medición y un gasto de recursos computacionales extremadamente elevados. Como consecuencia, los instrumentos de medición tradicionalmente se han optimizado para tener un gran rango de medida con una resolución aceptable para elementos de un tamaño medio-grande (llamadas macro geometrías, elementos geométricos de tamaño mayor a 1 mm, como pueden ser planos, cilindros, esferas y sus características físicas) o para ser capaces de evaluar elementos de muy pequeño tamaño (llamados micro geometrías, como la rugosidad superficial y elementos de dimensiones micrométricas) con una resolución muy alta pero en un campo de visión reducido.

Para la evaluación de macro geometrías se utilizan comúnmente instrumentos como las máquinas de medición por coordenadas (CMM) y los laser trackers. Ambos sistemas emplean elementos de contacto (palpadores en las CMM, reflectores en los laser trackers) para realizar las mediciones en las piezas, empleando un sistema de coordenadas basado en la localización de puntos individuales en un espacio tridimensional, a lo largo de los ejes X, Y y Z.

Las CMM emplean una estructura formada por guías lineales mediante las cuales el palpador se desplaza a lo largo de los 3 ejes para contactar directamente con la pieza a medir, la cual está anclada a una mesa de precisión; la forma de esta estructura depende principalmente de la arquitectura de la CMM, pero en todo caso otorga una estabilidad suficiente para la obtención de medidas de alta precisión y repetibilidad. Los puntos obtenidos son registrados como coordenadas XYZ en un sistema cartesiano mediante reglas ópticas y encoders lineales.

Los laser trackers, por su parte, utilizan un rayo láser que es dirigido mediante un reflector que se coloca en contacto con la pieza a medir, y su posición es registrada por un interferómetro o un medidor de distancia absoluta. Al contrario que las CMM, los laser tracker trabajan en un espacio de coordenadas esféricas, obteniendo el valor de la distancia y dos ángulos ortogonales mediante encoders angulares. Son capaces de medir grandes distancias [3] (las CMM están limitadas por su tamaño y, por tanto, su volumen efectivo de medida); sin embargo, debido a los posibles errores generados en los encoders angulares [4], el nivel de precisión es mucho menor que el de las CMM.

Para la caracterización de micro geometrías se emplean dispositivos tanto de contacto directo como ópticos. Aunque generalmente se usan en la industria para evaluar rugosidad

superficial y para la digitalización de superficies, su capacidad se extiende también a la medición de micro geometrías con dimensiones nanométricas.

En general, estos instrumentos se basan en la adquisición del valor de altura de un determinado punto, para la obtención ya sea de un punto único (caso de los microscopios confocales), de un perfil lineal (perfilómetros laser o de contacto) o de una superficie (microscopios de variación focal, FVM). Los instrumentos basados en la obtención de superficies son, generalmente, los más avanzados para la reconstrucción de micro geometrías, siendo capaces de caracterizar superficies 2,5D. La técnica que emplean permite adquirir nubes de puntos variando la altura de un rayo de luz en un rango determinado, obteniendo una resolución vertical de nanómetros.

Junto con el avance de las tecnologías digitales y computacionales, se han desarrollado nuevos instrumentos y técnicas metrológicas capaces de adquirir datos de piezas reales y reconstruir a partir de ellos un volumen 3D digital, en el cual es posible extraer dimensiones y medidas GD&T. Algunos de estos instrumentos y técnicas son los escáneres laser y la fotogrametría, que son empleados para la caracterización de áreas a gran escala (edificios, excavaciones geológicas, etc.); por otro lado, los escáneres ópticos son utilizados como herramientas en brazos de medición portátiles para obtener nubes de puntos de piezas industriales más pequeñas. Estos dispositivos están sin embargo limitados a la medición de la superficie externa de los objetos, no siendo capaces de inspeccionar zonas internas [5].

Como gran innovación en la metrología industrial, la tomografía computarizada de rayos X (XCT) se ha erigido como una solución para la inspección no destructiva de piezas y ensamblajes, debido a su capacidad para medir no sólo la superficie externa del objeto, sino también los elementos internos. Esta técnica ha sido utilizada a lo largo de los años [6] en el ámbito de la medicina, para la obtención de radiografías y la inspección interna de cuerpos humanos; recientemente, ésta ha sido adaptada para la toma de mediciones de alta precisión en el campo de la ingeniería industrial.

La XCT se basa en la adquisición de imágenes 2D de rayos X de la pieza a medir, la cual es anclada en un plato rotatorio. Un detector registra las proyecciones a lo largo de la rotación de 360º y, mediante un algoritmo especializado, se realiza una reconstrucción del objeto virtual. En este punto, es necesario un post procesado de los datos: un software específico se emplea para filtrar los datos y determinar la superficie del objeto (tanto interna como externa). En los casos necesarios se procede a extraer los datos metrológicos posteriormente.

Como se ha indicado previamente, la XCT tiene la ventaja de poder caracterizar los elementos internos y externos, constituyendo una solución para la inspección de defectos internos y porosidades. Además, su resolución y rango de medida le otorga una alta versatilidad, permitiendo evaluar tanto macro geometrías como micro geometrías, incluso formas complejas como superficies libres y estructuras en celosía.

Sin embargo, esta tecnología presenta algunas desventajas. La XCT se basa en la penetración de los objetos por rayos X, generando un histograma de valores de gris que varía dependiendo de la atenuación. Este parámetro está directamente relacionado con la densidad del material, su número atómico y el espesor de la pieza; como consecuencia, cualquier variación en la geometría de la pieza a medir puede afectar al resultado de la medición. Los parámetros del dispositivo normalmente deben ser ajustados para cada pieza o ensamblaje, por tanto, la generalización en el proceso de medición resulta complicada. Esto ha dificultado la estimación de la incertidumbre de los dispositivos de XCT; actualmente, la normativa empleada para regular los cálculos necesarios para la estimación de la incertidumbre está todavía en desarrollo, y para cada caso se suelen realizar aproximaciones.

La mejora continua de técnicas metrológicas como la XCT está motivada por el desarrollo de los procesos de fabricación, los cuales son capaces de generar diseños innovadores de alta complejidad con altos requisitos de calidad. En este apartado, la fabricación aditiva (AM) se erige como la tecnología más versátil en el campo de la producción industrial. La AM comenzó como un proceso innovador con el que replicar objetos virtuales en la realidad, basándose en la adición de material capa por capa; sin embargo, el propósito inicial se limitaba a prototipos formales, ya que las características mecánicas y térmicas de las piezas no eran adecuadas. La mejora de estas propiedades ha permitido el uso de las piezas producidas como productos acabados y funcionales.

El concepto de la AM engloba una serie de técnicas: modelado por deposición fundida (FDM), fusión laser por lecho de polvo (LPBF), estereolitografía (SLA), etc., en las cuales diferentes tipos de materiales se pueden emplear dependiendo del principio de fabricación. Los materiales más comunes son los polímeros y los metales; por ejemplo, en aplicaciones con altos requerimientos de calidad (como la aeronáutica, aeroespacial o las herramientas de precisión), el uso de aleaciones de metal se está extendiendo debido a sus excelentes capacidades mecánicas y térmicas. Sin embargo, la producción de piezas en AM metálica es costosa, ya que las máquinas son caras y sus requisitos técnicos y ambientales son altos. Por otra parte, los polímeros tienen un gran interés en la industria,

ya que tienen una mejor relación calidad-precio para ciertas aplicaciones. Además, está muy extendido el uso de materiales poliméricos mejorados en productos acabados de alta calidad como polímeros técnicos (polyether ether ketone (PEEK), polyethylene terephthalate glycol (PETG)) o polímeros reforzados con fibras de vidrio o carbono.

8.1.2. Objetivos

El objetivo principal de esta tesis es el desarrollo de una metodología experimental para el análisis de la precisión de la XCT en la evaluación de piezas de AM polimérica. Para ello, se han analizado una serie de situaciones que constituyen oportunidades de investigación y se han diseñado y fabricado piezas de test, cada una adaptada al experimento planteado. Se han empleado una serie de instrumentos metrológicos de referencia para la calibración de las piezas producidas, con los cuales se han podido realizar comparativas con las mediciones obtenidas por XCT para identificar tendencias y errores sistemáticos. El objetivo final ha sido profundizar en el conocimiento relacionado con la medición de este tipo de piezas por XCT, siendo capaces de aplicar la metodología desarrollada y generar una serie de directrices para futuros casos y mejorar los procesos de estimación de la incertidumbre y la trazabilidad.

Este objetivo final se puede dividir en diferentes objetivos parciales, los cuales son desarrollados a lo largo de la tesis:

i. Revisión del estado del arte e identificación de aspectos clave. Revisión profunda de la literatura existente con la intención de identificar los aspectos más importantes acerca de las dos tecnologías empleadas: principales características de la XCT, fuentes de error existentes en la medición, oportunidades prospectivas en AM, propiedades de los materiales, etc.
ii. Análisis de los procesos actuales usados en XCT. Estudio de las metodologías comúnmente empleadas en la toma de datos mediante XCT, así como los procedimientos de cálculo de incertidumbres.
iii. Análisis de los métodos tradicionales de evaluación para piezas poliméricas de AM. Aplicación de los procesos comunes de medición en piezas poliméricas de AM para identificar errores sistemáticos y tendencias, mediante el uso de piezas de test que incluyan geometrías convencionales.
iv. Diseño de piezas de test para cada caso específico. Con los conocimientos obtenidos previamente, se diseñan, adaptan y optimizan una serie de piezas de test para su medición por XCT y por los instrumentos de referencia.

v. Desarrollo de una metodología de evaluación conjunta. Para cada situación identificada, se genera un ciclo diseño-fabricación-evaluación en el cual el objeto de test es evaluado y rediseñado o modificado en caso necesario.

vi. Validación del procedimiento. Mediante cálculos estadísticos, análisis de resultados y estimaciones de incertidumbre en base a la normativa existente, se verifica la idoneidad de la metodología propuesta. Además, las tendencias sistemáticas identificadas son registradas en directrices para cada situación específica.

8.2. Conclusiones y trabajo futuro

En esta sección se describen las contribuciones que resultan de esta tesis, tanto las contribuciones generales en relación con los objetivos planeados inicialmente como las específicas de cada uno de los experimentos realizados, así como el trabajo futuro programado.

8.2.1. Contribuciones

Como se ha planteado en la sección 1.2, el principal objetivo de esta tesis es el desarrollo de una metodología basada en resultados experimentales para el análisis de la precisión de la tomografía computarizada (XCT) en la evaluación de piezas de fabricación aditiva (AM) polimérica. De esta forma, se pretende i) alcanzar un conocimiento más profundo de este tipo de mediciones, ii) ser capaz de aplicar el proceso desarrollado a futuros procesos de evaluación y iii) mejorar las técnicas de evaluación de la trazabilidad y estimación de la incertidumbre de medida.

Los hitos logrados y contribuciones generales, en relación con los objetivos planeados para esta tesis, se muestra en la siguiente lista.

i. La primera revisión del estado del arte ha permitido al autor identificar los temas de investigación más prometedores en relación con la evaluación mediante XCT de piezas de AM polimérica. Con este conocimiento como base, se han planeado una serie de experimentos para cubrir los nichos de investigación encontrados: caracterización de la rugosidad superficial de piezas de diferentes técnicas de AM polimérica mediante XCT, evaluación del efecto de la atenuación en la medición por XCT de ensamblajes metal-polímero, estimación de la precisión de la caracterización por XCT de celosías

fabricadas por AM polimérica y estimación general de la incertidumbre en mediciones por XCT de piezas de AM polimérica.

ii. Los procedimientos típicos de medición por XCT se han estudiado y aplicado o modificado para los experimentos planificados: ajuste de parámetros del dispositivo dependiendo de la pieza evaluada, selección de instrumentos de referencia para la calibración de las piezas de test (CMM para macro geometrías, FVM para micro geometrías y rugosidades), y cálculo de incertidumbres adaptado al tipo de pieza y al entorno de medición. Para ello, se ha usado tanto el método de sustitución como la aproximación por múltiples mediciones (en caso necesario). Se han desarrollado una serie de buenas prácticas durante los experimentos y se han ido mejorando conforme avanzaba la investigación, permitiendo obtener resultados de mayor calidad y fiabilidad.

iii. Se han estudiado y adaptado para cada caso las metodologías empleadas tradicionalmente para la evaluación y calibración de este tipo de piezas, incluyendo métodos para la medición de ciertas geometrías: orientación de la superficie a medir en FVM, alineación de piezas en CMM, número de repeticiones para obtener datos de repetibilidad aceptables, etc. Esta metodología se ha aplicado de forma exitosa en las piezas de test diseñadas.

iv. Se ha diseñado cada uno de los objetos de test acorde a los consejos de diseño encontrados en la literatura, generando un ciclo diseño-fabricación-medición mediante el cual se ha podido analizar fallos de diseño y oportunidades de mejora. Como resultado, se han ido optimizando las piezas de test y se han obtenido buenos resultados; además, se ha ampliado el conocimiento sobre el diseño de este tipo de piezas, lo cual que servirá para investigaciones futuras.

v. Las técnicas de evaluación por XCT desarrolladas se han ido refinando en conjunto con los objetos diseñados, como consecuencia del ciclo diseño-fabricación-medición mencionado previamente, alcanzando un alto nivel de adaptación al objeto medido. Esto ha permitido extrapolar los procedimientos seguidos de un experimento a otro, ya que los conocimientos obtenidos son transversales.

vi. Finalmente, los procedimientos de cálculo de incertidumbres aplicados han permitido verificar las metodologías propuestas, ya que han alcanzado un nivel adecuado de trazabilidad y repetibilidad en los experimentos realizados.

Centrándose en cada uno de los aspectos de investigación estudiados y como se ha descrito en cada uno de los capítulos de este documento, se resumen en la siguiente lista las contribuciones específicas realizadas en esta tesis.

Acerca de la caracterización de la rugosidad superficial en piezas de AM polimérica (capítulo 3):

- Se ha fijado una ratio mínima de Ra'/Vx ≈ 0.75 (coeficiente entre la rugosidad media teórica y el tamaño de vóxel) como deseable para una evaluación de la rugosidad superficial de forma adecuada mediante XCT. Por supuesto, una mejor resolución (por tanto, un tamaño de vóxel menor) conllevaría mayor precisión en la evaluación de micro geometrías. Sin embargo, una magnificación demasiado grande podría resultar en tomografías incompletas en caso de objetos grandes y un incremento exponencial del tiempo de medida. Con esta relación se puede hacer una estimación de la magnificación adecuada para cada pieza y cada micro geometría; de todas formas, este experimento está centrado en piezas de AM polimérica, y por tanto los resultados no son extrapolables a otro tipo de materiales o procesos de fabricación.
- En cuanto a la evaluación de la rugosidad superficial en diferentes tecnologías de AM polimérica, se ha encontrado que el uso de parámetros de rugosidad lineal es adecuado para las piezas de FDM y Polyjet; sin embargo, los parámetros de rugosidad de área son necesarios para una correcta caracterización de piezas de SLS. A la misma conclusión se ha llegado para la estimación de la rugosidad real mediante modelos predictivos [37,38]. La razón principal es el post procesado necesario para limpiar las superficies. SLS utiliza aire comprimido para eliminar el polvo no sinterizado después de la fabricación; sin embargo, un porcentaje significativo se queda atrapado entre los escalones generados por las capas. Además, se crean una serie de canales llamados geometrías reentrantes, las cuales sólo son posibles de medir mediante XCT. Por el contrario, la FDM no necesita ningún tipo de post procesado, mientras que las piezas fabricadas en Polyjet se limpian mediante agua a presión, que elimina prácticamente todo el material de soporte, con un efecto muy bajo en la rugosidad superficial. Cabe mencionar que, en caso de las piezas de Polyjet, se han generado escalones artificiales para obtener

valores teóricos equiparables a los de otras tecnologías, ya que el espesor de capa nominal es mucho menor.

En relación con la atenuación en la evaluación por XCT de ensamblajes metal-polímero (capítulo 4):

- Se ha observado que la evaluación dimensional de macro geometrías poliméricas es posible en ensamblajes metal-polímero con una precisión aceptable, incluso en casos con metales de alta densidad (acero). Es cierto que a mayor densidad del metal, más artefactos se encuentran en el polímero. Sin embargo, las desviaciones dimensionales de los diámetros de las esferas y las distancias entre ellas son bajas, ya que no dependen de la superficie determinada en la pieza. Por tanto, el ruido externo les afecta en menor medida. Esto se debe tomar con precaución en el caso de los errores de forma y la medición de rugosidades, ya que ambas características son muy dependientes de la determinación superficial (no en vano se han encontrado mayores distorsiones).
- Partiendo de una optimización de parámetros de XCT para ensamblajes metal-polímero, el valor de la intensidad relativa (I/I_0) puede ser empleado como un indicador para la precisión esperada de la XCT midiendo este tipo de ensamblajes, ya que está directamente relacionado con la atenuación de los rayos X. Como consecuencia, hay una correlación de la I/I_0 con los niveles de ruido y las distorsiones en las tomografías. Sin embargo, no se puede emplear únicamente la I/I_0 para la evaluación de la calidad de las tomografías, ya que los resultados no pueden ser extrapolados automáticamente: más parámetros deben ser identificados y empleados conjuntamente para ello. De todas formas, para diferentes ensamblajes en los que estén presentes los mismos materiales, puede servir de referencia.

Acerca de la precisión de la XCT en mediciones de celosías poliméricas (capítulo 5):

- Se ha demostrado que, incluso con una resolución menor, la repetibilidad de las mediciones de la XCT en elementos de estructuras de celosías es mayor, en comparación con un FVM (cuya función es la obtención de superficies de alta calidad). La principal razón es la capacidad de la tomografía para caracterizar elementos internos y estructuras que no están a la vista, en contraste con el FVM que sólo es capaz de medir elementos externos. Aunque la XCT se usa

comúnmente para la evaluación de celosías, la trazabilidad de las mediciones es todavía un desafío y por tanto es necesario realizar comparativas con otros instrumentos calibrados. Con esta investigación, se ha obtenido un mayor conocimiento de la precisión de esta tecnología (XCT) para la medición de estas geometrías en concreto (celosías). Sin embargo, el estudio está limitado a celosías hechas por AM polimérica; una mayor investigación es necesaria para otros materiales de interés en la industria, como metales o materiales compuestos.

- Se ha observado que la posición relativa de la celda dentro de la propia estructura de la celosía completa no afecta a la precisión de la XCT dimensionando cada barra, ya que las celdas internas presentan desviaciones similares a las externas. Este aspecto es importante por dos razones: i) la atenuación no afecta significativamente a la caracterización de las barras. El espesor de estos elementos es generalmente muy bajo, y cualquier distorsión podría causar grandes diferencias en la determinación de la superficie (y por tanto, peor precisión). ii) Si es necesario realizar mediciones de referencia para una comparativa con la tomografía (por ejemplo para la verificación de ciertos resultados), las celdas exteriores pueden ser representativas de la estructura completa. Esto puede permitir el uso de instrumentos como el FVM (que no puede caracterizar elementos internos) para hacer este control de calidad de la XCT.

Finalmente, en relación con los estudios para la estimación de la incertidumbre de la XCT en mediciones de objetos de AM polimérica (capítulo 6):

- Se ha observado que la repetibilidad y la comparabilidad con instrumentos de referencia (en este caso, una CMM) en la evaluación de esferas de precisión poliméricas es significativamente mayor que en la medición de esferas poliméricas de AM; la caracterización de la superficie en estas últimas, debido al efecto escalera producido por las características del propio proceso de fabricación, es más complicada para instrumentos de medición por palpado (como la CMM) y ligeras modificaciones en los puntos obtenidos resultan en grandes variaciones dimensionales. Además, su evaluación por XCT es muy dependiente de la determinación de la superficie, ya que el perfil de rugosidad de las esferas difiere considerablemente para altas y bajas resoluciones. Como

consecuencia, incluir esferas poliméricas de alta calidad en el diseño del patrón de referencia para el cálculo de incertidumbres resulta adecuado para mejorar significativamente la repetibilidad de las mediciones. Como se menciona en el resto de los experimentos acerca de piezas poliméricas de esta tesis, esta conclusión debe ser limitada por el momento a polímeros, ya que diferentes materiales pueden obtener diferentes resultados y por tanto serían necesarios experimentos adicionales para otros casos.

- La optimización del proceso de medición y la introducción de procedimientos normalizados ha mejorado enormemente la repetibilidad de las mediciones por XCT obtenidas en el experimento preliminar, El estudio continúa en desarrollo, pero los primeros resultados son prometedores y sugieren que esta modificación en la metodología es beneficiosa para lograr el objetivo final del proyecto (la correcta estimación de incertidumbres en mediciones por XCT de piezas de AM polimérica).

8.2.2. Trabajo futuro

Una serie de investigaciones futuras han sido programadas en relación con los resultados obtenidos para cada uno de los aspectos investigados, con el objetivo de profundizar en el conocimiento obtenido acerca de las mediciones por XCT de piezas de AM polimérica. En los siguientes párrafos se describe un resumen del trabajo futuro planteado.

Los experimentos realizados acerca de la caracterización superficial mediante XCT de diferentes tecnologías de AM polimérica se han limitado a superficies planas. Sin embargo, este aspecto intrínseco de la AM está presente en todo tipo de formas; por tanto, se podría realizar una investigación más a fondo en superficies con diferentes formas no planas. Un primer acercamiento se ha hecho en el diseño de piezas que incluyen superficies paramétricas, como un paraboloide hiperbólico, ondas senoidales y superficies definidas por perfiles Chirp (funciones onduladas cuya frecuencia varía dependiendo de su posición). En estos casos, los modelos teóricos descritos en la sección 3.1.1 deben ser adaptados, ya que fueron ideados para perfiles planos. Un mayor avance en este campo de estudio podría conseguir una evaluación completa de la rugosidad superficial por XCT en este tipo de piezas, sin importar la forma (que en este caso se limita a rampas planas).

En esta tesis se han realizado avances relevantes para lograr generalizar los criterios para la selección de ajustes y estimación de la precisión con respecto al efecto de la atenuación en mediciones por XCT de los ensamblajes metal-polímero. Sin embargo, los experimentos realizados se han limitado al estudio de dos metales: acero y aluminio, y los resultados descritos en la sección 4.2 muestran que las tendencias varían dependiendo del material de la pieza. Por tanto, una ampliación del experimento se debe realizar para obtener datos de otros materiales, para ser capaces de enriquecer el estudio y poder lograr una generalización completa. En este punto, el software empleado para realizar simulaciones de tomografías ha servido para obtener resultados aceptablemente precisos en comparación con los datos experimentales; esto permite aumentar la libertad de diseño de experimento, ya que no están limitados por la fabricación del objeto (al ser virtual).

En el ámbito de la medición por XCT de estructuras en celosía, el estudio realizado ha permitido una experimentación con resultados fructíferos para la definición de su precisión. Sin embargo, como se indica previamente, está limitado a materiales poliméricos y a cierto tipo de estructuras (basadas en celdas y barras). En este caso, podría ser interesante incluir en una futura investigación otras formas y distribuciones, como formas orgánicas (giroides, formas libres, etc.). Como añadido, los archivos digitales de las celosías reales pueden servir como herramienta para el cálculo de tensiones y deformaciones por el método de elementos finitos, aspecto que se está estudiando en el grupo de investigación. Por último, las observaciones realizadas respecto a la porosidad de las piezas pueden ser útiles para este estudio propuesto.

Por último, el estudio respecto a la estimación de la incertidumbre en mediciones por XCT de piezas de AM polimérica continúa en desarrollo como se comenta en la sección 6.4; por tanto, el primer paso en un trabajo futuro es analizar más en profundidad los resultados obtenidos y continuar con los experimentos para poder evaluar la precisión y adecuación de las metodologías propuestas, validando de esta forma los resultados prometedores explicados en esta tesis. Estos nuevos procedimientos podrían ayudar en la definición de la normativa relativa al cálculo de incertidumbres en XCT, en la que otros académicos previamente han puesto sus esfuerzos, ya que el conocimiento obtenido por el grupo de investigación puede ser aplicado en este aspecto.

9. Dissemination of results

In this section, a summary of the scientific production resulting from this thesis is presented, including published articles (both in indexed and non-indexed journals), papers currently under review and conference contributions.

9.1. Published articles

- **IOP Conference Series, 2021:** J.A. Albajez, S. Nuño, L.C. Díaz, D. Gallardo, J.A. Yagüe, R. Jiménez, M. Torralba. Reference standard for the uncertainty estimation of X–ray Computed Tomography measurements of complex macro- and micro-geometries. IOP Conf Ser Mater Sci Eng 1193 (2021) 012065. https://doi.org/10.1088/1757-899X/1193/1/012065.
- **Additive Manufacturing, 2023:** D. Gallardo, L.C. Díaz, R. Jiménez, M. Torralba, J.A. Albajez, J.A.Y. Fabra. X-Ray Computed Tomography performance in metrological evaluation and characterisation of polymeric additive manufactured surfaces. Addit Manuf 75 (2023). https://doi.org/10.1016/j.addma.2023.103754.
  Impact factor: 10,3 (2023) Engineering, Manufacturing – 4/68, Q1.
- **Key Engineering Materials, 2023:** D. Gallardo, M. Concha, L.C. Díaz, R. Jiménez, M. Torralba, J.A. Albajez, J.A. Yagüe-Fabra. Surface Characterisation and Comparison of Polymeric Additive Manufacturing Features for an XCT Test Object. Key Eng Mater 959 (2023) 35–44. https://doi.org/10.4028/p-tn0lzd.
- **Polymers, 2024:** D. Gallardo, L.C. Díaz, J.A. Albajez, J.A. Yagüe-Fabra. Progress toward the Definition of X-ray Computed Tomography Accuracy in the Characterization of Polymer-Based Lattice Structures. Polymers (Basel) 16 (2024) 1419. https://doi.org/10.3390/polym16101419.
  Impact factor: 4,7 (2023) Polymer Science – 18/94, Q1.
- **CIRP Journal of Manufacturing Science and Technology, 2024:** D. Gallardo, L.-C Díaz, F. Zanini, J.A. Albajez, S. Carmignato, J.A. Yagüe-Fabra, On the effect of material density in dimensional evaluations by X-ray computed tomography of metal-polymer multi-material parts. CIRP Journal of Manufacturing Science and Technology 54 (2024) 1-13 doi: https://doi.org/10.1016/j.cirpj.2024.08.003.

Impact factor: 4,6 (2023) Engineering, Manufacturing – 18/68, Q2.

9.2. Conference contributions

- **MESIC 2021**: J.A. Albajez, S. Nuño, L.C. Díaz, D. Gallardo, J.A. Yagüe, R. Jiménez, M. Torralba. Reference standard for the uncertainty estimation of X–ray Computed Tomography measurements of complex macro-and micro-geometries. Oral presentation. Gijón (virtual), June 2021.
- **Jornada De Jóvenes Investigadores Del I3A 2022:** D. Gallardo, L.C. Díaz, J.A. Albajez, J.A. Yagüe-Fabra, R. Jiménez, M. Torralba, Evaluación de la estabilidad dimensional de esferas calibradas poliméricas para su aplicación en un patrón de referencia para tomografía computarizada (CT). Oral presentation. Zaragoza, June 2022.
- **CEM 2022:** D. Gallardo, L.C. Díaz, J.A. Albajez, J.A. Yagüe-Fabra, R. Jiménez, M. Torralba. Evaluación de macro y micro geometrías en Patrones de Fabricación Aditiva mediante Tomografía Computarizada. Oral presentation. Ávila (virtual), September 2022.
- **EUSPEN 2023:** D. Gallardo, L.C. Díaz, J.A. Albajez, J.A. Yagüe-Fabra. Case study of X-ray Computed Tomography performance in polymeric additive manufacturing features evaluation. Poster. Copenhagen, June 2023.
- **MESIC 2023:** D. Gallardo, M. Concha, L.C. Díaz, R. Jiménez, M. Torralba, J.A. Albajez, J.A. Yagüe-Fabra. Surface Characterisation and Comparison of Polymeric Additive Manufacturing Features for an XCT Test Object. Oral presentation. Sevilla, June 2023.
- **3DMC 2023:** D. Gallardo, L.C. Díaz, J.A. Albajez, J.A. Yagüe-Fabra. Effect of metal artifacts in polymer macro dimensional 3D evaluation by XCT in multi material parts. Poster. Bilbao, September 2023.
- **EUSPEN 2024:** D. Gallardo, L.C. Díaz, J.A. Albajez, J.A. Yagüe-Fabra. Simulation-based approach on relative intensity effect in multi material X-Ray computed tomography evaluation. Poster. Dublin, June 2024.

9.3. Research stay at University of Padova

Position: Visiting PhD researcher in the Department of Manufacturing and Engineering at the University of Padova.

Period: 01/09/2022 – 30/11/2022 (3 months).

Supervisor: Full professor Prof. Simone Carmignato

Purpose: Collaboration with the host research group in the investigation regarding XCT characterization of metal-polymer assemblies, as well as the improvement on the definition of uncertainty estimation procedures for this type of parts.

Contributions:

- D. Gallardo, L.-C Díaz, F. Zanini, J.A. Albajez, S. Carmignato, J.A. Yagüe-Fabra, On the effect of material density in dimensional evaluations by X-ray computed tomography of metal-polymer multi-material parts. CIRP Journal of Manufacturing Science and Technology 54 (2024) 1-13. doi: https://doi.org/10.1016/j.cirpj.2024.08.003.

References

[1] P. Howarth, F. Redgrave, P.T.B. Germany, S. Madsen, S. Grafisk, Metrology–in short, 3rd edition, EURAMET Project, 1101, 2008.

[2] JCGM, JCGM 200:2008 - International vocabulary of metrology-Basic and general concepts and associated terms (VIM), 2008. www.bipm.org.

[3] H. Shang, C. Liu, R. Wang, Measurement methods of 3D shape of large-scale complex surfaces based on computer vision: A review, Measurement 197 (2022) 111302. https://doi.org/10.1016/J.MEASUREMENT.2022.111302.

[4] L. Xie, Y. Lian, F. Du, Y. Wang, Z. Lu, Optical methods of laser ultrasonic testing technology in the industrial and engineering applications: A review, Opt Laser Technol 176 (2024) 110876. https://doi.org/10.1016/J.OPTLASTEC.2024.110876.

[5] E. Morse, Design for Metrology – A new idea?, Procedia CIRP 84 (2019) 165–168. https://doi.org/10.1016/j.procir.2019.04.240.

[6] H. Villarraga-Gómez, E.L. Herazo, S.T. Smith, X-ray computed tomography: from medical imaging to dimensional metrology, Precis Eng 60 (2019) 544–569. https://doi.org/10.1016/j.precisioneng.2019.06.007.

[7] H. Villarraga-Gómez, L. Körner, R. Leach, S.T. Smith, Amplitude-wavelength maps for X-ray computed tomography systems, Precis Eng 64 (2020) 228–242. https://doi.org/10.1016/j.precisioneng.2020.03.005.

[8] W.A. Kalender, X-ray computed tomography, Phys Med Biol 51 (2006). https://doi.org/10.1088/0031-9155/51/13/R03.

[9] K. Naresh, K.A. Khan, R. Umer, W.J. Cantwell, The use of X-ray computed tomography for design and process modeling of aerospace composites: A review, Mater Des 190 (2020). https://doi.org/10.1016/j.matdes.2020.108553.

[10] W. Sun, D.R. Symes, C.M. Brenner, M. Böhnel, S. Brown, M.N. Mavrogordato, I. Sinclair, M. Salamon, Review of high energy X-ray computed tomography for non-destructive dimensional metrology of large metallic advanced manufactured components, Reports on Progress in Physics 85 (2022). https://doi.org/10.1088/1361-6633/ac43f6.

[11] R. Deriche, Using Canny's criteria to derive a recursively implemented optimal edge detector, Int J Comput Vis 1 (1987) 167–187. https://doi.org/10.1007/BF00123164.

[12] S. Ontiveros, R. Jiménez, J.A. Yagüe-Fabra, M. Torralba, Analysis of surface extraction methods based on gradient operators for computed tomography in metrology applications, Materials 11 (2018). https://doi.org/10.3390/ma11081461.

[13] M. Torralba, R. Jiménez, J.A. Yagüe-Fabra, S. Ontiveros, G. Tosello, Comparison of surface extraction techniques performance in computed tomography for 3D complex micro-geometry dimensional measurements, International Journal of Advanced Manufacturing Technology 97 (2018) 441–453. https://doi.org/10.1007/s00170-018-1950-9.

[14] W. Dewulf, H. Bosse, S. Carmignato, R. Leach, Advances in the metrological traceability and performance of X-ray computed tomography, CIRP Annals 71 (2022) 693–716. https://doi.org/10.1016/j.cirp.2022.05.001.

[15] S. Wang, K. Xu, Surface roughness evaluation based on near point lighting photometric stereo, Opt Lasers Eng 170 (2023) 107775. https://doi.org/10.1016/J.OPTLASENG.2023.107775.

[16] H. Liu, D. Li, M. Xi, T. Li, K. Liu, X. Liu, Y. Wang, Chromatic confocal precision measurement accuracy analysis with surface roughness based on a scalar diffraction and raytracing hybrid model, Opt Lasers Eng 178 (2024) 108256. https://doi.org/10.1016/J.OPTLASENG.2024.108256.

[17] A. Townsend, L. Pagani, L. Blunt, P.J. Scott, X. Jiang, Factors affecting the accuracy of areal surface texture data extraction from X-ray CT, CIRP Ann Manuf Technol 66 (2017) 547–550. https://doi.org/10.1016/j.cirp.2017.04.074.

[18] A. Townsend, R. Racasan, P. Bills, L. Blunt, Development of an interlaboratory comparison investigating the generation of areal surface texture data per ISO 25178 from XCT, in: 7th Conference on Industrial Computed Tomography (ICT), Leuven, Belgium, 2017. www.iCT2017.org.

[19] N. Ortega, S. Plaza, A. Pascual, I. Holgado, L.N. López De Lacalle, Study of the influence of filter material on the roughness evaluation by means of CT, in: Euspen's 20th International Conference and Exhibition, Geneva, CH, 2020.

[20] S. Carmignato, V. Aloisi, F. Medeossi, F. Zanini, E. Savio, Influence of surface roughness on computed tomography dimensional measurements, CIRP Ann Manuf Technol 66 (2017) 499–502. https://doi.org/10.1016/j.cirp.2017.04.067.

[21] Geometrical product specifications (GPS) Surface texture: Profile Part 2: Terms, definitions and surface texture parameters (ISO 21920-2:2021, Corrected version 2022-06), 2023.

[22] Geometrical product specifications (GPS). Surface texture: Areal. Part 2: Terms, definitions and surface texture parameters (ISO 25178-2:2011), 2011.

[23] B. He, H. Zheng, S. Ding, R. Yang, Z. Shi, A review of digital filtering in evaluation of surface roughness, Metrology and Measurement Systems 28 (2021) 217–253. https://doi.org/10.24425/mms.2021.136606.

[24] Geometrical product specifications (GPS). Surface texture: Profile. Part 3: Specification operators (ISO 21920-3:2023), 2023. www.une.org.

[25] Geometrical product specifications (GPS). Surface texture: Areal. Part 3: Specification operators (ISO 25178-3:2012)., 2012.

[26] S. Petzold, J. Klett, T.A. Osswald, A Statistical Study of Surface Roughness for Polyamide 12 Parts Produced Using Selective Laser Sintering, International Polymer Processing Journal of the Polymer Processing Society 35 (2020) 126–138.

[27] J. Metelkova, L. Vanmunster, H. Haitjema, B. Van Hooreweder, Texture of inclined up-facing surfaces in laser powder bed fusion of metals, Addit Manuf 42 (2021). https://doi.org/10.1016/j.addma.2021.101970.

[28] M.E. Imanian, F.R. Biglari, Modeling and prediction of surface roughness and dimensional accuracy in SLS 3D printing of PVA/CB composite using the central composite design, J Manuf Process 75 (2022) 154–169. https://doi.org/10.1016/j.jmapro.2021.12.065.

[29] N.K. Maurya, V. Rastogi, P. Singh, Comparative study and measurement of form errors for the component printed by FDM and polyjet process, Instrumentation Mesure Metrologie 18 (2019) 353–359. https://doi.org/10.18280/i2m.180404.

[30] K. Nar, C. Majewski, R. Lewis, A comprehensive characterisation of Laser Sintered Polyamide-12 surfaces, Polym Test 106 (2022). https://doi.org/10.1016/j.polymertesting.2021.107450.

[31] A. Bhatt, Y. Huang, C.L.A. Leung, G. Soundarapandiyan, S. Marussi, S. Shah, R.C. Atwood, M.E. Fitzpatrick, M.K. Tiwari, P.D. Lee, In situ characterisation of surface roughness and its amplification during multilayer single-track laser powder bed fusion additive manufacturing, Addit Manuf 77 (2023). https://doi.org/10.1016/j.addma.2023.103809.

[32] A. Triantaphyllou, C.L. Giusca, G.D. Macaulay, F. Roerig, M. Hoebel, R.K. Leach, B. Tomita, K.A. Milne, Surface texture measurement for additive manufacturing, Surf Topogr 3 (2015). https://doi.org/10.1088/2051-672X/3/2/024002.

[33] A. Mirabal, I. Loza-Hernandez, C. Clark, D.E. Hooks, M. McBride, J.A. Stull, Roughness measurements across topographically varied additively manufactured metal surfaces, Addit Manuf 69 (2023). https://doi.org/10.1016/j.addma.2023.103540.

[34] N. Vidakis, M. Petousis, N. Vaxevanidis, J. Kechagias, Surface roughness investigation of poly-jet 3D printing, Mathematics 8 (2020) 1–14. https://doi.org/10.3390/math8101758.

[35] P. Jiang, M. Rifat, S. Basu, Impact of surface roughness and porosity on lattice structures fabricated by additive manufacturing- A computational study, in: Elsevier B.V., 2020: pp. 781–789. https://doi.org/10.1016/j.promfg.2020.05.114.

[36] D. Downing, J. Rogers, R. Tino, J. Elambasseril, C. Wallbrink, M. Qian, M. Brandt, M. Leary, A virtual stylus method for non-destructive roughness profile measurement of additive manufactured lattice structures, International Journal of Advanced Manufacturing Technology 125 (2023) 3723–3742. https://doi.org/10.1007/s00170-023-10865-9.

[37] I. Dzullijah, D. Songlin, S. Shoujin, Roughness Prediction For FDM Produced Surfaces, in: International Institute of Engineers, 2014. https://doi.org/10.15242/iie.e0214527.

[38] I. Buj-Corral, A. Domínguez-Fernández, R. Durán-Llucià, Influence of Print Orientation on Surface Roughness in Fused Deposition Modeling (FDM) Processes, Materials 12 (2019) 3834. https://doi.org/10.3390/ma12233834.

[39] L. Pagani, A. Townsend, W. Zeng, S. Lou, L. Blunt, X.Q. Jiang, P.J. Scott, Towards a new definition of areal surface texture parameters on freeform surface: Re-entrant features and functional parameters, Measurement (Lond) 141 (2019) 442–459. https://doi.org/10.1016/j.measurement.2019.04.027.

[40] A. Townsend, L. Pagani, P. Scott, L. Blunt, Areal surface texture data extraction from X-ray computed tomography reconstructions of metal additively manufactured parts, Precis Eng 48 (2017) 254–264. https://doi.org/10.1016/j.precisioneng.2016.12.008.

[41] M.A. De Pastre, A. Thompson, Y. Quinsat, J.A. Albajez García, N. Senin, R. Leach, Polymer powder bed fusion surface texture measurement, Meas Sci Technol 31 (2020). https://doi.org/10.1088/1361-6501/ab63b1.

[42] C. Sen, G. Dursun, A. Orhangul, G. Akbulut, Assessment of Additive Manufacturing Surfaces Using X-ray Computed Tomography, in: Procedia CIRP, Elsevier B.V., 2022: pp. 501–506. https://doi.org/10.1016/j.procir.2022.03.078.

[43] A. Thompson, N. Senin, I. Maskery, R. Leach, Effects of magnification and sampling resolution in X-ray computed tomography for the measurement of additively manufactured metal surfaces, Precis Eng 53 (2018) 54–64.

[44] W. Sun, C. Giusca, S. Lou, X. Yang, X. Chen, T. Fry, X. Jiang, A. Wilson, S. Brown, H. Boulter, Establishment of X-ray computed tomography traceability for additively manufactured surface texture evaluation, Addit Manuf 50 (2022). https://doi.org/10.1016/j.addma.2021.102558.

[45] M. Praniewicz, J. Fox, G. Ameta, F. Kim, P. Witherell, C. Saldana, Exploring Registration of Optical, CMM and XCT for Verification of Supplemental Surfaces to Define AM Lattices: Application to Cylindrical and Spherical Surfaces, in: Procedia CIRP, Elsevier B.V., 2020: pp. 181–186. https://doi.org/10.1016/j.procir.2020.05.182.

[46] Y. Chahid, R. Racasan, L. Pagani, A. Townsend, A. Liu, P. Bills, L. Blunt, Parametrically designed surface topography on CAD models of additively manufactured lattice structures for improved design validation, Addit Manuf 37 (2021). https://doi.org/10.1016/j.addma.2020.101731.

[47] F. Borges de Oliveira, A. Stolfi, M. Bartscher, L. De Chiffre, U. Neuschaefer-Rube, Experimental investigation of surface determination process on multi-material components for dimensional computed tomography, Case Studies in Nondestructive Testing and Evaluation 6 (2016) 93–103. https://doi.org/10.1016/j.csndt.2016.04.003.

[48] P. Hermanek, F. Borges De Oliveira, S. Carmignato, M. Bartscher, Experimental investigation of new multi-material gap reference standard for testing computed tomography systems, in: 7th Conference on Industrial Computed Tomography (ICT), Leuven, Belgium, 2017.

[49] R.H. Schmitt, A. Buratti, N. Grozmani, C. Voigtmann, M. Peterek, Model-based optimisation of CT imaging parameters for dimensional measurements on multimaterial workpieces, CIRP Annals 67 (2018) 527–530. https://doi.org/10.1016/j.cirp.2018.04.003.

[50] A. Jansson, P. Hermanek, L. Pejryd, S. Carmignato, Multi-material gap measurements using dual-energy computed tomography, Precis Eng 54 (2018) 420–426. https://doi.org/10.1016/j.precisioneng.2018.07.012.

[51] H. Villarraga-Gómez, E.P. Morse, S.T. Smith, Assessing the effect of penetration length variations on dimensional measurements with X-ray computed tomography, Precis Eng 79 (2023) 146–163. https://doi.org/10.1016/j.precisioneng.2022.10.001.

[52] A. Jansson, A. Reza Zekavat, L. Pejryd, J. Ekengren, A.-R. Zekavat, L. Pejryd, Effects of X-ray Penetration Depth on Multi Material Computed Tomography Measurements, in: 6th Conference on Industrial Computed Tomography, 2016. https://www.researchgate.net/publication/312498386.

[53] R. Jiménez-Pacheco, S. Ontiveros, J.A. Yagüe-Fabra, F. Zanini, S. Carmignato, J.A. Albajez, Assessment of gradient-based algorithm for surface determination in multi-material gap

measurements by x ray computed tomography, Materials 13 (2020) 1–11. https://doi.org/10.3390/ma13245650.

[54] X. Yang, W. Sun, C.L. Giusca, An automated surface determination approach for computed tomography, NDT and E International 131 (2022). https://doi.org/10.1016/j.ndteint.2022.102697.

[55] C. Heinzl, J. Kastner, E. Gröller, Surface extraction from multi-material components for metrology using dual energy CT, IEEE Trans Vis Comput Graph 13 (2007) 1520–1527. https://doi.org/10.1109/TVCG.2007.70598.

[56] M. Haitham Shammaa, Y. Ohtake, H. Suzuki, Segmentation of multi-material CT data of mechanical parts for extracting boundary surfaces, CAD Computer Aided Design 42 (2010) 118–128. https://doi.org/10.1016/j.cad.2009.08.003.

[57] R. Jiménez-Pacheco, S. Ontiveros, J.A. Yagüe-Fabra, A surface extraction analysis in a multi-material test part for computed tomography in metrology applications, Procedia Manuf 13 (2017) 487–494. https://doi.org/10.1016/j.promfg.2017.09.068.

[58] M. Reiter, F.B. de Oliveira, M. Bartscher, C. Gusenbauer, J. Kastner, Case Study of Empirical Beam Hardening Correction Methods for Dimensional X-ray Computed Tomography Using a Dedicated Multi-material Reference Standard, J Nondestr Eval 38 (2019). https://doi.org/10.1007/s10921-018-0548-3.

[59] F. Borges de Oliveira, M. Bartscher, U. Neuschaefer-Rube, R. Tutsch, J. Hiller, Multi-material acceptance testing for CT-based coordinate measurement systems, in: Lecture Notes in Mechanical Engineering, Pleiades journals, 2019: pp. 131–154. https://doi.org/10.1007/978-3-030-18177-2_14.

[60] Computed tomography in dimensional metrology VDI/VDE 2630 Part 1.3: Accuracy of coordinate measuring machines characteristics and their testing, 2011.

[61] A. Jansson, L. Pejryd, L. Pejryd, Characterisation of additive manufacturing metal-carbon-fibre composite bond by dual-energy computed tomography, in: Dimensional Accuracy and Surface Finish in Additive Manufacturing, Leuven, 2017. www.euspen.eu.

[62] M. Curto, A.P. Kao, W. Keeble, G. Tozzi, A.H. Barber, X-ray computed tomography evaluations of additive manufactured multimaterial composites, J Microsc 285 (2022) 131–143. https://doi.org/10.1111/jmi.13034.

[63] F. Zanini, S. Carmignato, Reference object for traceability establishment in X-ray computed tomography measurements of fiber length in fiber-reinforced polymeric materials, Precis Eng 77 (2022) 33–39. https://doi.org/10.1016/j.precisioneng.2022.05.003.

[64] W. Tao, M.C. Leu, Design of lattice structure for additive manufacturing, in: International Symposium on Flexible Automation, ISFA 2016, Institute of Electrical and Electronics Engineers Inc., 2016: pp. 325–332. https://doi.org/10.1109/ISFA.2016.7790182.

[65] M. Helou, S. Kara, Design, analysis and manufacturing of lattice structures: An overview, Int J Comput Integr Manuf 31 (2018) 243–261. https://doi.org/10.1080/0951192X.2017.1407456.

[66] M. Praniewicz, J.C. Fox, C. Saldana, Toward traceable XCT measurement of AM lattice structures: Uncertainty in calibrated reference object measurement, Precis Eng 77 (2022) 194–204. https://doi.org/10.1016/j.precisioneng.2022.05.010.

[67] Computed tomography in dimensional measurement. VDI/VDE 2630 Part 2.1: Determination of the uncertainty of measurement and the test process suitability of coordinate measurement systems with CT sensors, 2015.

[68] F. Zanini, S. Carmignato, E. Savio, Two different experimental approaches for the uncertainty determination of X-ray computed tomography dimensional measurements on lattice structures, CIRP J Manuf Sci Technol 47 (2023) 205–214. https://doi.org/10.1016/j.cirpj.2023.10.004.

[69] E. Savio, H.N. Hansen, L. De Chiffre, Approaches to the Calibration of Freeform Artefacts on Coordinate Measuring Machines, CIRP Annals 51 (2002) 433–436. https://doi.org/10.1016/S0007-8506(07)61554-6.

[70] E. Trapet, E. Savio, L. De Chiffre, New advances in traceability of CMMs for almost the entire range of industrial dimensional metrology needs, CIRP Annals 53 (2004) 433–438. https://doi.org/10.1016/S0007-8506(07)60733-1.

[71] G. Ameta, J. Fox, P. Witherell, Tolerancing and verification of additive manufactured lattice with supplemental surfaces, in: Procedia CIRP, Elsevier B.V., 2018: pp. 69–74. https://doi.org/10.1016/j.procir.2018.02.023.

[72] J. Singh Rathore, C. Vienne, Y. Quinsat, C. Tournier, Influence of resolution on the X-ray CT-based measurements of metallic AM lattice structures, Welding in the Wolrd 64 (2020) 1367–1376. https://doi.org/10.1007/s40194-020-00920-4/Published.

[73] M.R. Karamooz Ravari, S. Nasr Esfahani, M. Taheri Andani, M. Kadkhodaei, A. Ghaei, H. Karaca, M. Elahinia, On the effects of geometry, defects, and material asymmetry on the mechanical response of shape memory alloy cellular lattice structures, Smart Mater Struct 25 (2016). https://doi.org/10.1088/0964-1726/25/2/025008.

[74] S. Okubo, Y. Yamauchi, K. Kitazono, Effects of random and controlled irregularity in strut lattice structure of PA12 on compression anisotropy, Addit Manuf 63 (2023). https://doi.org/10.1016/j.addma.2022.103385.

[75] W. Radlof, H. Panwitt, C. Benz, M. Sander, Image-based and in-situ measurement techniques for the characterization of the damage behavior of additively manufactured lattice structures under fatigue loading, in: Procedia Structural Integrity, Elsevier B.V., 2021: pp. 50–59. https://doi.org/10.1016/j.prostr.2022.03.006.

[76] K. Ferreira, N. Anwer, C. Mehdi-Souzani, Characterization of L-PBF lattice structures geometric defects, in: Procedia CIRP, Elsevier B.V., 2021: pp. 846–851. https://doi.org/10.1016/j.procir.2021.05.033.

[77] A. Riot, E. Panettieri, A. Cosculluela, M. Montemurro, Influence of manufacturing process-induced geometrical defects on the energy absorption capacity of polymer lattice structures, Defence Technology (2023). https://doi.org/10.1016/j.dt.2023.09.003.

[78] A. Sombatmai, V. Uthaisangsuk, S. Wongwises, P. Promoppatum, Multiscale investigation of the influence of geometrical imperfections, porosity, and size-dependent features on mechanical behavior of additively manufactured Ti-6Al-4V lattice struts, Mater Des 209 (2021). https://doi.org/10.1016/j.matdes.2021.109985.

[79] M.A. de Pastre, Y. Quinsat, C. Lartigue, Shape defect analysis from volumetric data - Application to lattice struts in additive manufacturing, Precis Eng 76 (2022) 12–28. https://doi.org/10.1016/j.precisioneng.2022.02.011.

[80] M.A. de Pastre, Y. Quinsat, Virtual volume correlation of lattice structures: From volumetric data to geometrical and dimensional defects identification, Addit Manuf 61 (2023). https://doi.org/10.1016/j.addma.2022.103347.

[81] H.D. Carlton, N.A. Volkoff-Shoemaker, M.C. Messner, N.R. Barton, M. Kumar, Incorporating defects into model predictions of metal lattice-structured materials, Materials Science and Engineering: A 832 (2022). https://doi.org/10.1016/j.msea.2021.142427.

[82] B.S. Rupal, X. Li, H.R.Z. Rajani, Z. Chen, A.J. Qureshi, Porosity and Shape Deviation Analysis of Lattice Structures Manufactured Using Laser Powder Bed Fusion Process, in: Procedia CIRP, Elsevier B.V., 2022: pp. 48–53. https://doi.org/10.1016/j.procir.2022.10.007.

[83] N. Elenskaya, M. Tashkinov, Numerical simulation of deformation behavior of additively manufactured polymer lattice structures with a porosity gradient, in: Procedia Structural Integrity, Elsevier B.V., 2021: pp. 692–697. https://doi.org/10.1016/j.prostr.2022.01.139.

[84] M. Grazia Guerra, M. Lafirenza, V. Errico, A. Angelastro, In-process dimensional and geometrical characterization of laser-powder bed fusion lattice structures through high-resolution optical tomography, Opt Laser Technol 162 (2023). https://doi.org/10.1016/j.optlastec.2023.109252.

[85] A. du Plessis, G. Schwaderer, I. Cristofolini, M. Zago, M. Benedetti, Dimensional metrology of additively manufactured lattice structures by combined tactile probe and X-ray tomography, Material Design and Processing Communications 3 (2021). https://doi.org/10.1002/mdp2.216.

[86] J.S. Rathore, C. Mang, C. Vienne, Y. Quinsat, C. Tournier, A methodology for computed tomography-based nondestructive geometrical evaluations of lattice structures by holistic strut measurement approach, Journal of Manufacturing Science and Engineering, Transactions of the ASME 143 (2021). https://doi.org/10.1115/1.4049492.

[87] Geometrical product specifications (GPS). Acceptance and reverification tests for coordinate measuring machines (CMM). Part 2: CMMs used for measuring linear dimensions, 2010. www.une.org.

[88] Geometrical product specifications (GPS) - Acceptance and reverification tests for coordinate measuring systems (CMS) - Part 5: Coordinate measuring machines (CMMs) using single and multiple stylus contacting probing systems using discrete point and/or scanning measuring mode (ISO 10360-5:2020), 2020.

[89] Geometrical product specifications (GPS). Acceptance and reverification tests for coordinate measuring systems (CMS). Part 10: Laser trackers (ISO 10360-10:2021), 2021.

[90] B. Muralikrishnan, M. Shilling, V. Lee, ASME B89.4.23 Performance Evaluation Tests and Geometry Errors in X-Ray Computed Tomography Systems, J Res Natl Inst Stand Technol 126 (2021). https://doi.org/10.6028/jres.126.042.

[91] Geometrical product specifications (GPS). Coordinate measuring machines (CMM). Technique for determining the uncertainty of measurement. Part 3: Use of calibrated workpieces or measurement standards. (ISO 15530-3:2011), 2011.

[92] A. Stolfi, M.K. Thompson, L. Carli, L. De Chiffre, Quantifying the Contribution of Post-Processing in Computed Tomography Measurement Uncertainty, in: Procedia CIRP, Elsevier B.V., 2016: pp. 297–302. https://doi.org/10.1016/j.procir.2016.02.123.

[93] Á. Rodríguez-Sánchez, A. Thompson, L. Körner, N. Brierley, R. Leach, Review of the influence of noise in X-ray computed tomography measurement uncertainty, Precis Eng 66 (2020) 382–391. https://doi.org/10.1016/j.precisioneng.2020.08.004.

[94] N. Grozmani, A. Buratti, R.H. Schmitt, Investigating the influence of workpiece placement on the uncertainty of measurements in industrial computed tomography, in: 9th Conference on Industrial Computed Tomography, Padova, 2019. http://www.ndt.net/?id=23750.

[95] M. Ferrucci, E. Ametova, Charting the course towards dimensional measurement traceability by x-ray computed tomography, Meas Sci Technol 32 (2021). https://doi.org/10.1088/1361-6501/abf058.

[96] N. Ortega, S. Plaza, A. Pascual, I. Holgado, A. Lamikiz, A methodology to obtain traceability for internal and external measurements of Inconel 718 components by means of XRCT, NDT and E International 120 (2021). https://doi.org/10.1016/j.ndteint.2021.102436.

[97] F. Zanini, M. Sorgato, E. Savio, S. Carmignato, Dimensional verification of metal additively manufactured lattice structures by X-ray computed tomography: Use of a newly developed calibrated artefact to achieve metrological traceability, Addit Manuf 47 (2021). https://doi.org/10.1016/j.addma.2021.102229.

[98] Conformity assessment - General requirements for the competence of proficiency testing providers (ISO/IEC 17043:2023), 2023.

[99] S. Carmignato, Accuracy of industrial computed tomography measurements: Experimental results from an international comparison, CIRP Ann Manuf Technol 61 (2012) 491–494. https://doi.org/10.1016/j.cirp.2012.03.021.

[100] S. Ontiveros, J.A. Yagüe-Fabra, R. Jiménez, G. Tosello, S. Gasparin, A. Pierobon, S. Carmignato, H.N. Hansen, Dimensional measurement of micro-moulded parts by computed tomography, Meas Sci Technol 23 (2012). https://doi.org/10.1088/0957-0233/23/12/125401.

[101] A.-F. Obaton, C. Gottlieb Klingaa, C. Rivet, K. Mohaghegh, S. Baier, J. Lasson Andreasen, L. Carli, L. De Chiffre, Reference standards for XCT measurements of additively manufactured parts, in: 10th Conference of Industrial Computed Tomography (ICT), Wels, Austria, 2020. www.ict-conference.com/2020.

[102] J.D. Thousand, S.T. Smith, A direct silicon bonded reference object for performance assessment of computed tomography systems, Precis Eng 58 (2019) 16–24. https://doi.org/10.1016/j.precisioneng.2019.04.017.

[103] S. Moylan, J. Slotwinski, A. Cooke, K. Jurrens, M.A. Donmez, An additive manufacturing test artifact, J Res Natl Inst Stand Technol 119 (2014) 429–459. https://doi.org/10.6028/jres.119.017.

[104] T. Grimm, User's guide to rapid prototyping, Society of Manufacturing Engineers, 2004.

[105] I. Gibson, D. Rosen, B. Stucker, Additive Manufacturing Technologies. 3D Printing, Rapid Prototyping, and Direct Digital Manufacturing, Second edition, Springer, 2015.

[106] A. Wiberg, J. Persson, J. Ölvander, Design for additive manufacturing – a review of available design methods and software, Rapid Prototyp J 25 (2019) 1080–1094. https://doi.org/10.1108/RPJ-10-2018-0262.

[107] M.A. de Pastre, S.C. Toguem Tagne, N. Anwer, Test artefacts for additive manufacturing: A design methodology review, CIRP J Manuf Sci Technol 31 (2020) 14–24. https://doi.org/10.1016/j.cirpj.2020.09.008.

[108] K. Lussenburg, A. Sakes, P. Breedveld, Design of non-assembly mechanisms: A state-of-the-art review, Addit Manuf 39 (2021). https://doi.org/10.1016/j.addma.2021.101846.

[109] C.A. Chatham, T.E. Long, C.B. Williams, A review of the process physics and material screening methods for polymer powder bed fusion additive manufacturing, Prog Polym Sci 93 (2019) 68–95. https://doi.org/10.1016/j.progpolymsci.2019.03.003.

[110] S. Singh, S. Ramakrishna, R. Singh, Material issues in additive manufacturing: A review, J Manuf Process 25 (2017) 185–200. https://doi.org/10.1016/j.jmapro.2016.11.006.

[111] A. García-Collado, J.M. Blanco, M.K. Gupta, R. Dorado-Vicente, Advances in polymers based Multi-Material Additive-Manufacturing Techniques: State-of-art review on properties and applications, Addit Manuf 50 (2022). https://doi.org/10.1016/j.addma.2021.102577.

[112] R. Singh, A. Gupta, O. Tripathi, S. Srivastava, B. Singh, A. Awasthi, S.K. Rajput, P. Sonia, P. Singhal, K.K. Saxena, Powder bed fusion process in additive manufacturing: An overview, in: Mater Today Proc, Elsevier Ltd, 2019: pp. 3058–3070. https://doi.org/10.1016/j.matpr.2020.02.635.

[113] T. Hofstätter, D.B. Pedersen, G. Tosello, H.N. Hansen, Applications of Fiber-Reinforced Polymers in Additive Manufacturing, Procedia CIRP 66 (2017) 312–316. https://doi.org/10.1016/j.procir.2017.03.171.

[114] B. Karaş, P.J. Smith, J.P.A. Fairclough, K. Mumtaz, Additive manufacturing of high density carbon fibre reinforced polymer composites, Addit Manuf 58 (2022). https://doi.org/10.1016/j.addma.2022.103044.

[115] D. Zindani, K. Kumar, An insight into additive manufacturing of fiber reinforced polymer composite, International Journal of Lightweight Materials and Manufacture 2 (2019) 267–278. https://doi.org/10.1016/j.ijlmm.2019.08.004.

[116] Y. Abderrafai, M. Hadi Mahdavi, F. Sosa-Rey, C. Hérard, I. Otero Navas, N. Piccirelli, M. Lévesque, D. Therriault, Additive manufacturing of short carbon fiber-reinforced polyamide composites by fused filament fabrication: Formulation, manufacturing and characterization, Mater Des 214 (2022). https://doi.org/10.1016/j.matdes.2021.110358.

[117] S. Yuan, F. Shen, C.K. Chua, K. Zhou, Polymeric composites for powder-based additive manufacturing: Materials and applications, Prog Polym Sci 91 (2019) 141–168. https://doi.org/10.1016/j.progpolymsci.2018.11.001.

[118] N. Yaragatti, A. Patnaik, A review on additive manufacturing of polymers composites, in: Mater Today Proc, Elsevier Ltd, 2020: pp. 4150–4157. https://doi.org/10.1016/j.matpr.2020.10.490.

[119] R. Leach, S. Carmignato, Precision Metal Additive Manufacturing, 2021.

[120] R.K. Leach, D. Bourell, S. Carmignato, A. Donmez, N. Senin, W. Dewulf, Geometrical metrology for metal additive manufacturing, CIRP Annals 68 (2019) 677–700. https://doi.org/10.1016/j.cirp.2019.05.004.

[121] Additive manufacturing. General principles. Fundamentals and vocabulary. (ISO/ASTM 52900:2021), 2022.

[122] H. Bikas, A.K. Lianos, P. Stavropoulos, A design framework for additive manufacturing, International Journal of Advanced Manufacturing Technology 103 (2019) 3769–3783. https://doi.org/10.1007/s00170-019-03627-z.

[123] G.A.O. Adam, D. Zimmer, Design for Additive Manufacturing-Element transitions and aggregated structures, CIRP J Manuf Sci Technol 7 (2014) 20–28. https://doi.org/10.1016/j.cirpj.2013.10.001.

[124] G.A.O. Adam, D. Zimmer, On design for additive manufacturing: Evaluating geometrical limitations, Rapid Prototyp J 21 (2015) 662–670. https://doi.org/10.1108/RPJ-06-2013-0060.

[125] J. Hulme, A.H. Sakhaei, M. Shafiee, Mechanical analysis and additive manufacturing of 3D-printed lattice materials for bone scaffolds, Mater Today Proc (2023). https://doi.org/10.1016/j.matpr.2023.02.278.

[126] M. Schmid, K. Wegener, Additive Manufacturing: Polymers applicable for laser sintering (LS), in: Procedia Eng, Elsevier Ltd, 2016: pp. 457–464. https://doi.org/10.1016/j.proeng.2016.06.692.

[127] A. Wegner, New polymer materials for the laser sintering process: Polypropylene and others, in: Phys Procedia, Elsevier B.V., 2016: pp. 1003–1012. https://doi.org/10.1016/j.phpro.2016.08.105.

[128] D. Drummer, K. Wudy, F. Kühnlein, M. Drexler, Polymer Blends for Selective Laser Sintering: Material and Process Requirements, in: Phys Procedia, Elsevier B.V., 2012: pp. 509–517. https://doi.org/10.1016/j.phpro.2012.10.067.

[129] D. Drummer, M. Drexler, F. Kühnlein, Effects on the Density Distribution of SLS-Parts, in: Phys Procedia, Elsevier B.V., 2012: pp. 500–508. https://doi.org/10.1016/j.phpro.2012.10.066.

[130] D. Kwon, E. Park, S. Ha, N. Kim, Effect of humidity changes on dimensional stability of 3D printed parts by selective laser sintering, International Journal of Precision Engineering and Manufacturing 18 (2017) 1275–1280. https://doi.org/10.1007/s12541-017-0150-0.

[131] P. Foteinopoulos, A. Papacharalampopoulos, P. Stavropoulos, On thermal modeling of Additive Manufacturing processes, CIRP J Manuf Sci Technol 20 (2018) 66–83. https://doi.org/10.1016/j.cirpj.2017.09.007.

[132] G. Ameta, J. Fox, P. Witherell, Tolerancing and verification of additive manufactured lattice with supplemental surfaces, in: Procedia CIRP, Elsevier B.V., 2018: pp. 69–74. https://doi.org/10.1016/j.procir.2018.02.023.

[133] B. Msallem, N. Sharma, S. Cao, F.S. Halbeisen, H.F. Zeilhofer, F.M. Thieringer, Evaluation of the dimensional accuracy of 3D-printed anatomical mandibular models using FFF, SLA, SLS, MJ, and BJ printing technology, J Clin Med 9 (2020). https://doi.org/10.3390/jcm9030817.

[134] V.M. Rivas Santos, A. Thompson, D. Sims-Waterhouse, I. Maskery, P. Woolliams, R. Leach, Design and characterisation of an additive manufacturing benchmarking artefact following a design-for-metrology approach, Addit Manuf 32 (2020). https://doi.org/10.1016/j.addma.2019.100964.

[135] Additive manufacturing Test artefacts Geometric capability assessment of additive manufacturing systems (ISO/ASTM 52902:2023), 2024. www.une.org.

[136] D. Gallardo, M. Concha, L.-C. Díaz, R. Jiménez, M. Torralba, J.A. Albajez, J.A. Yagüe-Fabra, Surface Characterisation and Comparison of Polymeric Additive Manufacturing Features for an XCT Test Object, Key Eng Mater 959 (2023) 35–44. https://doi.org/10.4028/p-tn0lzd.

[137] D. Gallardo, L.C. Díaz, R. Jiménez, M. Torralba, J.A. Albajez, J.A.Y. Fabra, X-Ray Computed Tomography performance in metrological evaluation and characterisation of polymeric additive manufactured surfaces, Addit Manuf 75 (2023). https://doi.org/10.1016/j.addma.2023.103754.

[138] Geometrical product specifications (GPS). Surface texture: Profile. Part 3: Specification operators (ISO 21920-3:2021), 2021. www.iso.org.

[139] H. Villarraga-Gómez, C.B. Lee, S.T. Smith, Dimensional metrology with X-ray CT: A comparison with CMM measurements on internal features and compliant structures, Precis Eng 51 (2018) 291–307. https://doi.org/10.1016/j.precisioneng.2017.08.021.

[140] D. Gallardo, L.-C. Díaz, F. Zanini, J.A. Albajez, S. Carmignato, J.A. Yagüe-Fabra, On the effect of material density in dimensional evaluations by X-ray computed tomography of metal-polymer multi-material parts, CIRP J Manuf Sci Technol 54 (2024) 1–13. https://doi.org/10.1016/j.cirpj.2024.08.003.

[141] H. Villarraga-Gómez, S.T. Smith, Effect of geometric magnification on dimensional measurements with a metrology-grade X-ray computed tomography system, Precis Eng 73 (2022) 488–503. https://doi.org/10.1016/j.precisioneng.2021.10.015.

[142] K. Kim, Y. Lee, Improvement of signal and noise performance using single image super-resolution based on deep learning in single photon-emission computed tomography imaging system, Nuclear Engineering and Technology 53 (2021) 2341–2347. https://doi.org/10.1016/j.net.2021.01.011.

[143] S. Lou, S.B. Brown, W. Sun, W. Zeng, X. Jiang, P.J. Scott, An investigation of the mechanical filtering effect of tactile CMM in the measurement of additively manufactured parts, Measurement (Lond) 144 (2019) 173–182. https://doi.org/10.1016/j.measurement.2019.04.066.

[144] A.M. Hernandez, J.M. Boone, Tungsten anode spectral model using interpolating cubic splines: Unfiltered x-ray spectra from 20 kV to 640 kV, Med Phys 41 (2014). https://doi.org/10.1118/1.4866216.

[145] X. Ma, M. Buschmann, E. Unger, P. Homolka, Classification of X-Ray Attenuation Properties of Additive Manufacturing and 3D Printing Materials Using Computed Tomography From 70 to 140 kVp, Front Bioeng Biotechnol 9 (2021). https://doi.org/10.3389/fbioe.2021.763960.

[146] M. Berger, J. Hubbel, S. Seltzer, J. Chang, J. Coursey, R. Sukumar, D. Zucker, K. Olsen, XCOM: photon cross section database, (2010).

[147] J. Punnoose, J. Xu, A. Sisniega, W. Zbijewski, J.H. Siewerdsen, Technical Note: Spektr 3.0 - A computational tool for x-ray spectrum modeling and analysis, Med Phys 43 (2016) 4711–4717. https://doi.org/10.1118/1.4955438.

[148] H. Villarraga-Gómez, A. Amirkhanov, C. Heinzl, S.T. Smith, Assessing the effect of sample orientation on dimensional X-ray computed tomography through experimental and simulated data, Measurement (Lond) 178 (2021). https://doi.org/10.1016/j.measurement.2021.109343.

[149] D. Gallardo, L.-C. Díaz, J.A. Albajez, J.A. Yagüe-Fabra, Progress toward the Definition of X-ray Computed Tomography Accuracy in the Characterization of Polymer-Based Lattice Structures, Polymers (Basel) 16 (2024) 1419. https://doi.org/10.3390/polym16101419.

[150] Computed tomography in dimensional measurement. VDI/VDE 2630 Part 1.1: Basics and definitions, 2009.

[151] Computed tomography in dimensional measurement VDI/VDE 2630 Part 1.2: Influencing variables on measurement results and recommendations for computed tomography dimensional measurements, 2010. www.vdi-richtlinien.de.

[152] Computed tomography in dimensional metrology VDI/VDE 2630 Part 1.4: Measurement procedure and comparability, 2010. www.vdi-richtlinien.de.

[153] J.A. Albajez, S. Nuño, L.C. Díaz, D. Gallardo, J.A. Yagüe, R. Jiménez, M. Torralba, Reference standard for the uncertainty estimation of X–ray Computed Tomography measurements of complex macro-and micro-geometries, IOP Conf Ser Mater Sci Eng 1193 (2021) 012065. https://doi.org/10.1088/1757-899X/1193/1/012065.

[154] D. Gallardo, L. Díaz, J.A. Albajez, J.A. Yagüe-Fabra, R. Jiménez, M. Torralba, Evaluación de la estabilidad dimensional de esferas calibradas poliméricas para su aplicación en un patrón de referencia para tomografía computarizada (CT)., Jornada De Jóvenes Investigadores Del I3A 10 (2022). https://doi.org/https://doi.org/10.26754/jjii3a.20227047.

[155] P. Shah, R. Racasan, P. Bills, Comparison of different additive manufacturing methods using computed tomography, Case Studies in Nondestructive Testing and Evaluation 6 (2016) 69–78. https://doi.org/10.1016/j.csndt.2016.05.008.

[156] G. Moroni, S. Petrò, Design for X-ray computed tomography, Procedia CIRP 84 (2019) 173–178. https://doi.org/10.1016/j.procir.2019.04.342.

[157] S. Carmignato, A. Voltan, E. Savio, Metrological performance of optical coordinate measuring machines under industrial conditions, CIRP Ann Manuf Technol 59 (2010) 497–500. https://doi.org/10.1016/j.cirp.2010.03.128.

[158] A. Townsend, R. Racasan, L. Blunt, Surface-specific additive manufacturing test artefacts, Surf Topogr 6 (2018). https://doi.org/10.1088/2051-672X/aabcaf.

[159] O. Sato, A. Balsamo, Report describing the procedure for a posteriori type A evaluation of measurement uncertainty. Deliverable D1 of the EUCoM project., 2021. http://eucom-empir.eu/wp-content/uploads/sites/20/2022/07/EUCoM-D1-v2. pdf.

[160] O. Sato, T. Takatsuji, Y. Miura, S. Nakanishi, GD&T task specific measurement uncertainty evaluation for manufacturing floor, in: Measurement: Sensors, Elsevier Ltd, 2021. https://doi.org/10.1016/j.measen.2021.100141.